ENEA

Agenzia Nazionale per le Nuove Tecnologie,
l'Energia e lo Sviluppo Economico Sostenibile

Ministero dello Sviluppo Economico

RICERCA DI SISTEMA ELETTRICO

Analisi del trasporto del trizio nei sistemi SFR

F. Franza, A. Ciampichetti, M. Zucchetti

ANALISI DEL TRASPORTO DEL TRIZIO NEI SISTEMI SFR
A. Ciampichetti – ENEA, F. Franza, M. Zucchetti - POLITO

Settembre 2011

Titolo

Analisi del trasporto del trizio nei sistemi SFR

Descrittori

Tipologia del documento: Rapporto Tecnico

Collocazione contrattuale: Accordo di programma ENEA-MSE: tema di ricerca "Nuovo nucleare da fissione"

Argomenti trattati: Radioprotezione
Prodotti di fissione
Tecnologia dei metalli liquidi
Generation IV Reactors

Sommario

Uno degli isotopi radioattivi più difficili da contenere all'interno dei reattori SFR è il trizio in quanto diffonde prontamente attraverso i materiali strutturali alle temperature operative e conseguentemente può essere rilasciato in ambiente. Al fine di studiare ed analizzare possibili accorgimenti necessari per ridurre l'entità dei rilasci di trizio in ambiente è stato sviluppato un codice di calcolo in linguaggio MATLAB (SFR-TPC), il quale viene utilizzato per valutare i rilasci di trizio in ambiente e gli inventari di trizio all'interno dei reattori SFR.

L'analisi condotta con l'utilizzo del codice SFR-TPC su un reattore di tipologia "a vasca" denominato PFBR (Prototype Fast Breeder Reactor), ha mostrato che, sotto alcuni ipotesi conservtive, solo circa 1.6 mg/y di trizio (su 3.874 g/y prodotti nel core e rilasciati nel refrigerante primario) raggiungono il ciclo del vapore e vengono conservativamente considerati come rilasci in ambiente. Nonostante le ipotesi conservative assunte il dato di rilascio ottenuto non costituisce un elevato rischio radiologico purché si adotti un opportuno set di misure mitigative per il trasporto di trizio

Note

Copia n.			In carico a:			
2			NOME			
			FIRMA			
1			NOME			
			FIRMA			
0	EMISSIONE	16-9-2011	NOME	A. Ciampichetti	M. Tarantino	P. Meloni
			FIRMA			
REV.	DESCRIZIONE	DATA		REDAZIONE	CONVALIDA	APPROVAZIONE

Contents

INTRODUZIONE E SOMMARIO DEL LAVORO

Uno degli isotopi radioattivi più difficili da contenere all'interno dei reattori SFR (Sodium-cooled Fast Reactors) è il trizio in quanto, essendo un isotopo dell'idrogeno, diffonde prontamente attraverso i materiali strutturali alle temperature operative e conseguentemente può essere rilasciato in ambiente.

Al fine di studiare ed analizzare possibili accorgimenti necessari per ridurre l'entità dei rilasci di trizio in ambiente è stato sviluppato un codice di calcolo in linguaggio MATLAB (SFR-TPC), il quale viene utilizzato per valutare i rilasci di trizio in ambiente e gli inventari di trizio all'interno dei reattori SFR.

Il trizio che viene generato nel core attraverso le fissioni ternarie e l'attivazione del boro, raggiunge quasi interamente il refrigerante primario, attraverso il quale entra nello scambiatore intermedio (IHX); successivamente, permeando attraverso le pareti dei tubi dell'IHX e del generatore di vapore (SG), raggiunge prima il sodio secondario e successivamente il vapore nel loop terziario di power - conversion (generatori di vapore, turbine, condensatori ecc). Il rateo totale di trizio introdotto nel sodio primario dal nocciolo e dalle barre controllo per un reattore di 1000 MWe ammonta a circa 75000 Ci/y.

Al fine di ridurre i rilasci di trizio si possono adottare due principali tecniche: 1) rivestimento (o coating) dei tubi degli scambiatori di calore (IHX e/o SG) di un certo tipo di materiale (in genere ossidi) in grado di ridurre i flussi permeati di un certo fattore PRF (Permeation Reduction Factor), 2) inserimento di trappole fredde (o cold traps) nei rami freddi dei circuiti primari e secondari. Il cold trapping del sodio ha l'obbiettivo di ridurre la solubilità dell'idrogeno (e del trizio) nel sodio tramite raffreddamento, determinandone quindi la precipitazione in una limitata regione "fredda". Le trappole fredde rispetto al coating dei tubi sono dispositivi ampiamente utilizzati per la loro efficienza, economicità e compattezza. Tuttavia alcune campagne sperimentali sono state condotte con l'obbiettivo di stimare l'attitudine di alcuni acciai a formare uno strato di ossido in grado di ridurre i flussi permeati; ad esempio l'INCOLOY 800 (lega al nickel candidata per la costruzione dei generatori di vapore in questa tipologia di impianti) ha mostrato PRF derivanti dalla propria ossidazione naturale (lato vapore) varianti tra 20 e 400. Per quanto riguarda invece le superfici a

contatto con il sodio, diversi studi hanno evidenziato che alcuni metalli come Fe, Ni e Cr (metalli tipici nell'ossidazione) difficilmente danno origine a ossidi stabili in quanto il sodio costituisce un ambiente riducente. Le pareti a contatto con il sodio vengono quindi conservativamente considerate "pulite" e prive di alcuna barriera antipermeazione (PRF=1).

L'analisi condotta con l'utilizzo del codice SFR-TPC su un reattore di tipologia "a vasca" denominato PFBR (Prototype Fast Breeder Reactor), ha mostrato che, assumendo PRF=1 e PRF=10 per IHX e SG rispettivamente (ipotesi conservative) e, ricircolando nelle cold traps lo 0.05 % della portata totale di sodio fluente nel nocciolo e nei loop secondari con un'efficienza di rimozione media del 80 % (parametri operativi che consentono di rispettare il target progettuale di contenimento delle cold traps), solo circa 1.6 mg/y di trizio (su 3.874 g/y prodotti nel core e rilasciati nel refrigerante primario) raggiungono il ciclo del vapore e vengono conservativamente considerati come rilasci in ambiente. Inoltre, aumentando di dieci volte la portata di sodio nelle cold traps (lo 0.5 % della portata totale di sodio fluente nel nocciolo e nei loop secondari), le attività specifiche di trizio nel sodio primario e secondario allo stato stazionario ammontano rispettivamente a 8 MBq/kg e 0.11 MBq/kg, le quali risultano confrontabili con quelle misurate in alcuni impianti in dismissione simili per tipologia a quello oggetto di studio (PFBR). Ad es. il reattore SuperPhénix ha mostrato attività specifiche di H^3 nel Na primario tra 5 e 20 MBq/kg.

Nonostante le ipotesi conservative assunte il dato di rilascio ottenuto non costituisce un elevato rischio radiologico purché si adotti un opportuno set di misure mitigative per il trasporto di trizio (cold traps e barriere alla permeazione derivanti o meno da processo di ossidazione naturale opportunamente controllati).

Chapter 0

Description of an SFR pool-type design

General description of SFR systems

The Sodium-Cooled Fast Reactor (SFR) system is one of six types of plants in Next Generation Nuclear Plant (NGNP). The NGNP [1] is in the pre-conceptual design phase with major design selections (e.g., reactor core type, core outlet temperature, etc.) still to be carried out. SFR features a fast-spectrum reactor and a closed fuel recycle system. The primary mission for SFR is the management of high-level wastes and, in particular, the management of plutonium and other actinides [1]. With innovations to reduce capital costs, the mission can extend to electricity production, given the proven capability of sodium reactors to utilize almost all of the energy in the natural uranium versus the 1% utilized in thermal spectrum systems [1].

The SFR system features a fast-spectrum reactor and closed fuel recycle system. The majority of natural uranium is the isotope U^{238} making up about 99.3 %. The remaining 0.7 % is U^{235}, the isotope required for thermal fission in modern light water reactors. The fast neutrons are used to breed plutonium from U^{238} and these plutonium isotopes then undergo fission to produce heat. Therefore fast reactors can utilize uranium much more efficiently than thermal reactors. Since water acts as a moderator and will slow neutrons out the fast spectrum, liquid metals, such as sodium, are used as coolants in these fast reactors transferring the heat to a power conversion system used to produce electricity.

The primary coolant system can either be arranged in a pool layout schematized in **Figure** Errore. Nel documento non esiste testo dello stile specificato.**-1** (a common approach, where all primary system components are housed in a single vessel), or in a compact loop layout, favored in Japan.
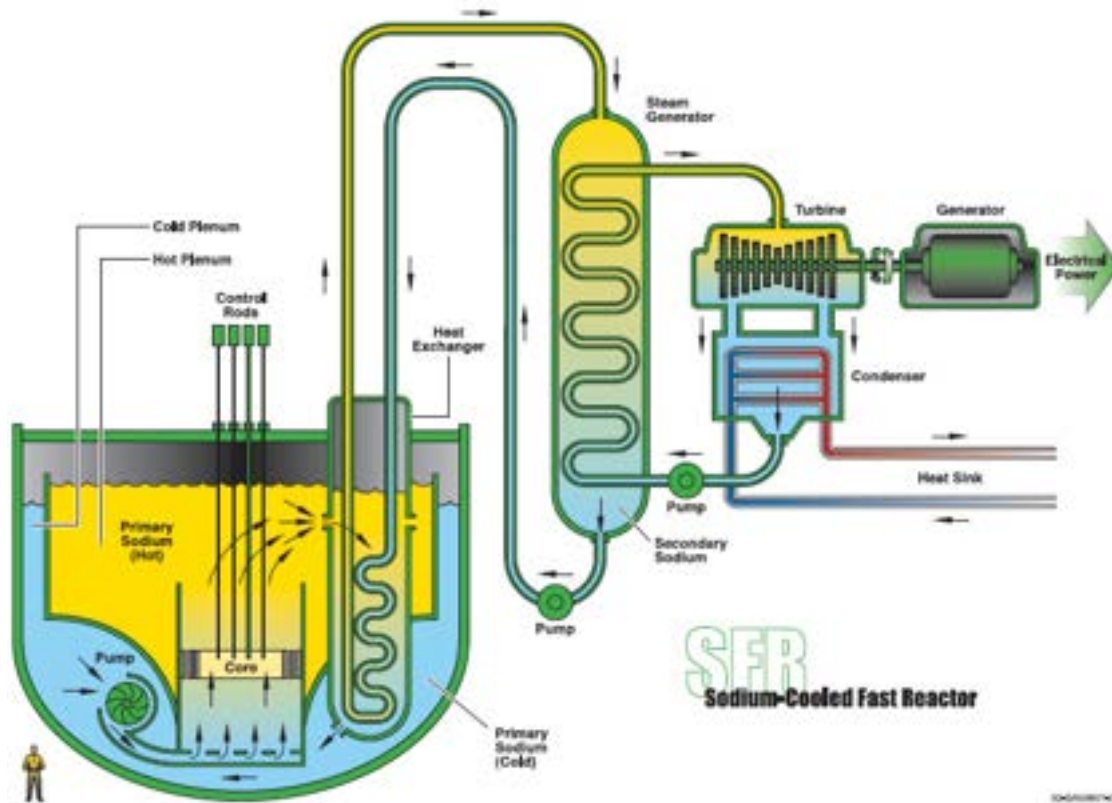
Figure Errore. Nel documento non esiste testo dello stile specificato.**-1 SFR pool type design configuration [1]**

In the pool type design the reactor core, the primary pumps, the IHXs (Intermediate Heat Exchangers) and the DHXs (Decay Heat Exchangers) are all immersed in a pool of sodium coolant within the reactor vessel, so the primary radioactive sodium does not leave the reactor vessel during normal operation. In this way LOCAs (Loss Of Coolant Accidents) affecting the primary sodium are extremely unlikely. The primary pump is totally submerged in the vessel, so the risk of having large sodium pipes under the core level (which could lead the core to become uncovered after a large LOCA) is eliminated. A disadvantage of this configuration is that a larger reactor vessel is required to host the heat exchangers and a larger quantity of primary sodium is needed. Moreover, the reactor vessel requires more complex internal structures.

In the loop type SFR design the primary coolant is circulated through pumps and IHXs in pipes which are external to the reactor tank. The main advantages of this design are: compactness,

easier in-service inspection and maintenance, smaller amount of sodium needed. The big disadvantage of this configuration is the possibility of a sodium leakage, which is much higher than in a pool-type SFR.

The total thermal power generated in the reactor core is exchanged by a set of IHXs in the reactor vessel. IHX is in general a straight tube heat exchanger of counter current shell and tube type. Liquid sodium is circulated through the core using one/two primary sodium pumps. The sodium enters the core and leaves at an higher temperature. The hot primary sodium is radioactive and is not used directly to produce steam, in fact it transfers the heat to secondary sodium through set of IHXs. The non-radioactive secondary sodium is circulated through a certain number of independent secondary loops, each having a sodium pump, a given number of intermediate heat exchangers and of steam generators (SG).

From the tritium analysis point of view, the IHX is a crucial component, since a portion of tritium entering the primary sodium permeates firstly through the IHX pipes walls and then through the SG ones reaching the feed water and escaping into the environment.

Selection of materials for SFR components

In order to perform a tritium transport analysis in SFR systems, some data on materials attitudes to allow tritium transport (i.e. tritium permeabilities and solubilities). For this reason attention will be focused on pool containment, IHX and SG materials.

In SFRs austenitic stainless steels are employed in the entire liquid sodium system even if the temperatures of some components are low enough to use less expensive ferritic steels [2]. **Table** Errore. Nel documento non esiste testo dello stile specificato.**-1** lists the structural materials selected for major components such as reactor vessel, intermediate heat exchanger (IHX), and piping in currently operating or designed Fast Breeder Reactors (FBRs) all over the world. The grades selected include 304, 304L, 316, 316L, 321, 347 and their equivalents. These steels have also poor creep ductility. In high temperature sodium, austenitic stainless steels have good resistance to general corrosion and localized corrosion.

Thus, for the IHX components, we see that austenitic stainless steels are preferred for sodium operation inside SFR intermediate heat exchanger. This is a precious information from the tritium permeation point of view. The permeability of tritium through a metallic materials is a key

component in a tritium transport analysis. Therefore, when IHX is modeled, we need to keep in mind that austenitic stainless steel are preferred for SFR's IHXs installation.

Reactor	Country	Reactor Vessel	IHX	Primary circuit piping hot leg (cold leg)*	Secondary circuit piping hot leg(cold leg)
Rapsodie	France	316 SS	316 SS	316 SS (316 SS)	316 SS (316 SS)
Phenix	France	316L SS	316 SS	(316 SS)	321 SS (304 SS)
PFR	U.K.	321 SS	316 SS	(321 SS)	321 SS (321 SS)
JOYO	Japan	304 SS	304 SS	304 SS (304 SS)	2.25Cr-1Mo (2.25Cr-1Mo)
FBTR	India	316 SS	316 SS	316 SS (316 SS)	316 SS (316 SS)
BN-600	Russia	304 SS	304 SS	304 SS	304 SS (304 SS)
Super Phenix-1	France	316L(N) SS	316L(N) SS	(304L(N) SS)	316L(N) SS
FFTF	U.S.A.	304 SS	304 SS	316 SS (316 SS)	316 SS (304 SS)
MONJU	Japan	304 SS	304 SS	304 SS (304 SS)	304 SS (304 SS)
SNR-300	Germany	304 SS	304 SS	304 SS (304 SS)	304 SS (304 SS)
BN-800	Russia	304 SS	304 SS	304 SS	304 SS (304 SS)
CRBRP	U.S.A.	304 SS	304 and 316 SS	316 SS (304 SS)	316H (304H)
DFBR	Japan	316FR SS	316 FR	316FR (304 SS)	304 SS (304 SS)
EFR	Europe	316L(N) SS	316L(N) SS	316L(N) SS	316L(N) SS

Table Errore. Nel documento non esiste testo dello stile specificato.**-1 Materials selected in SFRs for major components [2]**

Materials selected for SFR steam generator application should meet requirements of high temperature service such as high temperature mechanical properties including creep and low cycle fatigue, resistance to loss of carbon to liquid sodium which leads to reduction in strength, resistance

to wastage in case of small leaks leading to sodium-water reaction and resistance to stress corrosion cracking in sodium and water media [2]. For SFR steam generators, a range of materials starting from ferritic steels (2.25Cr- 1Mo, Nb stabilized 2.25Cr-1Mo, 9Cr-1Mo (grade 9), Modified 9Cr-1Mo (grade 91)), austenitic stainless steels (AISI 304/316/321) and Nickel alloys (Incoloy 800) were examined [2]. In view of the poor resistance to aqueous stress corrosion cracking (SCC), austenitic stainless steels of 300 series wouldn't be considered for the steam generator [2]. Incoloy 800 shows better resistance to SCC than austenitic steels, but it is not immune to stress corrosion cracking in chloride and caustic environments [2]. Therefore, ferritic steels are the most preferred for steam generator applications [2] (**Table** Errore. Nel documento non esiste testo dello stile specificato.**-2**). Among the ferritic steels, 2.25Cr-1Mo and 9Cr-1Mo steels and their variants were preferred for SFR steam generators.

Reactor	Sodium inlet (K)	Steam outlet (K)	Tubing material	
			Evaporator	Superheater
Phenix	823	785	2.25Cr-1Mo 2.25Cr-1Mo stabilised	321 SS
PFR	813	786	2.25Cr-1Mo stabilised Replacement unit in 2.25Cr-1Mo	316 SS Replacement unit in 9Cr-1Mo
FBTR	783	753	2.25Cr-1Mo stabilised	
BN-600	793	778	2.25Cr-1Mo	304 SS
Super Phenix-1	798	763	Alloy 800 (once through integrated)	
MONJU	778	760	2.25Cr-1Mo	304 SS
SNR-300	793	773	2.25Cr-1Mo stabilised	2.25Cr-1Mo stabilised
BN-800	778	763	2.25Cr-1Mo	2.25Cr-1Mo
CRBR	767	755	2.25Cr-1Mo	2.25Cr-1Mo
DFBR	793	768	Modified 9Cr-1Mo (grade 91) (once through integrated)	
EFR	798	763	Modified 9Cr-1Mo (grade 91) (once through integrated)	

Table Errore. Nel documento non esiste testo dello stile specificato.**-2 Materials selected for steam generator in major SFRs [2]**

From the tritium transport analysis point of view, the steam generator represents the second joint between the tritium source and the environment, since it directly belongs to the heat transport

system immediately after the IHX. Thus, a detailed investigation of SG material properties has to be carried out. In conclusion linking past experiences and selection criteria for SG materials, in a tritium analysis applied to SFR systems, Incoloy 800 and ferritic steels would be considered.

Chapter 0

Theoretical aspects of hydrogen isotopes kinetics in matter

Chemical and radiological properties of tritium

Transport of different chemical species of tritium in the environment (i.e., HT and HTO) is related to physical and chemical processes. Physical processes are bulk transport (tritium moves because of its dissolution inside heat transfer fluids) and diffusional transport (tritium motion is driven by concentration gradient). Reactions and state changes of chemical species are chemical processes [1].

Tritium is a radioactive isotope of hydrogen with the half life of 12.32 years. The nucleus of a tritium atom consists of a proton and two neutrons. This contrasts with the nucleus of an ordinary hydrogen atom and a deuterium atom. Ordinary hydrogen comprises over 99.9%, deuterium comprises 0.02%, and tritium comprises about a 10^{-16} % of naturally occurring hydrogen (Ref. [4]). The physical and chemical properties of tritium are very close to those of hydrogen [1]. Typically, tritium exists as a form of HT tritium gas ($H^1 - H^3$) because of isotope exchange reactions between $T_2(H^3 - H^3)$ and H_2 [4]. Tritiated water HTO is another common form of tritium. In tritiated water, a tritium atom replaces one of the hydrogen atoms so the chemical form is HTO rather than H_2O. Tritium in the environment has three sources: natural production, release from atmospheric weapon tests, and routine or accidental releases from the nuclear industry [1].

Inhalation, ingestion and skin exposure are the three main routes of exposure to tritium for man [1]. The radiological impact of tritium results from the combination of the characteristics and the behavior of the radionuclide. Some parameters enhance the radiotoxicity of tritium: for example, its radioactive half-life relatively long (12.35 years), its uptake by humans is likely to take place and as an isotope of hydrogen, it has a high biological importance [1]. The decay of tritium is given by:

$$^3_1H \rightarrow \, ^3_2He + \, ^0_{-1}\beta + \overline{v_e} \tag{2-1}$$

The β (or electron)'s kinetic energy varies, with an average of 5.7 keV [1], and a maximum of 19 keV [1] while the remaining energy is carried off by the nearly undetectable electron antineutrino $\overline{v_e}$.

The radiotoxicity of tritium is relatively low; the dose coefficients per unit of incorporation (the effective dose per built-in Becquerel) have been evaluated at 1.8×10^{-15} Sv/Bq for HT (inhalation), 1.8×10^{-11} Sv/Bq for HTO (ingestion or inhalation) [1]. As for other radionuclides, the theoretical risk of death by cancer due to tritium incorporation has been calculated to be $6.5 \times 10^{-2} Sv^{-1}$ incorporated [1]. The World Health Organization (WHO) places the limit at an annual effective dose of 0.1 mSv, corresponding to the daily consumption of tritiated water at a concentration of 10000 Bq/L during a year [1].

Solubility of hydrogen in metals: derivation of the Sievert's law

Hydrogen dissolves in and permeates through most materials, thus it is important to understand the permeation, diffusion and dissolution of atomic hydrogen in materials in which hydrogen and its isotopes are present.

More recently, these topics have received attention from the hydrogen energy community; hydrogen dissolution and permeation can be significant, especially in liquid metals. Thus, it is also necessary to understand the behavior of hydrogen in these materials, in order to predict the transport mechanisms inside the nuclear heat installations, and to estimate the tritium losses into the environment. Tritium permeation mechanisms are studied mainly in liquid metals for nuclear fusion devices, but in this study the attention is addressed also in liquid metals involved in next generation nuclear power plant, such as liquid sodium.

The Sievert's law

After crossing the outer surface of a solid, hydrogen moves into the subsurface where it occupies a solution site of the host lattice. There are two parameters characterizing the ability of materials to dissolve gas: the Sievert's constant K_s and the solubility S.

The **solubility** of a gas in a material is defined as the concentration of the gas dissolved at the chemical equilibrium $(S = C_{eq}[mol/m^3])$, under a given pressure and temperature. The concentration of hydrogen in the bulk of the material, in the most general form, is expressed as a function of both temperature and pressure and is defined as [5]:

$$C_{eq} = f(T) \cdot p^n \tag{2-2}$$

The parameter n may be different in different conditions. In dilute solution $n = 1/2$ for diatomic gases, and this is the case of the so called Sievert's law, and $f(T)$ characterizes the **Sievert's constant.** The Sievert's law can be derived starting from ideal gas law and from basic thermodynamic relationship relating molar volume $V_m[m^3/mol]$, the chemical potential $\mu[J/mol]$ the temperature $T[K]$ and the pressure $p[Pa]$ according to the following equations [6]:

$$V_m = \frac{RT}{p} \tag{2-3}$$

$$\left(\frac{d\mu}{dp}\right)_T = V_m \tag{2-4}$$

Substituting Eq. (2-3) into Eq. (2-4), the chemical potential of an ideal gas can be written in the form [6]:

$$(d\mu)_T = RT(d\ln p)_T \tag{2-5}$$

Assuming chemical and thermodynamic equilibrium between the diatomic hydrogen molecule (gas phase) and hydrogen atoms in a metal (solid phase) we find the following equilibrium:

$$\frac{1}{2} H_2(g) \Leftrightarrow \underline{H}(s) \tag{2-6}$$
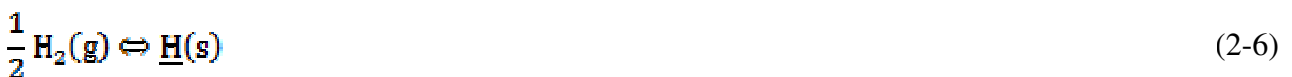
At chemical equilibrium, the chemical potential of the gas $\mu[J/mol]$ must equal the chemical potential of hydrogen dissolved in the material [6] as follows:

$$\frac{1}{2} \mu_{H_2} = \mu_{\underline{H}} \tag{2-7}$$

In this context we assume that atomic hydrogen dissolved in the material behaves as a dilute solution, thus, integrating the expression reported in Eq. (2-5) between the standard state (defined at

standard temperature and pressure) and the generic thermodynamic state (defined at temperature and pressure $T = 298.15$ [K] and $p = 1013200$ [Pa]) and considering chemical equilibrium between solid and gas phase (Eq. (2-7)), we obtain the following equation [6]:

$$\frac{1}{2}\left(\mu_{H_2}^0 + RT \ln p\right) = \mu_H^0 + RT \ln c_L \tag{2-8}$$

where c_L [at. fract] is the equilibrium concentration of hydrogen dissolved in the metal lattice and the superscript 0 refers to the standard state. The difference in chemical potential between the standard states is related to the enthalpy of formation of H-atoms in the metal ΔH_s and the entropy of formation ΔS_s [6]:

$$\mu_H^0 - \frac{1}{2}\mu_{H_2}^0 = \Delta H_s - T\Delta S_s \tag{2-9}$$

Combining Eqs. (2-8) and (2-9) the concentration of hydrogen that is dissolved in the metal lattice and in equilibrium with the hydrogen gas can be expressed as [6]:

$$c_L(p, T) = K(T) \cdot p^{1/2} \tag{2-10}$$

Where:

$$K(T) = K_0 \exp\left(-\frac{\Delta H_s}{RT}\right) \tag{2-11}$$

The concentration at the chemical equilibrium of hydrogen in metal lattice c_L (or solubility S) can be written in the final form [6]:

$$S\left(p_{H_2}, T\right)\left[\frac{mol_H}{m^3}\right] = c_L = K_s(T) \cdot \sqrt{p_{H_2}} \tag{2-12}$$

Where:

$$K_s(T)\left[\frac{mol}{m^3\sqrt{Pa}}\right] = K_{0,s} \exp\left(-\frac{E_s}{RT}\right) \tag{2-13}$$

is the Sievert's constant (which is a function of temperature) and $E_s = \Delta H_s$ is called heat of solution. Ideal behavior is a good engineering approximation at elevated temperatures and relatively low pressures [6]. It is important to emphasize that the Sievert's law is a simplified way to describe the equilibrium mechanism between two different system (gas phase and solid phase), and to relate this equilibrium to the gas partial pressure, which is very important to study the hydrogen isotopes permeation in materials and characterizes the driving force of the permeation. For our purposes it is relevant to determine the Sievert's constant for all different materials present in the specific type of power plant and through which tritium can move.

Solubility of hydrogen in liquid sodium

Since we are dealing with SFR systems, it would be of relevance to treat, in a theoretical way, all chemical issues regarding presence of hydrogen (and its isotopes), in liquid sodium, especially regarding solubility of hydrogen in sodium.

Na – Na-H binary system exhibits a monotectic reaction, which is a case of a non complete solubility between Na and Na-H system (as shown in **Figure** Errore. Nel documento non esiste testo dello stile specificato.**-2**). The monotectic invariant temperature and the equilibrium hydrogen pressure at that temperature were determined by Skuratov et al. [7] as 911 ± 0.5 K and 107.3 ± 4 bar, respectively.
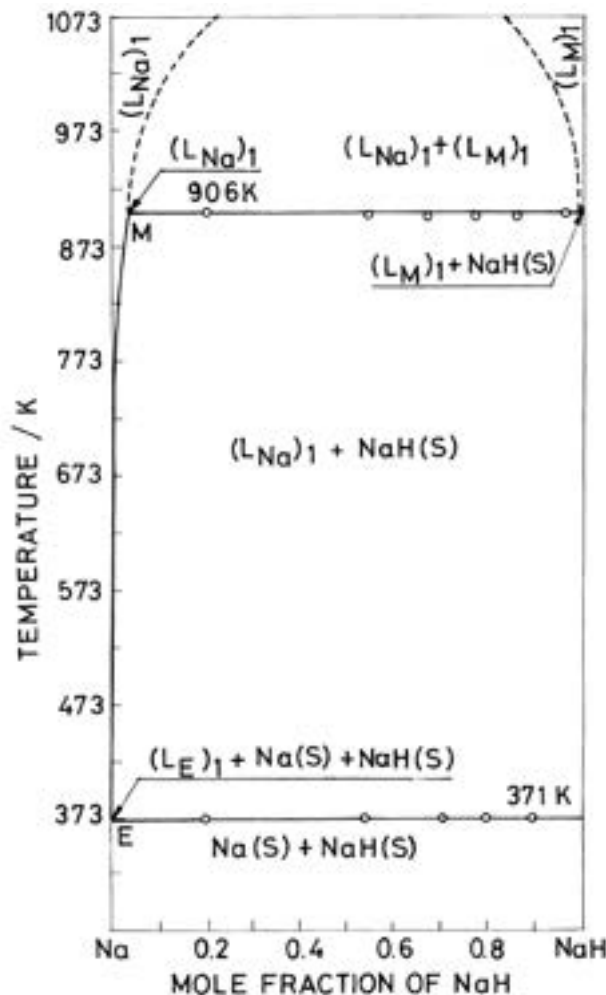
Figure Errore. Nel documento non esiste testo dello stile specificato.**-2 Phase diagram of Na – Na-H system [7]**

Dissolution of hydrogen in sodium can be represented by a Barn-Heber cycle, as shown below [7]:
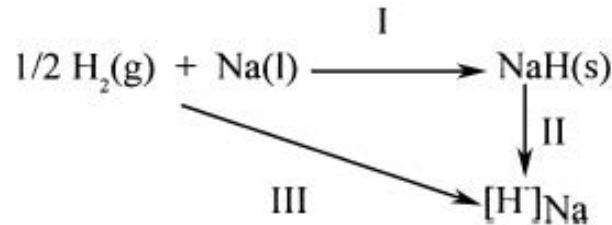
Figure Errore. Nel documento non esiste testo dello stile specificato.**-3 Barn-Haber cycle [7]**

The process I is very important to understand the hydrogen (and tritium) impurities removal mechanisms from sodium in SFR (see cold traps in par. 0), while the process III is the basic chemical equilibrium considered for tritium concentration modeling in sodium inside heat transport facilities (e.g. the core, the Intermediate Heat Exchanger and the Steam generator) assuming that tritium dissolves in ionic form in liquid form, and a chemical equilibrium between dissolved tritium ions and tritium in gaseous phase.

Solubility data of hydrogen in liquid sodium

Below the monotectic temperature (see **Figure** Errore. Nel documento non esiste testo dello stile specificato.**-2**), hydrogen dissolves in sodium up to a concentration beyond which solid sodium hydride saturated with sodium metal precipitates. Thompson, based on a solvation model, postulated that hydrogen in solution would be present as hydride ion [7]. In the single phase region consisting of liquid sodium (with dissolved hydrogen in it), the following equilibrium with gaseous hydrogen exists [7] (process III of Born – Heber cycle reported in **Figure** Errore. Nel documento non esiste testo dello stile specificato.**-3**):

$$\frac{1}{2} H_2(g) + e^- \Leftrightarrow [H^-]_{Na} \tag{2-14}$$

and the equilibrium constant K_{eq} is determined by [7]:

$$K_{eq} = \frac{a_{H^-}}{\sqrt{p_{H_2}}} = \frac{\gamma_{H^-} C_{H^-}}{\sqrt{p_{H_2}}} \tag{2-15}$$

where $a_{H^-} = \gamma_{H^-} \cdot C_{H^-}$ is the activity of hydrogen in sodium and γ_{H^-} is the activity coefficient and p_{H_2} is the hydrogen partial pressure in gas phase. The Sievert's constant of hydrogen in liquid

sodium can be expressed by means of concentration in ion form (C_{H^-}), and activity coefficient (γ_{H^-}) as follows:

$$K_s(T) = \frac{K_{eq}}{\gamma_{H^-}} = \frac{C_{H^-}}{\sqrt{p_{H_2}}}$$ (2-16)

For the dilute solutions of hydrogen in sodium, Henry's zeroth order law can be applied [7]. i.e. $(\gamma_{H^-})^\infty$ is finite. Under these conditions, Sievert's constant, K_S would remain constant. For a given temperature, the concentration range up to which this law is applicable can be ascertained from the experimental data.

Data on solubility of hydrogen in liquid sodium have been reported by several workers. These measurements can be broadly classified under two categories: (i) measurements using manometric techniques with sodium contained in static pots or sealed capsules and (ii) measurements in large sodium loops [7]. In the first category of experiments, techniques based either on absorption of hydrogen by sodium or desorption of hydrogen from Na-NaH samples of known compositions were used. In the second category of experiments the equilibrium hydrogen pressures were determined using hydrogen monitors [7]. Solubility data reported by various authors are shown in **Figure** Errore. Nel documento non esiste testo dello stile specificato.**-4** and the details of techniques used by them are reported in Ref. [7].
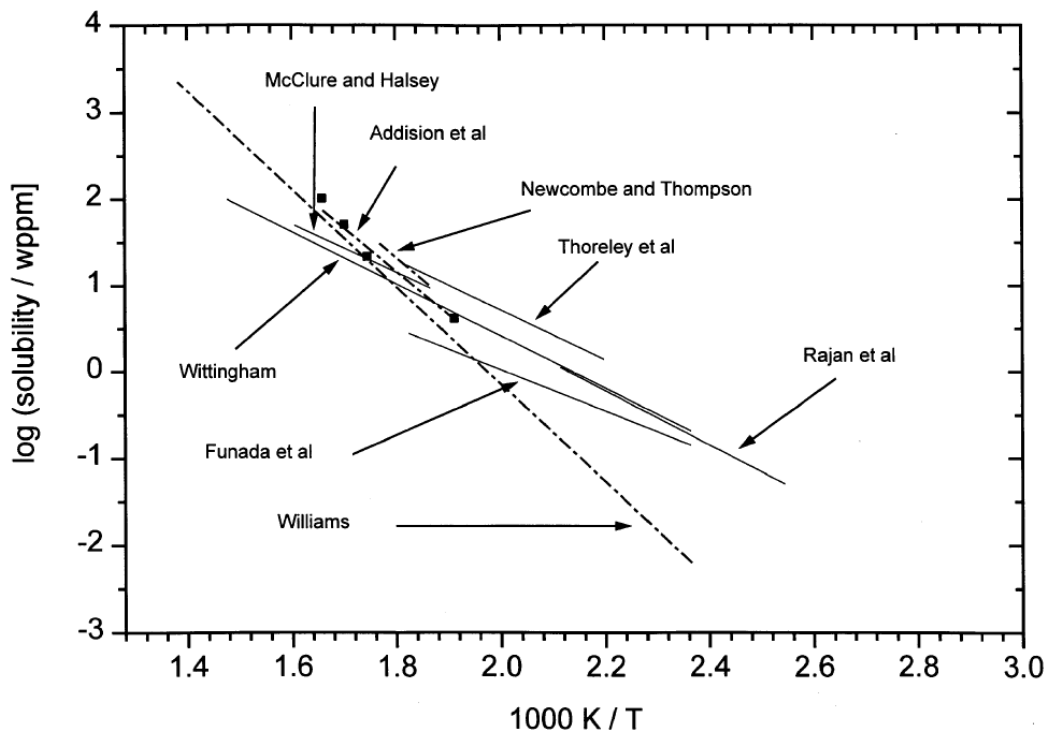
Figure Errore. Nel documento non esiste testo dello stile specificato.**-4 Solubility of hydrogen in sodium [7]**

Since solubility here is defined as a function of temperature, we are interested in the empirical equations obtained by different authors. Not all solubility relations are reported here, but only derived by Vissers et. al (Eq. (2-4)) and that obtained by Wittingham (Eq. (2-5)) defined as follows:

$$\log\{S(T) \ [wppm]\} = 6.067 - \frac{2880}{T} \qquad (2\text{-}17)$$

$$\log\{S(T) \ [wppm]\} = 6.467 - \frac{3023}{T} \qquad (2\text{-}18)$$

The above equations identify the solubility (or the concentration at the chemical equilibrium) of hydrogen in sodium for low hydrogen partial pressure, which implies that the dependency of the solubility on hydrogen partial pressure is quite low and therefore it is defined only as a function of temperature. However, for modeling tritium transport in SFRs the above equations are not relevant, because we are dealing with sodium in which a certain tritium amount is dissolved, and since tritium partial pressure is the driving force of permeation through structural materials, we need a mathematical tool that correlates dissolute tritium concentration and partial pressure, which is the case of the Sievert's constant.

Sievert's constant data of hydrogen in liquid sodium

Hydrogen Sievert's constant in sodium can be evaluated from nine main author's data [7].

- Davies et al;
- Meacham et al;
- Pulham et al;
- Witthingam et al;
- Vissers et al.;
- Ullmann's et al;
- Funada et al.;
- Kozlov et al;
- Trouvé et al.

All Sievert's constant data reported in **Table** Errore. Nel documento non esiste testo dello stile specificato.**-3** are plotted in **Figure** Errore. Nel documento non esiste testo dello stile specificato.**-5.**
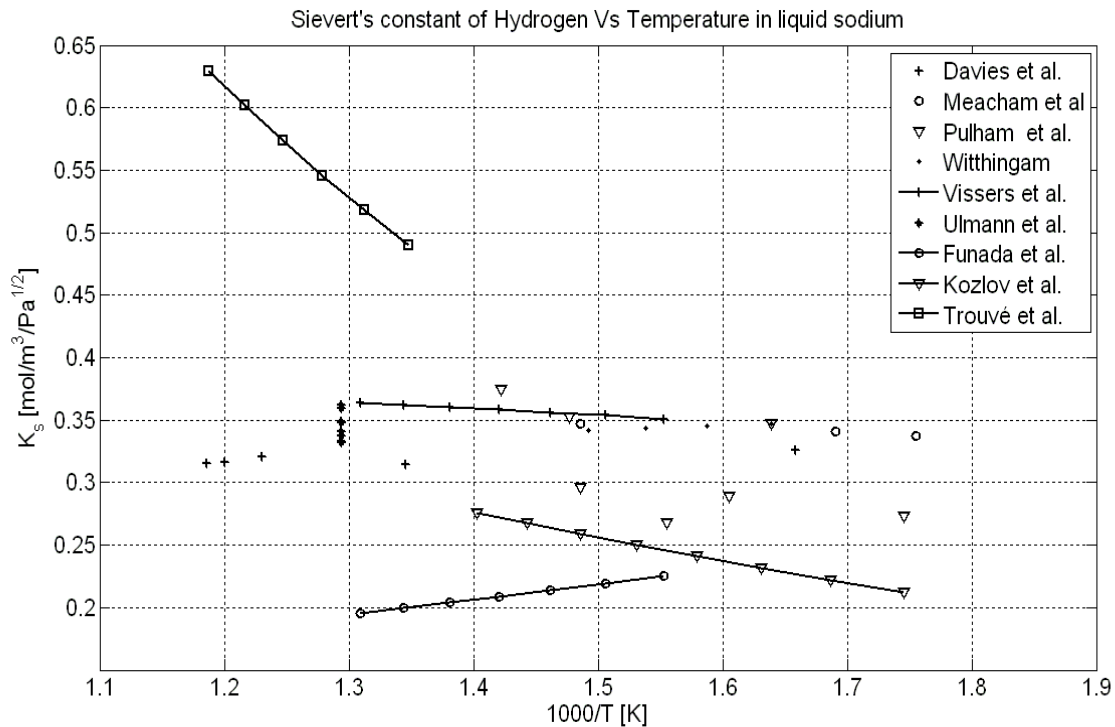
Figure Errore. Nel documento non esiste testo dello stile specificato.**-5 Hydrogen Sievert's constant in liquid sodium Vs 1000/T [K]**

Sievert's constant data for Na-H system reported in the literature ([7],[8]) are listed in Table Errore. Nel documento non esiste testo dello stile specificato.**-3,** with the temperature range of the measurements.

Author	$K_s(T) \left[\dfrac{mol}{m^3 \cdot \sqrt{Pa}}\right]$	Temperature
Davies et all	$\begin{bmatrix} 118 \\ 118 \\ 123 \\ 122 \end{bmatrix} \cdot \sqrt{\dfrac{1}{10^5}} \cdot \dfrac{\rho_{Na}}{PA_H} \cdot 10^{-6}$	$\begin{bmatrix} 603 \\ 743 \\ 813 \\ 843 \end{bmatrix} K$
Meacham et al.	$\begin{bmatrix} 121 \\ 123 \\ 128 \end{bmatrix} \cdot \sqrt{\dfrac{1}{10^5}} \cdot \dfrac{\rho_{Na}}{PA_H} \cdot 10^{-6}$	$\begin{bmatrix} 569.7 \\ 591.6 \\ 673.0 \end{bmatrix} K$
Pulham et al.	$\begin{bmatrix} 98 \\ 105 \\ 98 \\ 109 \\ 139 \end{bmatrix} \cdot \sqrt{\dfrac{1}{10^5}} \cdot \dfrac{\rho_{Na}}{PA_H} \cdot 10^{-6}$	$\begin{bmatrix} 573 \\ 623 \\ 643 \\ 673 \\ 703 \end{bmatrix} K$
Witthingam et al	$(126 \pm 4) \cdot \sqrt{\dfrac{1}{10^5}} \cdot \dfrac{\rho_{Na}}{PA_H} \cdot 10^{-6}$	$[610 - 677] K$

Vissers et al.
$$\sqrt{\frac{1}{10^5} \cdot \frac{\rho_{Na}}{PA_H}} \cdot 10^{-6} 10^{\left(2.298 - \frac{122}{T}\right)} \qquad [644 - 773]\ K$$

Ullmann et al.
$$\begin{bmatrix} 131.7 \\ 125.8 \\ 137.3 \\ 131.9 \\ 136.2 \\ 132.2 \\ 127.9 \\ 126.0 \\ 129.2 \end{bmatrix} \cdot \sqrt{\frac{1}{10^5} \cdot \frac{\rho_{Na}}{PA_H}} \cdot 10^{-6} \qquad [773]\ K$$

Funada et al.
$$\sqrt{\frac{1}{10^5} \cdot \frac{\rho_{Na}}{PA_H}} \cdot 10^{-6} \cdot 10^{\left\{\left(1.609 + \frac{198.1}{T}\right)\right\}} \qquad [643 - 803]\ K$$

Kozlov et al.
$$\frac{\rho_{Na}}{PM_{Na}} \cdot 10^{\left\{\left[-4.4 - 0.645\,\log X_H + \frac{(639\,\log X_H - 572)}{T}\right]\right\}} \qquad [573 - 723]\ K$$

Trouvé et al.
$$\left\{65 \exp\left(-\frac{200}{T}\right)\right\} \cdot \frac{p_S}{RT_S} \qquad [469 - 580]\ °C$$

Table Errore. Nel documento non esiste testo dello stile specificato.**-3 Hydrogen Sievert's constant data for liquid sodium**[1]

where PA_H and ρ_{Na} are the hydrogen atomic weight and the liquid sodium density respectively. The reported data show that variation of Sievert's constant is negligibly small in the temperature range of 603-843 K and in order to visualize more clearly all listed data, in this case they are reported in a linear scale plot instead of a log scale plot. The parameter ρ_{Na}, PA_H, p_S and T_S appearing in Table Errore. Nel documento non esiste testo dello stile specificato.**-3** are the sodium density, the hydrogen atomic weight (these two last terms were necessary in order to convert all Sievert's constant data in the same units) the standard pressure and the standard temperature respectively.

Influence of oxygen content on hydrogen Sievert's constant data.

Sievert's constant experiments clearly indicate an increase in its measured values with the increasing of dissolved oxygen concentration [7]. Presence of oxygen impurity would lead to an interaction with dissolved hydrogen, which can be represented by the following equilibrium [7]:

$$[O^{2-}]_{Na} + [H^-]_{Na} \Leftrightarrow [OH^-]_{Na} + 2e^- \tag{2-19}$$
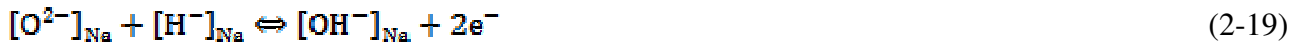
According to this chemical equilibrium reaction, The total hydrogen concentration is given by [7]:

$$(C_{H^-})_{tot} = C_{H^-} + C_{OH^-} = C_{H^-}[1 + K_{int} \cdot (C_{O^{2-}})_{tot}] \tag{2-20}$$

where K_{int} is a thermodynamic equilibrium constant (function of temperature) and $(C_{O^{2-}})_{tot}$ is the total oxygen concentration in sodium. Dissolved hydrogen concentration in sodium under equilibrium with a known hydrogen partial pressure would then increase with oxygen concentration in sodium. Since Sievert's constant, $K_s(T)$ in Eq. (2-16) is applicable only for C_{H^-} and not for $(C_{H^-})_{tot}$, data derived from experiments in oxygen contaminated sodium would result in an apparent increase in Sievert's constant with increase in oxygen concentration [7], as confirmed by the next relation obtained by introducing an apparent Sievert's constant K_s' that takes into account the oxygen content in sodium [7]:

$$K_s'(T, (C_{O^{2-}})_{tot}) = \frac{(C_{H^-})_{tot}}{\sqrt{P_{H_2}}} = \frac{C_{H^-}}{\sqrt{P_{H_2}}} \cdot [1 + K_{int} \cdot (C_{O^{2-}})_{tot}] \tag{2-21}$$

Using Eq. (2-16) we obtain [7]:

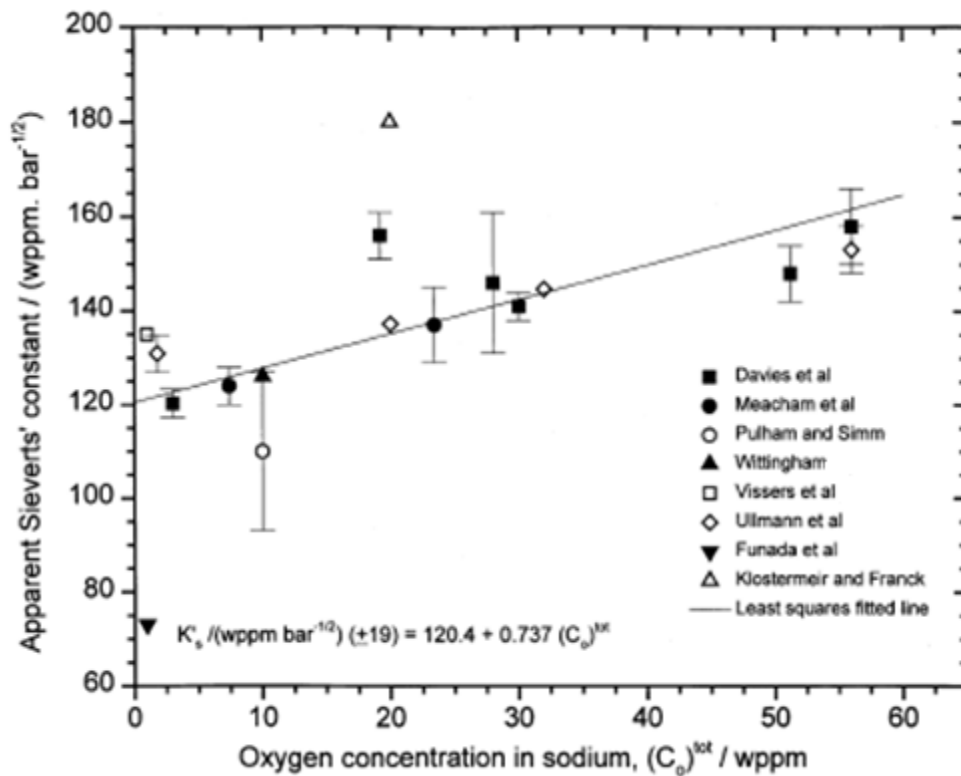$$K_s' = K_s \cdot [1 + K_{int} \cdot (C_{O^{2-}})_{tot}] \tag{2-22}$$

Figure Errore. Nel documento non esiste testo dello stile specificato.**-6 Variation of Sievert's constant with dissolved oxygen [7]**

Taking K_s' to be independent of temperature (as a first approximation), arithmetic mean of the Sievert's constant measured at known values of oxygen concentration in sodium are plotted in Figure Errore. Nel documento non esiste testo dello stile specificato.**-6**. The data in Figure Errore. Nel documento non esiste testo dello stile specificato.**-6**, fitted to a straight line by the method of least squares, can be expressed by the following equation [7]:

$$K_s'\left[\frac{\text{wppm}}{\sqrt{\text{bar}}}\right] = 120 + 0.737 \cdot (C_{O^{2-}})_{tot} \pm 19, \quad [(C_{O^{2-}})_{tot} < 56 \text{ wppm}] \tag{2-1}$$

The dependence of Sievert's constant is reported in Figure Errore. Nel documento non esiste testo dello stile specificato.**-6** :

This variation of Sievert's constant with oxygen concentration in sodium should be taken into account while estimating tritium permeation fluxes through heat exchangers, which is the target of this study. For a tritium permeation model the Sievert's constant is key parameter, and it is necessary to pay attention to it. However, for our purposes the oxygen content is not considered, but can be used in order to take into account of all incident parameters (such as oxygen content).

Equilibrium hydrogen pressure over Na(l) – NaH(s)

As already illustrated at the beginning of this section, the hydrogen dissolved in sodium can origin solid sodium hydride NaH(s) (see process I of Born – Heber cycle reported in **Figure** Errore. Nel documento non esiste testo dello stile specificato.**-3**). The hydrogen pressure over the two phase Na(l) - NaH(s) mixtures, represent the following equilibrium occurs:

$$\frac{1}{2}H_2(g) + Na(l) \Leftrightarrow NaH(s) \tag{2-2}$$

This pressure has been measured as a function of temperature by several workers. Measurements have been carried out by determining hydrogen pressures over either solid NaH (i.e., decomposition pressures) and liquid sodium covering a wide temperature range of 373 to 1032 K [7] (monotectic temperature in Na - NaH system is 906.2 K [7]). The experimental results are characterized by Arrhenius type relations as those reported for hydrogen solubility in Eqs. (2-4) and (2-5); these results are reported in Ref. [7]. For our purposes they are not so relevant, but this brief discussion was meant to make the reader to understand that, if the above chemical equilibrium occurs (when hydrogen is not dissolved in liquid sodium in the atomic form, according to the solvation model represented by chemical equilibrium (2-1)), hydrogen can be removed as a solid impurity from sodium by means of solid sodium hydride (NaH) precipitation reducing the sodium temperature and thus, reducing its solubility in liquid sodium. This mechanism is verified inside the sodium cold traps (see par. 0), that are needed in order to remove significant tritium quantities from primary and secondary sodium, in order to reduce tritium losses and inventories.

Sievert's constant data of hydrogen in various liquid metals

Since Sievert's constant is a crucial parameter also in fusion reactors (where tritium is the fuel and is produced by breeding reactions inside liquid lithium or eutectic alloy lead-lithium), it could be interesting to report in the same Arrhenius plot the hydrogen Sievert's constant in sodium and that of lithium and lead-lithium, which are two liquid metals studied to be used as tritium breeders in fusion reactors (see **Figure** Errore. Nel documento non esiste testo dello stile specificato.**-7**).

In order to have a good data visualization not all curves reported in **Figure** Errore. Nel documento non esiste testo dello stile specificato.**-5** are plotted, but only the maximum and the minimum for each liquid metals (Aiello et al [9] and Chan et al [10] for lead-lithium, Trouvé et al [8] and Funada et al [7] for liquid sodium, Moryama et al [11] and Smith et al [12] for liquid lithium respectively).

This plot is crucial for our Sievert's constant discussion. In fact the first consideration to be performed regards the position in this plot of hydrogen Sievert's constant in sodium. As shown in **Figure** Errore. Nel documento non esiste testo dello stile specificato.**-7** the sodium is located between the liquid lithium, which occupies the top of the plot, and the lead-lithium which is located in the bottom. From these considerations we can affirm that hydrogen permeation in sodium is not worrying like in lead lithium, but it is more worrying that those concerning the lithium. Similarly, the same considerations can be made discussing about the tritium inventory problem, which is less problematic then that in liquid lithium, but more than that in lead lithium. These considerations allow us to conclude that Sievert's constant is the key parameter which correlates the driving force of tritium losses into the environment (the partial pressure), and the tritium inventory (or the concentration), which are the fundamental parameters in a tritium transport assessment of a plant, whose objective is to estimate the radioactivity leaving the plant (for people and environmental matrix safety), and the radioactivity staying in the plant during normal power production operations.
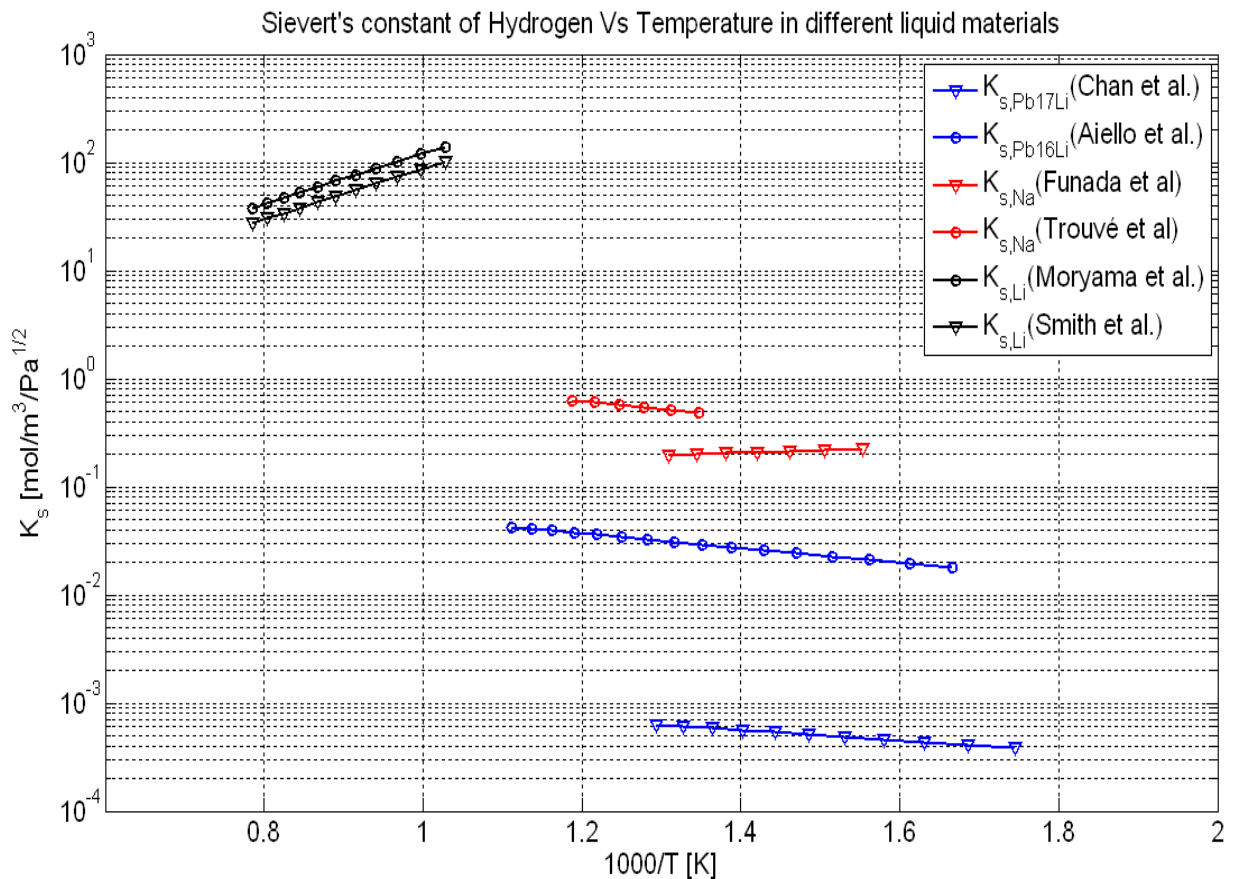
Figure Errore. Nel documento non esiste testo dello stile specificato.**-7 Hydrogen Sievert's constant in different liquid metals Vs 1000/T [K]**

Modeling of permeation

In order to find out the main mechanisms of hydrogen permeation and the techniques adopted for solubility and diffusivity measurements a permeation model is needed. In fact the Sievert's constant determination can be developed from indirect calculation of an hydrogen permeated flux in a certain volume [9]. In the simplest model of hydrogen permeation through a membrane, three processes have to be considered:

- The chemisorption, where hydrogen molecules in the gas phase dissociate on the solid material surface providing adsorbed atoms which may diffuse into the solid;
- The desorption by which adsorbed atoms recombine and are released as molecules;
- The diffusion, by which hydrogen atoms move through the membrane.

The first two of these processes are known as "surface processes" and under certain conditions (i.e. low partial pressures [6]) they may completely control the permeation rate. Under other conditions, instead, diffusion may be the limiting factor. In the first case the process is called "surface – limited permeation", while the second "diffusion – limited permeation". When surface conditions modify the kinetics of hydrogen transport, the square root dependence of pressure is often lost [6]. Very low pressure (<10 Pa) also precludes the square root dependence on pressure and diffusion-controlled transport [6]. Moreover, the apparent changes in hydrogen transport appear to be the result of changing the rate-controlling step from lattice diffusion to a surface process (such as adsorption and dissociation), and surface layers do not change the intrinsic hydrogen permeability of the material. There are two limiting cases of permeation:

- Diffusion – limited model;
- Surface – limited model.

In this paragraph only the diffusion – limited model is going to be examined by the mathematical point of view.

Diffusion – limited model

Hereafter is considered the hydrogen permeation through a membrane in which the characteristic time of the surface effects (i.e. the time relevant for gas adsorption in the high pressure side and recombination in the low pressure side) is negligible with respect to the time of diffusion through the solid.

The membrane of thickness d, with surfaces at $x = 0$ and $x = d$, diffusion coefficient $D\ [m^2/s]$ independent on hydrogen concentration, initially does not contain dissolved hydrogen. Then at time $t = 0$ one side of the membrane is pressurized with hydrogen at concentration C_0. Assuming suitable initial boundary conditions the problem is mathematical described by 1-D time dependent diffusion equation with no volumetric source inside the domain. The overall mathematical relation is given by [13]:

$$
\begin{cases}
\dfrac{\partial C(x,t)}{\partial t} = D\dfrac{\partial^2 C(x,t)}{\partial x^2}; \\
C(0 < x < d, t = 0) = 0; \\
C(x = 0, t > 0) = C_0; \\
C(x = d, t > 0) = 0.
\end{cases}
\tag{2-3}
$$

The analytical solution with the reported initial boundary condition has derived from Eigen value problem and the solution is found using Fourier's series and adopting the separation of variables technique. Thus, the concentration $C(x,t)$ is a function of two variables x and t and is defined as [13]:

$$C(x,t) = C_0\left(1 - \frac{x}{d}\right) - \frac{2C_0}{\pi}\sum_{n=1}^{+\infty}\frac{1}{n}\sin\left(\frac{n\pi}{d}x\right)\exp\left(-\frac{n^2\pi^2 D}{d^2}t\right) \tag{2-4}$$

The second boundary condition in Eq. (2-3) means that the exit surface is always in contact with a negligible hydrogen pressure with respect the high pressure side. Using Fick's law, the gas flux from the exit surface as a function of time can be calculated as [13]:

$$J(d,t)\left[\frac{mol}{m^2 \cdot sec}\right] = -D\frac{\partial C(x,t)}{\partial x}\bigg|_{x=d} = \frac{D \cdot C_0}{d}\left[1 + 2\sum_{n=1}^{+\infty}(-1)^n\exp\left(-D\frac{n^2\pi^2}{d^2}t\right)\right] \tag{2-5}$$

Considering also the formulation of a certain hydrogen concentration at the equilibrium formulated by the Sievert's law (Eq. (2-12)), it is possible to express the value of parameter C_0 by means of hydrogen partial pressure p_{H_2} in the high pressure side and the hydrogen Sievert's constant inside the membrane material; thus the total flux coming out from the exit surface is characterized by the following expression [13]:

$$J(d,t)\left[\frac{mol}{m^2 \cdot sec}\right] = -D\frac{\partial C(x,t)}{\partial x}\bigg|_{x=d} = \frac{DC_0}{d}\left[1 + 2\sum_{n=1}^{+\infty}(-1)^n\exp\left(-D\frac{n^2\pi^2}{d^2}t\right)\right] \tag{2-6}$$

At steady state (i.e. $t \rightarrow \infty$) Eq. (2-6) becomes:

$$J\left[\frac{mol}{m^2 \cdot sec}\right] = \frac{P(T)}{d} \cdot \sqrt{p_{H_2}} \tag{2-7}$$

which is known as the Richardson's law, where:

$$P(T)\left[\frac{mol}{m \cdot sec \cdot \sqrt{Pa}}\right] = K_s(T) \cdot D(T) \tag{2-8}$$

is defined as the permeability of the material. Since K_s and D vary with temperature in an Arrhenius manner, also $P(T)$ can be written as:

$$P(T)\left[\frac{mol}{m \cdot sec \cdot \sqrt{Pa}}\right] = P_0 \cdot \exp\left(-\frac{E_p}{RT}\right) \tag{2-9}$$

where $E_p[J/mol] = E_s + E_d$ is the activation energy for permeation which is the sum of that of diffusion and solubility. This last expression is very indicative for a good intuition of hydrogen transport mechanisms, because it indicates that in order to have permeation through a certain solid

material, the hydrogen atom has to dissolve in the host material and diffuse through it; thus, by the numerical point of view the this is confirmed by the product of solubility and diffusivity (Eq. (2-8)).

In conclusion, when a wall with a thickness $t\,[m]$ and a permeability $P(T)$ is subjected to an high tritium partial pressure $p_h\,[Pa]$ and to a lower one $p_l\,[Pa]$ on the opposite side, the 1-D steady state permeated flux through the wall assumes the general form expressed in the following equation:

$$J_{ss}\left[\frac{mol}{m^2 \cdot sec}\right] = \frac{P(T)}{t} \cdot \left(\sqrt{p_h} - \sqrt{p_l}\right) \tag{2-10}$$

Theoretical aspects of hydrogen isotopes in water

The steam/water system in nuclear reactors in general may contain H_2. Hydrogen inside water could be present both in ionic form H^+ (natural dissolution dependent on the water pH), or in molecular form H_2, which may be or dissolved naturally or added for corrosion and safety problems [15]. The tritium atoms coming from secondary sodium inside the SG, enters in water and interacts chemically with hydrogen dissolved in H_2O. In this regard, since pure water is said to be neutral with a pH close to 7.0 (at which corresponds an ionic hydrogen concentration of $10^{-4}\,[mol_{H^+}/m^3_{H_2O}]$), the amount of ionic and molecular hydrogen dissolved in water is supposed to be much larger than that of tritium coming from a generic high pressure region (i.e., secondary sodium in SFRs); thus, all tritium atoms coming from this region in atomic form T recombines in molecular form T_2 and bounds chemically with dissolved molecular hydrogen H_2. Therefore, all atomic tritium atoms entering into the water via permeation, become atoms of HT, according to the following chemical equilibrium reaction:

$$T_2 + H_2 \Leftrightarrow 2HT \tag{2-11}$$
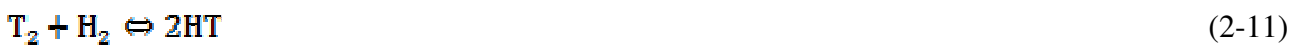
Since the equilibrium constant is quite large [14] (is a product-shifted chemical equilibrium), the HT isotopic exchange rate of this equilibrium will be not considered, and therefore only the permeable species HT (between the two gaseous and permeable species HT and T_2) will be considered in water inside SFR's steam generators.

Tritium in liquid water

The mass transfer of tritium through the steam generator tubes is assumed to be driven by the T_2 partial pressure in secondary sodium and the HT partial pressure in the water side. The HT

partial pressure inside water is controlled by two thermodynamic equilibria: a chemical equilibrium, in the liquid phase, among the species HT_L, HTO, H_2O and H_2 and a gas-liquid equilibrium between HT in liquid (HT_L) and HT in gas (HT_G).

In the cooling water, the following equilibrium due to the H_2 addition (dissolved in water or produced by corrosion of structural materials) is considered [15]:

$$HT + H_2O \Leftrightarrow H_2 + HTO \tag{2-12}$$

and the corresponding equilibrium constant is [15]:

$$K_{eq} = \frac{[H_2] \cdot [HTO]}{[HT_L] \cdot [H_2O]} \tag{2-13}$$

and the HT concentration in water can be calculated by [15]:

$$[HT_L] = \frac{1}{K_{eq}} \cdot \frac{[HTO]}{[H_2O]} \cdot [H_2] \tag{2-14}$$

where $[HTO]/[H_2O]$ is the molar tritiated water molar concentration and $[H_2]$ is the solved molar concentration.

A system consisting of two components (HT and water) and two phases (gas and liquid) has been considered. The equilibrium between the HT in the gaseous phase (HT_G) and the HT dissolved in the liquid (HT_L) is expressed by equating the fugacities [15]:

$$f_{liq} = f_{gas} \tag{2-15}$$

and:

$$\phi \cdot p(HT_G) = \gamma \cdot K_H(T) \cdot [HT_L] \tag{2-16}$$

where: f_{gas} is the HT fugacity in the gaseous phase, f_{liq} is the fugacity in the liquid phase, ϕ is the fugacity coefficient, $p(HT_G)$ is the partial pressure [Pa], $K_H(T)$ is the Henry constant $[Pa]$, γ is the activity coefficient≈ 1, and $[HT_L]$ is the HT molar concentration in the liquid phase. in the limit of ideal gas the fugacity is coincident to the pressure, hence we can state that the fugacity coefficient is almost equal to one $\phi \approx 1$. The partial pressure of tritium HT inside liquid water becomes:

$$p(HT_G) = K_H(T) \cdot [HT_L] \tag{2-17}$$

There are several ways of describing the solubility of a gas in water. Usually the Henry's law constant K_H is defined as [16]:

$$K_H \overset{\text{def}}{=} \frac{c_a}{p_g} \tag{2-18}$$

Here, c_a is the concentration of the a species in the aqueous phase and p_g is the partial pressure of that species in the gas phase. If K_H refers to standard conditions ($T^{\ominus} = 298.15\ K$) it will be denoted as $K_{H,w}^{\ominus}$. A simple way to describe Henry's law [16] as a function of temperature is:

$$K_H^w(T) = K_{H,w}^{\ominus} \cdot \exp\left(-\frac{\Delta H_{soln}}{R}\left(\frac{1}{T} - \frac{1}{T^{\ominus}}\right)\right) \tag{2-19}$$

where $\Delta H_{soln} < 0$ is the enthalpy of solution (the Henry's constant written in the form of Eq. (2-18) was observed to decrease with temperature increasing [17] and, as a consequence, the hydrogen solubility in water decreases with temperature increasing).

Tritium in vapor water

When water inside SG tubes evaporates, the constitutive relation between HT pressure and HT concentration is different. In fact, in case of superheated steam (vapor mass fraction y_{vap} =1), the water is considered to be treated as a single phase gas, and the concentration is proportional to the partial pressure inside steam, according to Dalton's law, which is related to ideal gas law. In a mixture of different gas i with a given pressure p_i, the total pressure of mixture is given by the summation of single gas species i pressure p_i as follows:

$$p_{tot} = \sum_i p_i = p_1 + p_2 + \cdots p_n \tag{2-20}$$

and the partial pressure of single species p_i is given by:

$$p_i = p_{tot} \cdot y_i \tag{2-21}$$

where y_i is the molar fraction of species i component in the total mixture of n component. If we consider a system composed by a mixture of superheated water $H_2O|_{vap}$, tritiated hydrogen HT_w, and tritiated water HTO_w, the HT partial pressure inside steam $p(HT_w)$ is given by:

$$p(HT_w) = p_w \cdot y_{HT} \tag{2-22}$$

where $y_{HT}[mol_{HT}/mol_w]$ is the molar fraction of HT inside steam, and $p_w[MPa]$ is the steam pressure inside the SG. Since we are interested in HT concentration expressed in recommended unit $[mol_{HT}/m_w^3]$, we defined the molar volume of steam $V_{mol}^w(T_w, p_w)[m_{vap}^3/mol_{vap}]$ given by:

$$V_{mol}^w(T_w, p_w)\left[\frac{m_w^3}{mol_w}\right] = \frac{PM_w\left[\frac{kg_{vap}}{mol_{vap}}\right]}{\rho_w(p_w, T_w)\left[\frac{kg_{vap}}{m_{vap}^3}\right]} \tag{2-23}$$

which correlates molar fraction $y_{HT}\left[mol_{HT}/mol_{vap}\right]$ to the volumetric concentration $C_{HT}^w\left[mol_{HT}/m_w^3\right]$ as:

$$y_{HT}\left[\frac{mol_{HT}}{mol_w}\right] = C_{HT}^w\left[\frac{mol_{HT}}{m_w^3}\right] \cdot V_{mol}^w(T_w, p_w)\left[\frac{m_w^3}{mol_w}\right] \tag{2-24}$$

Tritium isotope exchange rate

Chemical equilibrium of the isotope exchange reaction (2-12) is characterized by the equilibrium constant $K_{eq}(T)$ defined as follows:

$$K_{eq}(T) = \frac{\dot{F}_{eq,H_2} \cdot \dot{F}_{eq,HTO}}{\dot{F}_{eq,HT} \cdot \dot{F}_{eq,H_2O}} = \frac{(\dot{F}_{in,H_2} + \dot{\Delta}_{HT}) \cdot (\dot{F}_{in,HTO} + \dot{\Delta}_{HT})}{(\dot{F}_{in,HT} - \dot{\Delta}_{HT}) \cdot (\dot{F}_{in,H_2O} - \dot{\Delta}_{HT})} \tag{2-25}$$

where:

- $K_{eq}(T)$ is the chemical equilibrium constant of reaction;
- $\dot{F}_{eq,i}\left[mol_i/sec\right] = \dot{Q}_w(z_{SG}) \cdot C_{eq,i}(z_{SG}, t)$ is the molar flow rate of species i at the chemical equilibrium concentration $C_{eq,i}(z_{SG}, t)$;
- $\dot{F}_{in,i}(z_{SG}, t)\left[mol_i/sec\right]$ is the molar inlet flow rate of species i;
- $\dot{\Delta}_{HT}\left[mol/sec\right]$ is the amount of HT conversion rate by reaction (2-12).

As reported in Chapter 3, the term $\dot{\Delta}_{HT}$ is quite important because it enters in the HT and HTO balance equation (for HT species is a sink term whereas for HTO species is a source term), and it has to expressed as a function of HT and HTO concentrations, starting from values of K_{eq} and inlet water and hydrogen molar flow rate.

Since we pointed out that hydrogen content in water is given by corrosion considerations, the dissolved hydrogen concentration in water at the SG inlet is supposed to be fixed as an input data.

Relationships between tritium partial pressures and concentration

The objective of this section is to summarize all constitutive equations correlating the tritium partial pressure and the concentration depending on the matter tritium is present. This operation is

needed in order to insert all permeation fluxes and in isotope exchange rate into tritium mass balance equations (see next chapter). As described in previous section chemical equilibrium tritium concentration is characterized by different expressions depending on the case in which tritium is dissolved in sodium (Sievert's law), in liquid water (Henry's law) and in superheated steam (Dalton's law).

As already mentioned the tritium partial pressure is the driving force of permeation, thus the permeation fluxes entering the mass balance equation must be expressed as a function of concentrations (which are the mathematical unknowns of the problem), but must take into account that tritium moves from and high partial pressure region to a lower one.

The constitutive relationships between tritium chemical equilibrium concentration C_{eq} and tritium partial pressure p_{gas} are summarized and reported in **Table** Errore. Nel documento non esiste testo dello stile specificato.**-4**, where $K_S^{Na}(T)$, $K_H^W(T)$, p_w and $V_{mol}^W(p_w, T)$ are the Sievert's constant of hydrogen in sodium, the Henry's constant of hydrogen in water, the steam pressure and the molar volume of steam respectively.

Equilibrium Concentration	Dissolution Fluid
$C_{eq}(p_{gas}, T)\big|_{Na} = K_S^{Na}(T) \cdot \sqrt{p_{gas}}$	**Liquid sodium**
$C_{eq}(p_{gas}, T)\big|_{H_2O,liq} = K_H^W(T) \cdot p_{gas}$	**Liquid Water**
$C_{eq}(p_{gas}, T)\big|_{H_2O,vap} = \dfrac{1}{V_{mol}^W(p_w, T) \cdot p_w} \cdot p_{gas}$	**Steam**

Table Errore. Nel documento non esiste testo dello stile specificato.**-4 Constitutive relations of tritium concentration for different dissolution fluids**

After this theoretical discussion, all ingredients necessary to develop a complete tritium permeation mathematical model were described and discussed.

Chapter 0

Development of a computational code for tritium transport analysis in SFRs

Introduction

The expectation that tritium contamination of plant installation in SFRs will be a significant design issue was confirmed [18]. Thus, a tritium transport model in the SFR design phase is required in order to estimate the total amount of tritium released into the environment and circulating inside the plant. In fact the model is applied to the overall SFR plant, considering all tritium transport processes inside nuclear plant installations and studying systematically tritium transport in each components. The objective in this work in fact is exactly to simulate tritium transport behavior in SFR components (according to SFR reference configuration reported in **Figure** Errore. Nel documento non esiste testo dello stile specificato.**-8**) and to predict tritium quantities in different SFR devices by means of solving mass conservation laws with computational tools (such as MATLAB packages).

In literature, different tritium permeation codes for SFRs are available, such as those developed by Kumar in 1974 [19] and by Kozlov et al. in 2005 [20], while more recently another computational code (the TPAC code) was created for Very High Temperature Gas Reactors [4]. In this chapter will be illustrated the computational code SFR-TPC (developed in the academic contest [21]) which is built to evaluate tritium losses and inventories from and inside an SFR system. This

code is essentially inspirited, by the computational and mathematical structure point of view, to the above mentioned codes.

Tritium transport mechanisms in SFRs

One potential problem of using SFR is tritium permeation from the primary coolant through heat exchangers into the environment. In SFRs tritium mostly comes from ternary fission of the fuel and neutron capture reactions inside boron-containing materials [22], such as control rods and neutron flux shielding blocks.

Tritium that enters in the primary coolant will be circulated or permeated to the secondary coolant through the intermediate heat transfer loop. The permeated tritium, successively, enters the product steam/water into steam generator through heat exchanger surfaces. The tritium transport paths in SFRs are shown in **Figure** Errore. Nel documento non esiste testo dello stile specificato.**-8**. The mechanisms of tritium transport are mainly diffusion, permeation and bulk transport.
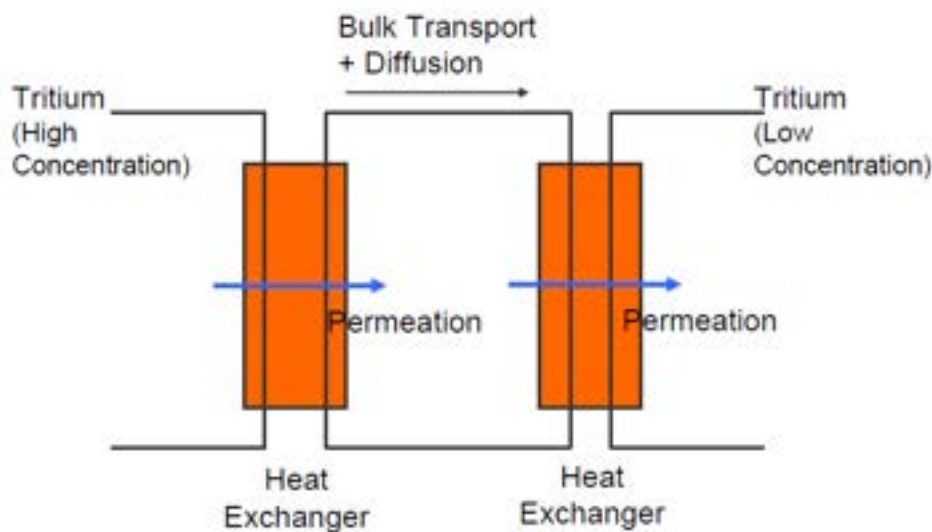
Figure Errore. Nel documento non esiste testo dello stile specificato.**-8 Tritium transport pathways scheme in a notional two loops heat transport system**

As an isotope of hydrogen, tritium is able to diffuse through the cladding and structural materials and especially through the walls of heat exchangers so that in SFRs, where the temperatures are higher than in water reactors, tritium is highly mobile [22]. This means that, in terms of plant operation and design, it is important to be able to predict the distribution of tritium in SFRs so that amounts of tritium released can be estimated with some certainty at the design stage and counter-measures can be taken if the levels are too high.

In a reactor system tritium escapes from the primary sodium:

- into the argon cover gas where the equilibrium is assumed to be instantaneous;

- by diffusion through the walls of the heat exchangers into the secondary sodium circuits;

- into the interspace gas between the vessels, by diffusion through the steel of the vessel and pipework;

- by crystallization of sodium tritide, or by isotopic exchange in the cold traps (SFR devices necessary to control hydrogen and tritium level as well in primary and secondary coolants, as reported in next chapter);

- by radioactive decay.

In order to calculate at any point in time the tritium concentration in various parts of the circuit a mass-balance of Σ sources - Σ losses = accumulation, has to be established for all the important media of the plant. A typical scheme for an SFR reactor (e.g., Super-Phénix) is illustrated in **Figure** Errore. Nel documento non esiste testo dello stile specificato.**-9** and the types of species involved are shown in **Table** Errore. Nel documento non esiste testo dello stile specificato.**-5**:
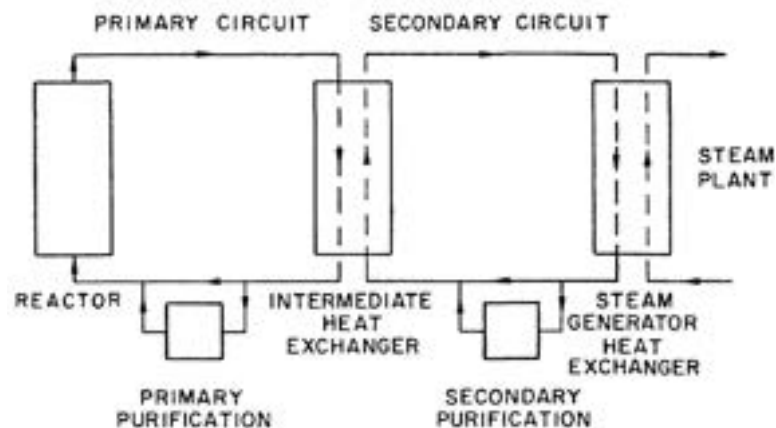
Figure Errore. Nel documento non esiste testo dello stile specificato.**-9 Schematic representation of a pool reactor** [22]

Medium	Type	Hydrogen species	Tritium
Cover gas	dissolved molecules	H_2	HT
Water	dissolved molecules	H_2O	HTO
Sodium	dissolved ions	H^-	T^-
Steels	dissolved atoms	H	T

Cold traps   crystallized molecules   NaH   NaT

Table Errore. Nel documento non esiste testo dello stile specificato.**-5 Type of hydrogen species involved in SFR media [22]**

Summary of the SFR-TPC code

The SFR-TPC code solves the tritium 1D time dependent mass balance equation for i species (with i = T⁻, HT and HTO) into fluid j (with j = primary sodium, secondary sodium and water) inside the k component (with k = core, IHX and SG) and computes the tritium concentrations, characterized by the following concentration functions:

- T⁻ concentration inside core sodium (lumped parameter) $C_{core}(t)$;

- T⁻ concentration inside primary sodium along IHX heat transfer coordinate z_{IHX} $C_{prim}(z_{IHX}, t)$;

- T⁻ concentration inside secondary sodium along IHX heat transfer coordinate z_{IHX} $C_{sec}^{IHX}(z_{IHX}, t)$;

- T⁻ concentration inside secondary sodium along SG heat transfer coordinate z_{SG} $C_{sec}^{SG}(z_{SG}, t)$;

- HT and HTO concentrations inside water along SG heat transfer coordinate z_{SG} $C_i^w(z_{SG}, t)$. In water/steam system different isotopic were considered and the 1D time dependent concentration for both species were calculated.

Once the concentrations listed above are calculated, the code proceeds with a post elaboration, evaluating tritium losses and inventories, which are the objective of the code. In particular, the tritium losses are given by the following terms:

- total tritium losses through SG shell surfaces $\phi_{shell}^{SG}(t)$;

- total tritium losses through pool surface $\phi_{pool}(t)$;

- total tritium permeation rate into steam/water bulk through SG pipes walls $\phi_{bulk}^{SG}(t)$;

- total tritium losses (sum of all losses tritium terms listed above) $\Phi_{tot}(t)$.

In the tritium losses computation, it was assumed that all tritium amount entering into the steam cycle (ϕ_{bulk}^{SG}) permeating through the SG pipes is considered totally lost into the environment.

Tritium inventories are characterized by the following contributions:

- total tritium inventory inside IHX's steels (tube and shell steels) $I_{steel}^{IHX}(t)$;

- total tritium inventory inside SG's steels (tube and shell steels) $I_{steel}^{SG}(t)$;

- total tritium inventory inside the primary sodium $I_{prim}(t)$;

- total tritium inventory in secondary sodium of a single heat transfer loop (sum of secondary sodium in IHXs of a single loop and secondary sodium in SGs of a single loop) $I_{sec}^{loop}(t)$;

- total tritium inventory in water/steam of a single heat transfer loop (sum of steam/water present in all SGs of a single heat transfer secondary loop) $I_{steam}^{loop}(t)$.

- total tritium inventory (sum of all losses tritium terms listed above) $I_{tot}(t)$.

$$\Phi_{bulk}^{SG}$$
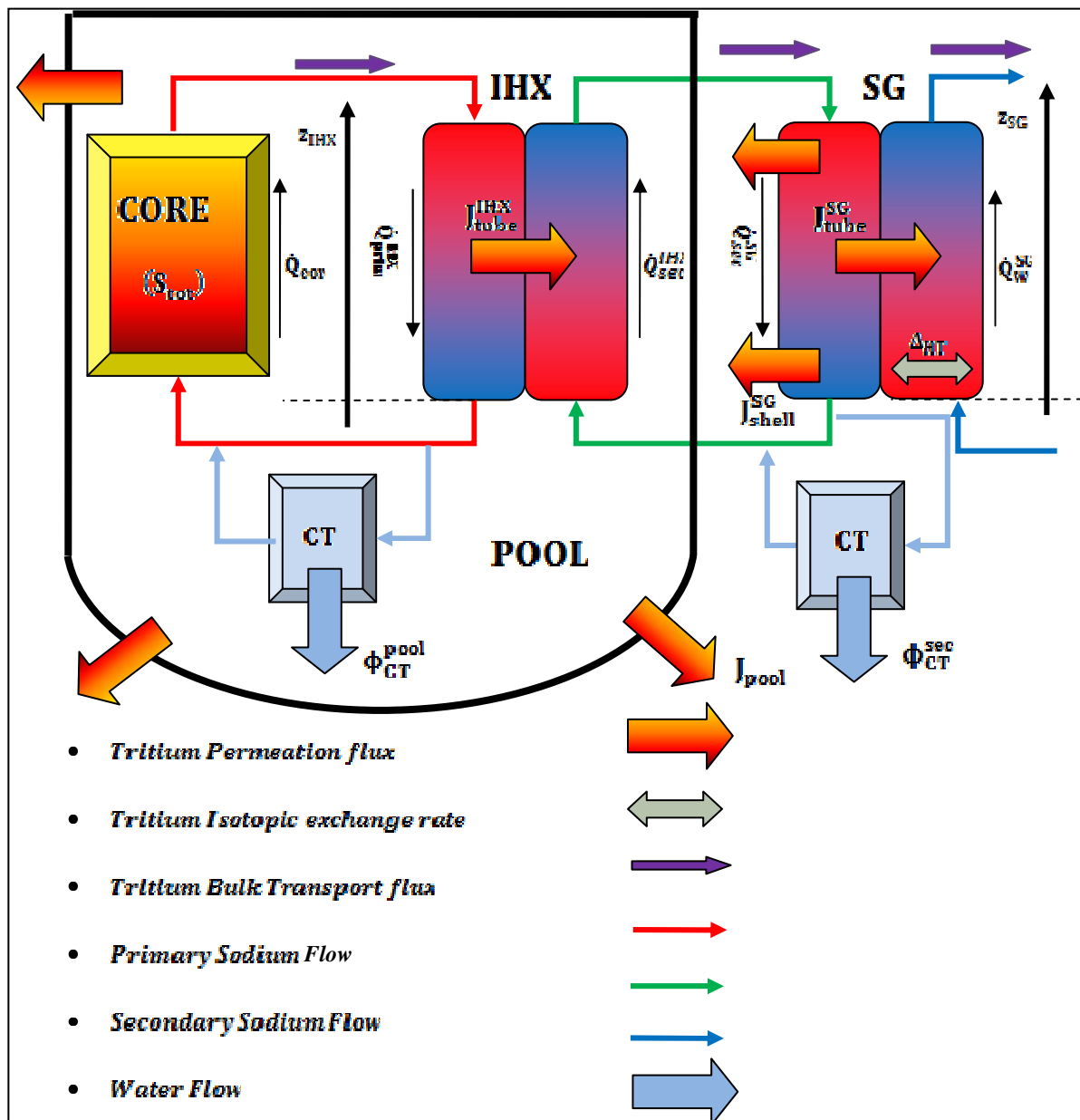
Figure Errore. Nel documento non esiste testo dello stile specificato.**-10 Sample scheme for Tritium analysis inside a SFR plant**

The following phenomena are taken into consideration in this code:

- Mass balance of the species (T in sodium and steels, HT and HTO in steam/water);

- Nuclear production inside the core via ternary fissions and neutron capture reactions;

- Tritium transport via bulk transfer with process coolants;

- Tritium permeation through the heat transfer surface;

- Isotope exchange between tritium containing and hydrogen containing chemicals:

- Nuclear decay.

SFR-TPC code performs the tritium transport analysis for two different notional steam generator configurations:

1) once through straight tube IHXs supplying once through straight tube steam generators (SG) in the secondary circuit;

2) once through straight tube IHXs supplying once through helicoidal tubes SGs in the secondary circuit.

After this qualitative discussion, and observing the reference configuration of an SFR plant reported in **Figure** Errore. Nel documento non esiste testo dello stile specificato.**-10**, a quantitative approach has to be performed, in order to treat, theoretical speaking, all physical processes related to tritium transport mechanisms, summarized as:

- tritium source inside primary coolant S_{tot};
- tritium permeation $J_{tube}^{IHX}(z_{IHX}, t)$, $J_{tube}^{SG}(z_{SG}, t)$, $J_{shell}^{SG}(z_{SG}, t)$, $J_{pool}(t)$;
- tritium isotopes exchange $\dot{\Delta}_{HT}(z_{SG}, t)$.

Tritium sources in SFRs

As already mentioned, the three main sources of tritium in SFR systems are:

- the fuel via ternary fission (both thermal and fast fissions);
- the boron carbide (B_4C) control and shielding rods;
- the impurities in the sodium, e.g. lithium.

Tritium birth from ternary fission.

Tritium is formed by ternary fission in an SFR core with the reported yields typically ranging from about 0.8 to $2.3 \cdot 10^{-4}$ atoms/fission, depending on the fissile nuclide and the neutron flux spectrum [23]. The available tritium yield data are summarized in **Table** Errore. Nel documento non esiste testo dello stile specificato.**-6** [23].

Source	Tritium Atoms/Fission (X 10⁻⁴)				
	U-233	U-235	U-238	Pu-239	Pu-241
Thermal Neutrons					
[Fluss 1972]	1.1	0.85 ± 0.09			
[Horrocks 1973]	0.88 ± 0.07	0.75 ± 0.08		1.51 ± 0.10	
[Albenesius 1960]		0.95 ± 0.08			
[Sloth 1962]		0.8 ± 0.01			
[Ray 1966]		0.87			
[Marshall 1966]				2.3	0.26
[Albenesius 1959]		0.5 – 1.0			
[Vorobiev 1969]		1.26			
[Dakowski, 1967]		1.24			
Fast Neutrons					
[Fluss 1972, Halpen 1971]		2.0 – 2.2			
[Buzzelli 1976]		1.4 – 1.7	10 – 20.6		

Table Errore. Nel documento non esiste testo dello stile specificato.**-6 Tritium Yield from ternary fission [23]**

The H^3 yields from thermal fissioning of U^{235} and Pu^{239} are reasonably well known. However, the H^3 yields from fast fissioning are not well known; reported H^3 yields from the fast fissioning of U^{238} are one order of magnitude greater than from the thermal fissioning of U^{235} and Pu^{239} and from the fast fissioning of U^{235} (see **Table** Errore. Nel documento non esiste testo dello stile specificato.**-6**). Since most of fissioning in an SFR core is from fast fissioning [24], this uncertainty in the fast fission H^3 yields introduces a nontrivial uncertainty in the total core production of tritium from ternary fission. However, as a first approximation, we can assume that the tritium production rate from ternary fission inside the fuel is directly proportional to neutron the fluxes, the fission cross section and the tritium yields of different uranium and plutonium isotopes.

Since the calculation of the source term is subjected to a large number of uncertainties and lacks of precise and suitable neutronic data, some literature data on tritium source from fuel ternary fission are available to estimate the tritium generation rate. In fact, the specific tritium production rate from SFR fuel is expected to be of the order $2 \text{ to } 4 \cdot 10^4 \, [\text{Ci/yr/1000 MW}_e]$ [22], which means that a 1000 MW$_e$ (assumed to be operated at 2500 MW$_{th}$) generates 4.13 g/y of tritium by means of ternary fissions. Thus, assuming this specific generation rate from ternary fission $S^{sp}_{tern} = 4 \cdot 10^4 [\text{Ci/y/1000 MW}_e] = 4 \cdot 10^4 \, [\text{Ci/y/2500MW}_{th}]$, the total tritium generation rate inside the fuel at a given thermal power $P_{th} [\text{MW}_{th}]$ is given by:

$$S_{tern}\left[\frac{Ci}{y}\right] = S_{tern}^{sp} \cdot \frac{P_{th}[MW_{th}]}{2500} \tag{3-1}$$

Hence, in SFR-TPC code the source term is calculated only using the thermal power, provided as an input data.

Tritium birth from boron activation.

The adopted approach to estimate the tritium source inside control and neutron flux shielding control rods, is similar to that adopted for fuel tritium source estimation.

The neutron capture reactions involved in the tritium production from boron are the following reactions

$$B^{10} + n \rightarrow 2\alpha + H^3 \tag{3-2}$$

$$B^{10} + n \rightarrow \alpha + Li^7 \tag{3-3}$$

$$Li^7 + n \rightarrow \alpha + n + H^3 \tag{3-4}$$

As it is possible to see, tritium may be produced directly from boron capture (3-2), or indirectly by producing firstly Li^7 atoms (3-3), and then, by means of neutron capture of Li^7 (3-4), tritium atoms are produced.

Estimation of the tritium production rates in B_4C control rods is approximate because of incomplete information on radial dependence of flux and neutron spectrum, and on the quantities of boron involved [22]. As done for tritium source estimation inside SFR fuel, some studies [16,22] report the specific tritium production rate inside boron control rods $S_{B_4C}^{sp}[Ci/yr/1000\,MW_e]$, which is supposed to be approximately of order of $6.5 \cdot 10^4[Ci/yr/1000\,MW_e] = 6.5 \cdot 10^4[Ci/yr/2500\,MW_{th}]$. Combining S_{tern}^{sp}, $S_{B_4C}^{sp}$, one might be induced to point out that the dominant contribute comes from boron activation. Actually, this is not true, because the important parameter is characterized by the portion of tritium generated inside core materials (boron or fuel) entering the primary coolant, which is the total release rate in the primary sodium as illustrated in par.

However, the total tritium production rate from boron activation is calculated as performed in Eq. (3-1), as follows:

$$S_{B_4C}\left[\frac{Ci}{yr}\right] = S_{B_4C}^{sp} \cdot \frac{P_{th}[MW_{th}]}{2500} \qquad (3\text{-}5)$$

Tritium birth from sodium impurities activation.

Restrictions placed on the lithium content of reactor-grade sodium makes the yield from this source relatively unimportant, however the major reactions include the reaction reported in (3-4) and:

$$Li^6 + n \rightarrow \alpha + H^3 \qquad (3\text{-}6)$$

specific tritium production rate from lithium impurities $S_{Li}^{sp}[Ci/yr/1000\,MW_e]$ should be less than 2 $2 \cdot 10^3[Ci/yr/1000\,MW_e]$. Once again. the total tritium production rate coming from lithium impurities is given by:

$$S_{Li}\left[\frac{Ci}{yr}\right] = S_{Li}^{sp} \cdot \frac{P_{th}[MW_{th}]}{2500} \qquad (3\text{-}7)$$

Tritium release rate into the primary coolant

The expected tritium generation rates in different media reported and discussed in last three paragraphs are summarized and listed in **Table** Errore. Nel documento non esiste testo dello stile specificato.**-7.**

Source	Expected Rate of Generation, Ci/1000 MWe-yr
Fission	$2 - 4 \times 10^4$
Activation of B_4C control rods	65,000[a]
Activation of B impurity in primary coolant	≤ 70
Activation of B impurity in core & blanket fuel	600
Activation of lithium in primary coolant	≤ 85
Activation of lithium in core and blanket fuel	≤ 1400

Table Errore. Nel documento non esiste testo dello stile specificato.**-7 Expected tritium generation rates in different media [22]**

The appearance of tritium in the SFR primary coolant occurs by escape of fission-generated tritium from fuel rods and by neutron activation of boron and impurities in contact with the coolant. The escape of fission-product tritium from fuel rods can occur through cladding defects, but more importantly, by permeation of the stainless steel cladding by elemental tritium. The latter mechanism is expected to result in release of nearly all the fission-product tritium into the primary coolant [22], whereas a little portion of 20 % of that born in the control rods may be released [25].

According to values listed in Table Errore. Nel documento non esiste testo dello stile specificato.**-7** the contribution of impurities is negligible compared to that coming from fuel and control rods. Thus, considering the specific production rates discussed in the above three paragraphs, the total specific tritium source released into the sodium coolant $S_{tot}^{sp}[\text{Ci/yr/1000 MW}_e]$ is expected to be $3.5 \text{ to } 7.5 \cdot 10^4 \, [\text{Ci/yr/1000 MW}_e] = 3.5 \text{ to } 7.5 \, 10^4 \, [\text{Ci/yr/2500 MW}_{th}]$, and the total tritium source released into the primary sodium, is defined as:

$$S_{tot}\left[\frac{Ci}{y}\right] = S_{tot}^{sp} \cdot \frac{P_{th}[\text{MW\_th}]}{2500} = \frac{75000}{2500} \cdot P_{th}[Mw_{th}] = 30 \cdot P_{th}[Mw_{th}] \tag{3-8}$$

A 1000 MW$_e$ SFR reactor gives a total generation rate of 7.75 g/y, which characterizes another confirm that tritium is a concern in SFRs. To keep the release as low as practicable, the cold traps will be required to remove at least 90 % of this tritium burden.

Numerical analysis of tritium transport in SFRs

In order to find the concentrations listed in the previous paragraph, a mass balance equations for each concentration functions is needed. Thus, SFR-TPC must be able to solve a system of partial differential equations (PDEs) where the unknowns are the concentrations and where all terms entering the equations are characterized by all tritium fluxes participating to the mass balances (see Chapter 2) and which must be expressed properly as a function of these concentrations. Moreover, since permeation fluxes are proportional to square roots of partial pressures (see Eq. (2-10)) and since in case of tritium dissolved in water, the HT partial pressure and the HT concentration are proportional (see **Table** Errore. Nel documento non esiste testo dello stile specificato.**-4**), the tritium permeation flux through SG pipe walls is proportional the square root of the HT concentration. Thus, the problem is characterized by a system of non-linear PDEs and therefore, SFR-TPC adopts a numerical approach to solve mass balance equation for each concentration functions listed above discretizing the control volume into a set of finite volumes (FVs) and the choice of numerical method was addressed to the Finite Volume Method (FVM), performing an integral balance inside the h finite volume $\delta V_{j,k}^h$ of the fluid j (with j = primary sodium, secondary sodium or water) inside the component k (with k = IHX or SG). This FV (which is the control volume of the spatial domain) is obtained discretizing volume of the fluid j inside the heat exchange k into a certain number of finite volumes (n_{FV}^k), as reported in Figure Errore. Nel documento non esiste testo dello stile specificato.**-11**.

In this representation is reported only the case in which k = IHX and j = primary sodium and secondary sodium, where a discretization length δz_{IHX} derived from a discretization of the total IHX heat transfer length into n_{FV}^{IHX} parts gives a discretized primary sodium volume δV_{prim}^{IHX} and a secondary sodium one δV_{sec}^{IHX} wrapped into the IHX shell with a diameter D_{shell}^{IHX}.

The SFR-TPC basically solves the continuity mass balance equation calculating the concentration $c_{i,j,k}^h(t)[mol_i/m^3]$ inside the h FV $\delta V_{j,k}^h$ for the tritium species i (with i = T⁻, HT and HTO) into the coolant j (with j = primary sodium, secondary sodium and water), inside the component or heat exchanger k (with k = core, IHX and SG) expressed in the most general form for the concentration $c_{i,j,k}^h(t)[mol_i/m^3]$ as follows:

$$\frac{dc_{i,j,k}^h(t)}{dt} = -\lambda_T \cdot c_{i,j,k}^h(t) + \frac{\dot{Q}_{j,k}^{h-1} \cdot c_{i,j,k}^{h-1}(t) - \dot{Q}_{j,k}^h \cdot c_{i,j,k}^h(t)}{\delta V_{j,k}^h} +$$

$$+ \frac{\dot{S}_{tot}}{\delta V_{j,k}^h} \pm \frac{J_{perm,j,k}^h(t) \cdot \delta A_{perm,k}^h}{\delta V_{j,k}^h} \pm \frac{\Delta_{HT}^h(t)}{\delta V_{j,k}^h}$$

(3-9)

where:

- $\dot{Q}_{j,k}^{h-1}[m^3/s]$ is the inlet volume flow rate of fluid j inside the FV $\delta V_{j,k}^h$, coming from FV $\delta V_{j,k}^{h-1}$;

- $\dot{Q}_{j,k}^h[m^3/s]$ is the outlet volume flow rate of fluid j from the FV $\delta V_{j,k}^h$;

- $\lambda_T[s^{-1}]$ is the decay constant of tritium;

- $\dot{S}_{tot}[mol/s]$ is the total tritium release rate into the primary coolant (see Eq. (3-8));

- $J_{perm,j,k}^h(t)[mol/m^2/s]$ is the permeation flux into the FV h of the fluid j inside the component k through the discretized permeation area $\delta A_{perm,k}^h[m^2]$ (see Eq. (2-10));

- $\Delta_{HT}^h(t)[mol/s]$ is the isotope exchange rate of the chemical equilibrium (see Eq. (2-25) and par. 0), thus is present only in mass balance equations for tritium in water (HT and HTO species).
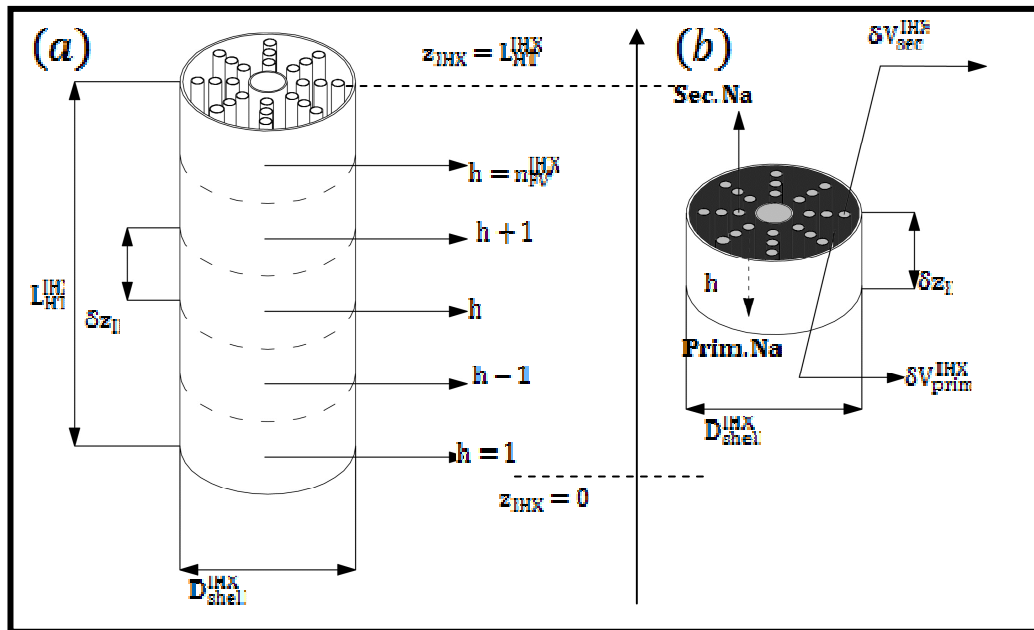
Figure Errore. Nel documento non esiste testo dello stile specificato.**-11 Assonometric view of IHX discretization and (b) detailed view of IHX discretization volume**

From the mathematical point of view the FV approach allows to translate the nature of the problem from a system of six non-linear PDEs (see par. 0) into a system of Λ Ordinary Differential Equations (ODEs), which must be implemented in a suitable solver (SFR-TPC uses MATLAB *ode23s* and *ode23tb* solvers [26] which are quite appropriate for stiff problems such as the studied one) and integrated numerically (with Runge-Kutta methods or Multistep methods [26]) This value Λ is equal to 1 (core sodium concentration) $+ 2 \cdot n_{FV}^{IHX}$ (n_{FV}^{IHX} FVs for both primary and secondary sodium inside the IHX) $+ 3 \cdot n_{FV}^{SG}$ (n_{FV}^{SG} FVs for both secondary sodium and water inside the SG, and inside the water both HT and HTO concentrations are computed.

Before running the code, the user must insert a large number of input data [21] (see par. 0), regarding thermalhydraulics and geometrical data (i.e. temperature, mass flow rates, tube diameters and thickness) of core fuel assembly, IHX and SG and other numerical setting (i.e. number of FVs into IHX and SG, the MATLAB solver and the final time value $t_{fin} [s]$ of the total time domain $\tau: t \in [0, t_{fin}]$ in which the computation is performed). Once the concentrations are computed, the code puts into a big matrix $\vec{C}$ all concentrations values ordered with a suitable criterion [21], and the calculation of tritium losses and inventories takes place.

SFR-TPC material properties database

In the SFR-TPC code were built a set material properties [21] regarding permeation properties (i.e. hydrogen permeabilities and Sievert's constant in sodium and inside all steels adopted for SFRs devices), chemical parameters (chemical equilibrium constants and Henry's constant) and different thermalhydraulics properties of sodium and water (such as density, enthalpy, etc). All these properties are expressed as a functions of temperature, thus the code computes also the temperature profiles along all coolants and all steels. Hereafter all material properties built into the SFR-TPC code (reported in Ref. [21]) are illustrated.

All chemical parameter relations of hydrogen in water such as equilibrium constant $K_{eq}(T)$ of chemical equilibrium (2-10) and Henry's constants discussed in par 0. are reported in **Table** Errore. Nel documento non esiste testo dello stile specificato.**-8**.

Property	Expression
Henry's constant	$K_H^w(T)\left[\dfrac{mol}{l \cdot atm}\right] = 7.8 \cdot 10^{-4} \cdot \exp\left\{500 \cdot \left(\dfrac{1}{T} - \dfrac{1}{298.15}\right)\right\}$
Equilibrium Constant	$\log\{K_{eq}(T)\} = 0.292 \cdot \log T + \dfrac{336.5}{T} - 1.055$

Table Errore. Nel documento non esiste testo dello stile specificato.**-8 SFR-TPC Chemical parameters of hydrogen species in water**

In **Table** Errore. Nel documento non esiste testo dello stile specificato.**-9** are reported all sodium properties:

Property	Expression
Enthalpy	$h_l^{Na}(T) - h_s(T_s)\left[\dfrac{kJ}{kg}\right] = -365.77 + 1.6582 \cdot T +$ $-4.2395 \cdot 10^{-4} \cdot T^2 + +1.4847 \cdot 10^{-7} \cdot T^3 + 2.996 \cdot T^{-1}$
Density	$\rho_l^{Na}(T)\left[\dfrac{kg}{m^3}\right] = 219 + 275.32\left(1 - \dfrac{T}{2503.7}\right) + 511.88\left(1 - \dfrac{T}{2503.7}\right)^{0.5}$
Heat Capacity	$C_p^{Na}(T)\left[\dfrac{kJ}{kg \cdot K}\right] = 1.6582 - 8.7490 \cdot 10^{-4} \cdot T + 4.4541 \cdot 10^{-7} \cdot T^2 - 2992.6 \cdot T^{-2}$
Sievert's constant	$\log\left\{K_S^{Na}(T)\left[\dfrac{wppm}{\sqrt{Pa}}\right]\right\} = 2.298 - \dfrac{122}{T}$

Table Errore. Nel documento non esiste testo dello stile specificato.**-9 SFR-TPC Sodium properties**

In **Table** Errore. Nel documento non esiste testo dello stile specificato.**-10** are reported the tritium permeabilities inside some structural steels:

Property	Expression
Austenitic steel (AISI SS316L)l	$P(T)\left[\dfrac{mol_{T_2}}{m \cdot sec \cdot \sqrt{Pa}}\right] = 3.24 \cdot 10^{-8} \cdot \exp\left\{-\dfrac{60075}{RT}\right\}$
Ferritic Steel (P91)	$P(T)\left[\dfrac{mol_{H}}{m \cdot sec \cdot \sqrt{Pa}}\right] = 3.32 \cdot 10^{-8} \cdot \exp\left\{-\dfrac{36700}{RT}\right\}$
Martensitic Steel (MANET)	$P(T)\left[\dfrac{mol_{H_2}}{m \cdot sec \cdot \sqrt{Pa}}\right] = 3.29 \cdot 10^{-8} \cdot \exp\left\{-\dfrac{42360}{RT}\right\}$
Incoloy 800	$P(T)\left[\dfrac{mol_{H_2}}{m \cdot sec \cdot \sqrt{Pa}}\right] = 3.94 \cdot 10^{-8} \cdot \exp\left\{-\dfrac{55600}{RT}\right\}$

Table Errore. Nel documento non esiste testo dello stile specificato.**-10 SFR-TPC Hydrogen/Tritium permeabilities inside steels**

In **Table** Errore. Nel documento non esiste testo dello stile specificato.**-11** is reported the list of the empirical expressions of Sievert's constant in the same steels and alloys:

Property	Expression
Austenitic steel (AISI SS316L)	$K_S(T)\left[\dfrac{mol_{T_2}}{m^3 \cdot \sqrt{Pa}}\right] = 144 \cdot \exp\left\{-\dfrac{45028}{RT}\right\}$
Ferritic Steel (P91)	$K_S(T)\left[\dfrac{mol_{H}}{m^3 \cdot \sqrt{Pa}}\right] = 0.6485 \cdot \exp\left\{-\dfrac{32550}{RT}\right\}$
Martensitic Steel (MANET)	$K_S(T)\left[\dfrac{mol_{H_2}}{m^3 \cdot \sqrt{Pa}}\right] = 0.373 \cdot \exp\left\{-\dfrac{26890}{RT}\right\}$
Incoloy 800	$K_S(T)\left[\dfrac{mol_{D_2}}{m^3 \cdot \sqrt{Pa}}\right] = 0.102 \cdot \exp\left\{-\dfrac{7800}{RT}\right\}$

Table Errore. Nel documento non esiste testo dello stile specificato.**-11 Hydrogen Sievert's constant inside steels**

where $R = 8.31 \, [J/mol/K]$ is the constant gas and $T[K]$ is the temperature.

Values of permeabilities, as shown in the above table, are reported in the same unit but referred to different isotopic species (T_2, H_2, H). The code takes into account of mass effect, subdividing by a factor $\sqrt{m_I}$ [13]. All permeability coefficient listed in **Table** Errore. Nel documento non

esiste testo dello stile specificato.**-10** are reported in the Arrhenius plot of **Figure** Errore. Nel documento non esiste testo dello stile specificato.**-12**, while hydrogen Sievert's constant data are visualized in **Figure** Errore. Nel documento non esiste testo dello stile specificato.**-13**
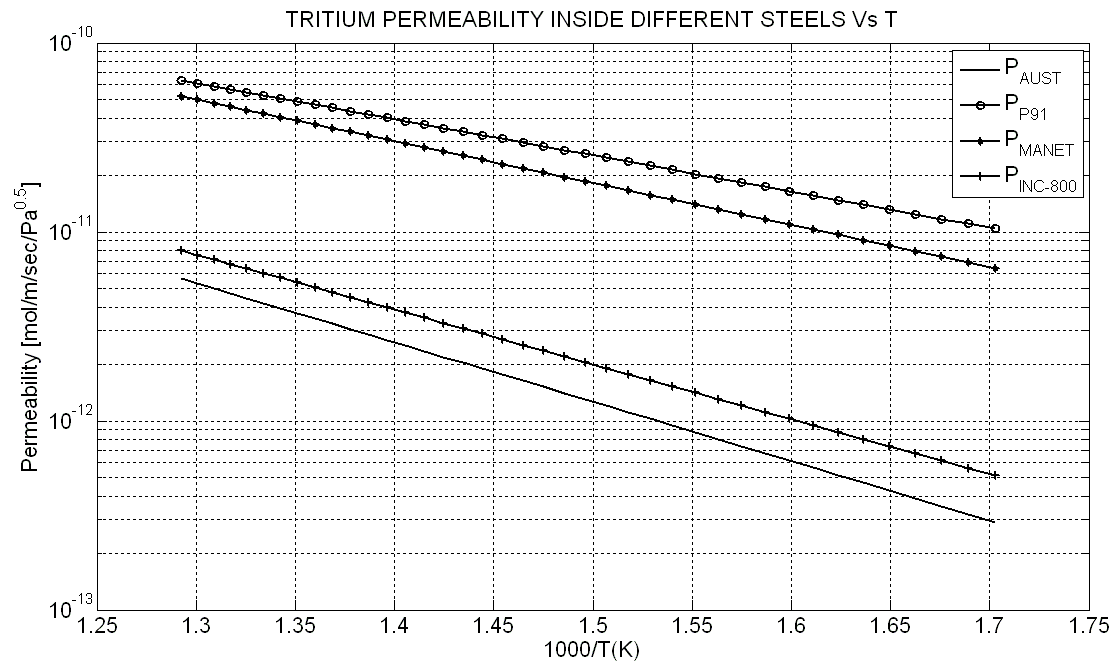
Figure Errore. Nel documento non esiste testo dello stile specificato.**-12 SFR-TPC Tritium Permeabilities Vs 1000/T inside steels**
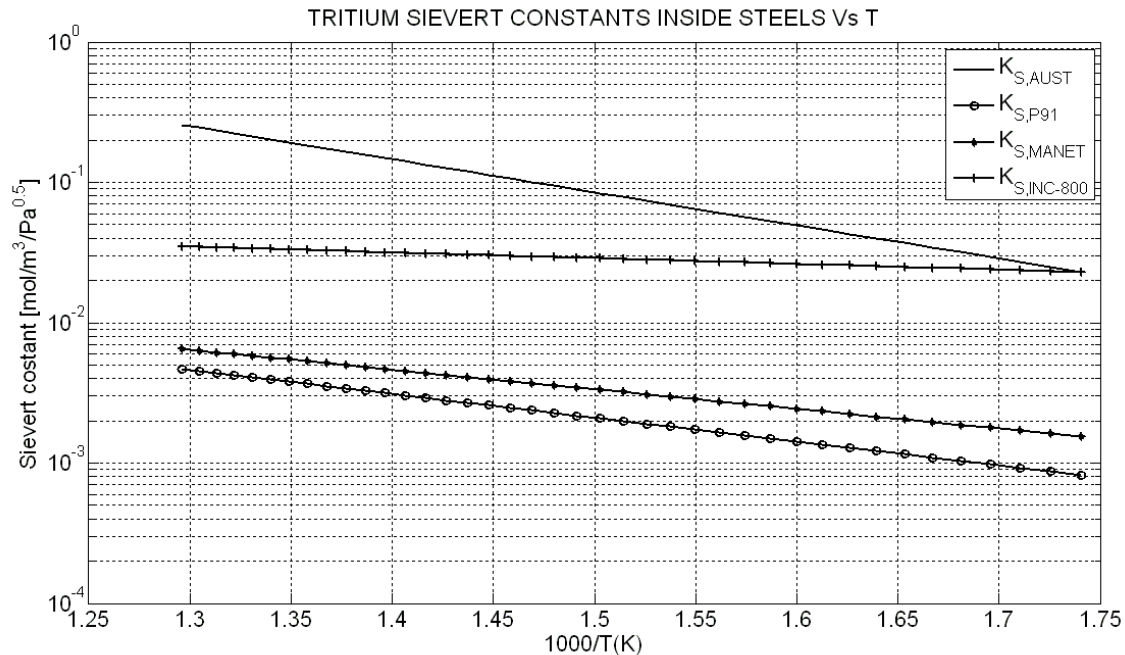
Figure Errore. Nel documento non esiste testo dello stile specificato.**-13 SFR-TPC Hydrogen Sievert's constant Vs 1000/T inside steels**

As will be described in par. 0 the Sievert's constant in steels is required in order to determine the tritium inventories inside IHX, SG and pool steels.

Modeling of tritium losses and inventories

When the overall ODEs system is defined, it is necessary to determine tritium losses and tritium inventories. These two quantities are characterized by integral quantity, obtained by integration in space phase of our tritium concentrations defined in our phase space (z_{IHX}, t) and (z_{SG}, t), according to **Figure** Errore. Nel documento non esiste testo dello stile specificato.**-10** schematization and to the description reported in par. 0.

Modeling of tritium losses.

The overall SFR plant tritium losses according to all outgoing tritium fluxes are indicated in Figure Errore. Nel documento non esiste testo dello stile specificato.**-10**, and they are summarized in the following list:

- tritium losses through the pool containment $\phi_{pool}(t)$;
- tritium losses through the SG shells $\phi_{shell}^{SG}(t)$;

- permeation flux through SG tubes and entering in the steam/water bulk $\phi_{bulk}^{SG}(t)$;

Considering negligible the tritium partial pressure outside the pool (conservative assumption), a permeation flux $J_{pool}(t)$ through the pool containment tank takes place (see Figure Errore. Nel documento non esiste testo dello stile specificato.**-10**) giving the tritium losses term ϕ_{pool}. Assuming a tritium concentration inside the pool sodium $\left(C_{pool}\right)$ equal to that in core sodium C_{core} (computed by the code), assuming a certain pool permeability $P_{pool}(\overline{T}_{tank})$ at a pool tank temperature $\overline{T}_{tank}$ and a certain pool area A_{pool}, the total tritium losses from pool containment $\phi_{pool}(t)$, is given by:

$$\phi_{pool}(t)\left[\frac{mol}{s}\right] = J_{pool}(t) \cdot A_{pool} =$$

$$= \left(\frac{P_{pool}(\overline{T}_{tank})}{t_{pool}} \cdot \frac{C_{pool}}{K_s^{Na}(\overline{T}_{pool})}\right) \cdot A_{pool} \tag{3-10}$$

where $K_{s,Na}(\overline{T}_{pool})$ is the tritium Sievert's constant in sodium at average pool sodium temperature $\overline{\overline{T}}_{pool}$ and t_{pool} is the pool thickness.

Assuming again that the outside tritium partial pressure is negligible, a tritium permeation flux through the SG shell walls $J_{shell}^{SG}(z_{SG},t)$ is founded (see Figure Errore. Nel documento non esiste testo dello stile specificato.**-10**). Considering a certain tritium concentration distribution along the SG heat transfer coordinate z_{SG} inside the secondary sodium $C_{sec}^{SG}(z_{SG},t)$ (computed by the code), the tritium losses through the SG shell is defined as :

$$\phi_{shell}^{SG}(t)\left[\frac{mol}{s}\right] = n_{SG} \cdot \int_{A_{shell}^{SG}} J_{shell}^{SG}(z_{SG},t) \cdot dA_{shell}^{SG} =$$

$$n_{SG} \cdot \int_{A_{shell}^{SG}} \left(\frac{P_{shell}^{SG}(T_{shell}^{SG})}{t_{shell}^{SG}} \cdot \frac{C_{sec}^{SG}(z_{SG},t)}{K_s^{Na}(T_{sec}^{SG})}\right) \cdot dA_{shell}^{SG} \tag{3-11}$$

where n_{SG} is the total number of SGs, A_{shell}^{SG} is the total permeation area of all SG shells, t_{shell}^{SG} is the SG shell thickness, $P_{shell}^{SG}(T_{shell}^{SG})$ is the SG shell permeability defined along the SG shell temperature profile $T_{shell}^{SG}(z_{SG})$ and T_{sec}^{SG} is the secondary sodium temperature distribution along the coordinate z_{SG}.

The last tritium losses contribution, which is also the most relevant one comes from tritium permeation flux $J_{tube}^{SG}(z_{SG},t)$ (see Figure Errore. Nel documento non esiste testo dello stile specificato.**-10**) from secondary sodium inside the SG into the steam/water through SG tubes surfaces. This quantity

is conservatively assumed to be lost into the environment, and the overall expression is derived combining Eq. (2-10) with Eq. (2-16) (for tritium partial pressure in secondary sodium) and Eq. (2-17) or (2-22) (for HT partial pressure in water) and the overall expression is reported in the following equation:

$$\phi_{bulk}^{SG}(t) \left[\frac{mol}{s}\right] = n_{SG} \cdot \int_{A_{perm}^{SG}} J_{tube}^{SG}(z_{SG}, t) \cdot dA_{perm}^{SG} =$$

$$= n_{SG} \cdot \int_{A_{perm}^{SG}} \frac{P_{tube}^{SG}(T_{tube}^{SG})}{t_{tube}^{SG}} \cdot \left(\frac{C_{sec}^{SG}(z_{SG}, t)}{K_s^{Na}(T_{sec}^{SG})} - \sqrt{\frac{C_{HT}^{w}(z_{SG}, t)}{K_{HT}^{w}(T_w)}} \right) \cdot dA_{perm}^{SG} \tag{3-12}$$

where A_{perm}^{SG} is the total SG tubes permeation area, $C_{HT}^{w}(z_{SG}, t)$ is the HT concentration in water, P_{tube}^{SG} is the SG tubes permeability (defined at SG tubes temperature profile $T_{tube}^{SG}(z_{SG})$) and $K_{HT}^{w}(T_w)$ is a function of water temperature $T_w(z_{SG})$ and is defined according to the thermodynamic state of water along heat transfer coordinate. In fact the water enters into the SG in sub-cooled liquid condition and it is heated up from the secondary sodium. Then, it evaporates along SG heat transfer length and goes out assuming the superheated steam condition. As reported in par. 0, the constitutive relationships between partial pressures and concentration are different in case of pure liquid water or superheated steam and therefore, this function $K_{HT}^{w}(T_w)$ takes into account the changing thermodynamic state passing from Henry's law (see Eq. (2-17)) to Dalton's law in case of superheated steam (see Eq. (2-24)). Inside the evaporation region was assumed that the function $K_{HT}^{w}(T_w)$ is equal to the Henry's constant at the saturation temperature.

Summing all tritium losses terms listed above it is possible to evaluate total tritium losses of an overall SFR plant $\phi_{tot}[g/y]$:

$$\phi_{tot}(t) \left[\frac{g}{y}\right] = \left[\phi_{pool}(t) + \phi_{shell}^{SG}(t) + \phi_{bulk}^{SG}(t) \right] \cdot PA_T \cdot N_s^y \tag{3-13}$$

where $PA_T \approx 3 \, [g/mol]$ is the tritium atomic weight and $N_s^y = 3.1536 \cdot 10^7 \, [s/y]$ is the number of seconds per year. From the above equation it is possible to point out that in order to fight the tritium losses from an SFR system, the SG is a key component because two terms out of three term entering the expression of ϕ_{tot} regard exactly the SG.

Modeling of Tritium Inventories

As already mentioned, for the tritium transport analysis point of view, it is of common interest to consider the tritium quantities staying inside the power plant facilities, which are characterized by the tritium inventories. The interest in this topic is related to the radiological risks for workers inside the plant (evaluation of annual dose per built-in Becquerel), or risks related to accidental conditions. In fact, in SFRs there are many accident event (such as UTOP, ULOF [27] or accident triggered by water-sodium interaction [7]), and they involve radionuclide releases. According with these releases we are willing to evaluate tritium inventories in those portions of SFR plants which are objects of radiological risks evaluation in case of accident condition (in the previous paragraph we evaluated tritium losses in case of operative SFR conditions), such as tritium inventory into primary sodium (relevant for accident related to failure of pool containment or for decomissioning issues [30]), or into secondary sodium contained in a secondary loop (which is an interesting quantity for failure of sodium pipe linking IHX and SG or for decomissioning issues too [30]).

In the tritium inventories assessments is also necessary to calculate the tritium contents inside structural materials, such as IHX and SG heat transfer pipes and IHX and SG shells. These quantities are relevant mainly when a decommissioning of SFR plant is effectuated, since activation of steels and others structural materials has to be evaluated before starting the decommissioning operations. However after this brief introduction, as listed in par. 0, the tritium inventories computation is characterized by the evaluation of:

- total tritium inventory in a single IHX's steels $I_{steel}^{IHX}(t)$;
- total tritium inventory in a single SG's steels $I_{steel}^{SG}(t)$;
- total tritium inventory inside the structural pool containment tank $I_{tank}(t)$;
- total tritium inventory inside primary sodium contained into the pool (sum of core sodium, pool sodium and IHX primary sodium) $I_{prim}(t)$;
- total tritium inventory inside the secondary sodium of a single heat transfer loop (sum of secondary sodium in IHXs of a single loop and secondary sodium in SGs of a single loop) $I_{sec}^{loop}(t)$;
- total tritium inventory inside the steam/water of a single heat transfer loop (sum of steam/water present in all SGs of a single heat transfer secondary loop) $I_{w}^{loop}(t)$.

- total tritium inventory inside the plant (sum of all above terms) $I_{tot}(t)$.

Tritium inventory inside the cold traps (see par. 0) has not so much relevance because, after a certain time period (typically 1-5 years [29]), a certain fraction of the trap mesh volume is filled of solid sodium hydride and tritide and therefore the cold trap should be plugged or substituted. For this reason this tritium inventory is not evaluated in the code. However, the total tritium retention rate inside the cold traps $\phi_{CT}^{tot}[mol/s]$ (see par. 0 and Eq. (4-13)) is a key parameter because the ratio between total tritium retention rate inside cold traps ϕ_{CT}^{tot} and the tritium release rate into primary sodium $\dot{S}_{tot}$ (see Eq. (3-8)) indicates the overall cold trap performances inside an SFR system.

Tritium inventory inside steels.

When the H^3 inventory has to be evaluated inside a metallic material it is assumed, as illustrated in Chapter 0, that Sievert's law is valid for solubility of hydrogen isotopes inside metals. Hence, according to this constitutive relation (see Eq. (2-12)), and assuming a diffusion-limited regime for the tritium permeation inside steels, an average concentration C_{steel}^k between the high pressure side concentration $C_{steel}^{h,k}$ and the low pressure side concentration $C_{steel}^{l,k}$ of structural steels of component k (with k = pool containment tank, IHX steels and SG steels) is used to determine tritium inventory inside k steels I_{steel}^k and it is defined as:

$$C_{steel}^k(z_k,t) = \frac{C_{steel}^{h,k}(z_k,t) + C_{steel}^{l,k}(z_k,t)}{2} \tag{3-14}$$

The concentrations $C_{steel}^{h,k}$ and $C_{steel}^{l,k}$ are defined by means of the Sievert's law, considering the hydrogen Sievert's constant inside the k steels $K_s^k(T_{steel}^k)$ (defined at average k steels temperature T_{steel}^k), the tritium partial pressure acting on the high pressure side of the k steels $p_{steel}^{h,k}$ and that acting on the low pressure one $p_{steel}^{h,k}$; their expressions are reported in the following equations:

$$C_{steel}^{h,k}(z_k,t) = K_s^k(T_{steel}^k) \cdot \sqrt{p_{steel}^{h,k}}, \tag{3-15}$$

$$C_{steel}^{l,k}(z_k,t) = K_s^k(T_{steel}^k) \cdot \sqrt{p_{steel}^{l,k}}, \tag{3-16}$$

Hence, the total inventory inside the k steels is calculated integrating the k steels concentration distribution $C_{steel}^k(z_k,t)$ in the k steels volume $V_{steel}^k[m^3]$ as follows:

$$I_{steel}^k(t)[mol] = \int_{V_{steel}^k} C_{steel}^k(z_k, t) \cdot dV_{steel}^k \tag{3-17}$$

According to this procedure and considering the total volumes of the IHX steels (V_{steels}^{IHX}), of the SG steels (V_{steels}^{SG}) and of pool containment structural steels (V_{steels}^{pool}), the total inventory inside all steels is given by summing all these tritium inventory terms calculated as done in Eq. (3-17).

Tritium inventory in primary sodium

In case of failure of tank containing all pool facilities, it is necessary to be aware of the potential amount of gas releasable with primary sodium leakage when the fracture takes place. Inside the pool containment all tritium inventories contributions are characterized by:

- Primary sodium inside the pool with a volume V_{pool} and a concentration $C_{pool}(t)$;
- Primary sodium inside core fuel assembly with a volume V_{core} and a concentration $C_{core}(t)$;
- Primary sodium inside IHX with a volume V_{prim}^{IHX} and a concentration $C_{prim}(z_{IHX}, t)$;

The tritium inventory inside the primary sodium (I_{prim}) is estimated in a simplifying and conservative way, assuming that all pool internal volume V_{pool} is occupied by sodium at a tritium concentration $C_{core}(t)$ which is the largest tritium concentration inside the plant [21]. Thus, I_{prim} is given by:

$$I_{prim}(t)[mol] = C_{core}(t) \cdot V_{pool} \tag{3-18}$$

Tritium inventory inside a secondary sodium loop.

In order to the estimate tritium quantity releasable when a failure occurs in a pipe linking IHX to SG, it is necessary to predict the total amount of tritium staying inside all secondary sodium volume, given by the sum of sodium flowing inside IHX, that inside SG and that inside linking pipelines (assumed negligible with respect to that inside the first two). Thus, the total amount of H^3 inside the sodium flowing in a secondary loop and then, releasable to the environment in case of rupture of a pipe carrying secondary sodium, is defined as a function of I_{sec}^{loop} and is given by:

$$I_{sec}^{loop}(t) = I_{sec,loop}^{IHX}(t) + I_{sec,loop}^{SG} \tag{3-19}$$

where $I_{sec,loop}^{IHX}$ and $I_{sec,loop}^{SG}$ are the secondary sodium tritium inventories inside n_{IHX}^{loop} of IHXs contained inside a secondary loop, and the tritium inventory inside n_{SG}^{loop} of SGs contained inside a secondary loop. Thus their expressions are defined as:

$$I_{sec}^{loop}(t)[mol] = n_{IHX}^{loop} \cdot \int_{V_{sec}^{IHX}} C_{sec}^{IHX}(z_{IHX}, t) \cdot dV_{sec}^{IHX} + n_{SG}^{loop} \cdot \int_{V_{sec}^{SG}} C_{sec}^{SG}(z_{SG}, t) \cdot dV_{sec}^{SG} \qquad (3\text{-}20)$$

where $C_{sec}^{IHX}(z_{IHX}, t)$ and $C_{sec}^{SG}(z_{SG}, t)$ are the tritium concentration of secondary sodium inside IHX and SG respectively, and V_{sec}^{IHX} and V_{sec}^{SG} are volumes of secondary sodium inside IHX and SG respectively.

Tritium inventory in water.

The last term is given by the tritium inventory inside the SGs water. In fact, if a rupture in a pipe carrying steam out from the SGs occurs, the tritium dissolved inside the water contained in a the number of SGs per secondary loop n_{SG}^{loop} can be released. Although this term is expected to be the less warring from the radiological point of view, it is computed anyway.

Considering the total tritium concentration inside water $C_T^W(z_{SG}, t)$ given by the sum of $C_{HT}^W(z_{SG}, t)$ and $C_{HTO}^W(z_{SG}, t)$ (both computed by the code), the tritium inventory inside the water of a single secondary loop $I_w^{loop}(t)$ is defined as:

$$I_w^{loop}(t)[mol] = n_{SG}^{loop} \cdot \int_{V_{sec}^{IHX}} C_T^W(z_{SG}, t) \cdot dV_w^{SG} \qquad (3\text{-}21)$$

where V_w^{SG} is volume of water contained in a single SG.

The total tritium inventory inside the plant $I_{tot}(t)$ is simply obtained by summing all above inventory terms, and is defined as:

$$I_{tot}(t)[g] = \left[\sum_k I_{steel}^k(t) + I_{prim}(t) + \frac{n_{SG}}{n_{IHX}} \cdot \left(I_{sec}^{loop}(t) + I_w^{loop}(t) \right) \right] \cdot PA_T \qquad (3\text{-}22)$$

where the values n_{SG} and n_{IHX} are the total number of SGs and IHX respectively. n_{SG}/n_{IHX} is the number of secondary loops inside the plant and $PA_T \approx 3 \, [g/mol]$ is the tritium atomic weight.

In this chapter the main tritium transport mechanisms in SFR systems were illustrated, and the mathematical procedures necessary to study these mechanisms were described.

In order to perform a tritium analysis inside such systems a computational code was developed (the SFR-TPC), and since was confirmed that tritium inside SFRs is a concern (as reported in par. 0

a 1000 MW$_e$ produces a quite warring quantity of tritium of about 7.8 g/y), some mitigation techniques must be adopted in order to prevent and mitigate potential tritium releases into the environment. In next chapter the SFR-TPC code will be used in order to study the effects coming from the application of the mitigations techniques available to mitigate tritium transport inside these nuclear plants.

Chapter 0

Investigation of the tritium transport mitigation techniques

As illustrated in the previous chapter, large tritium quantities are potentially releasable from a SFR system into the environment. In order to avoid a large amount of tritium dissolved in primary sodium and potentially permeated into secondary sodium and steam, a set of tritium containment tools are foreseen in an SFR system. The main mitigation measures are referred to:

- application of tritium permeation barriers on the heat exchanger tubes surfaces (i.e., coating the tubes surfaces with a certain material before the installation or forming an oxidation layer during the operation);
- Cold trapping of primary and secondary sodium.

In this chapter both techniques will be studied in term of performances using the SFR-TPC code and will be also discussed from the engineering point of view.

Tritium permeation barriers

Tritium/hydrogen barriers have evolved in a variety of applications during the last few decades. In general the presence of an oxidation layer (natural oxide or coating) characterizes a

barrier to the hydrogen permeation. Thus, the objective becomes here to investigate the permeation reduction factor (PRF) literature data of available for those materials adopted in SFR heat transfer facilities (i.e. IHX and SG tubes material), which were illustrated in par. 0 and given by the stainless austenitic steels for IHX and ferritic steels and nickel based alloy (i.e. Incoloy 800) for SG tubes.

To permeate a barrier-coated metal, an hydrogen isotope must be adsorbed on the surface, diffuse through the barrier, be incorporated into the base metal, diffuse through the base metal and undergo desorption at the opposite surface [31]. Simple surface oxides have provided a reduction in hydrogen permeation of about one order of magnitude for many structural materials [31]. In fact there are a number of results published in the literature which basically prove the permeation inhibiting effect of oxidic layers on austenitic steels and nickel based alloys steels ([31], [32]).

Theory of permeation in two-layer membranes

The hydrogen migration through the layers of a planar membrane is assumed to be limited by H atom diffusion in the bulk while the adsorption, dissociation, recombination, and desorption processes at the inlet and outlet surface are rapid [33]. In such case the hydrogen concentration at the inlet surface is in equilibrium with hydrogen partial pressure p according to the Sievert's law (see Eq. (2-12)). Steady-state permeation rate J_{ss}(see Eq. (2-10)) is driven by the difference in the hydrogen concentration in the membrane bulk. Coefficients D and K_S are assumed to be independent of hydrogen concentration and time, being only a material property. The rightmost term in eq. (2-10) is valid also for multi-layer membrane (i.e. base material and coated layer) if P represents the effective permeability coefficient P_{eff}.

Coating the membrane with an additional layer (barrier) always results in the reduced permeation if the diffusion remains the rate limiting process. The experimental proof of the barrier efficiency is a relative reduction of the steady-state permeation flux measured at the identical conditions (p, T). Its definition is the ratio of the steady-state permeation rate through the uncoated membrane versus one through the coated membrane, termed "the permeation reduction factor" (PRF):

$$PRF = \frac{J_{uncoated}}{J_{coated}} \tag{4-1}$$

being on the order of 100 or even 1000 for efficient barrier films [33].

For modeling purposes it is enough to consider that surface conditions of a certain metallic materials (i.e. presence of oxide layer, impurities, corrosion products) can affect the permeation regime and reduce the quantity of tritium permeation flux J_{perm} crossing a surface characterized by a certain thickness t and a certain permeability P(T). Hence, considering a certain PRF and the partial pressures acting on the high and the low pressure sides (p_h and p_l respectively), the permeation flux J_{perm} becomes:

$$J_{perm} = \frac{1}{PRF} \cdot \frac{P_T(T)}{t} \cdot \left(\sqrt{p_h} - \sqrt{p_l} \right) \tag{4-2}$$

A variety of experimental and developmental activities on tritium barriers for hydrogen isotope permeation are underway, including in situ reactor testing of these barriers [33]. For a SFR tritium permeation code is necessary to consider suitable PRFs inside IHX and SG to be inserted into the code for IHX and SG structural materials illustrated in par. 0 (shell and tubes material of both) in order to evaluate tritium losses into the environment and tritium inventories. In general, tritium losses are expected to reduce with IHX and SG PRF increases, whereas the tritium inventories would increase. However, numerical results at the end of this chapter will illustrate better this statement.

Various hydrogen/tritium permeation barriers

Since in a SFR system the tritium permeation occurs both through IHX and SG pipe walls, one may wonder if there might be some barrier effects on both heat exchangers coming from the formation of oxides on pipe surfaces, because the installation of coated tubes in SFR IHXs or SGs may be uneconomic. Thus, the natural permeation barrier (such as formation of oxide layers on the wall of heat exchanger) have attracted much attention for the reduction of hydrogen and tritium permeation.

Simple oxidation of metals may be effective for certain heat installations facilities. Some studies [34] show that oxide layers can decrease the hydrogen permeation rates even by more than two orders of magnitude and that the oxidation potential and temperature may be essential for the formation and the structure of oxide layer, and consequently for the permeation rate [34].

Tritium permeation barriers for IHX tubes

Austenitic stainless steels were individuated through one of the most candidate class of materials for IHX tubes installation (see par. 0). The problem thus becomes to understand if the formation of oxides in stainless steels adopted in IHXs could provide a potential barrier effect to the tritium permeation through IHX pipes walls. Since IHX deals with liquid sodium at high temperature on both sides (primary and secondary sodium), the corrosion of structural steels by liquid metals could be of interest in the oxide formation and deposition and therefore, in the tritium permeation reduction.

Liquid metal corrosion is one of the key factors that have to be considered when using liquid metal as a heat transfer medium such as the primary coolant in advanced nuclear reactors [35]. The corrosion processes can be simply summarized in three significant steps: (1) transport in the solid (metal or alloy), (2) dissolution of the steel constituents into the liquid, or mass exchange at the solid/liquid interface, and (3) transport of the corrosion products and impurities in the liquid. The transport processes in liquid and solid are coupled with each other at solid/liquid interface through mass exchange. The two processes (transports in liquid and solid) can also lead to impurity redistribution and new phase formation at the surface area of the solid contacting with the liquid metal.

In an isothermal liquid metal closed loop system, if the loop is made of same materials the corrosion may finally stop because of saturation of the corrosion products, while in a non-isothermal system (such as the primary coolant loop system of a nuclear reactor), the final state is a kinetic equilibrium in which the amount of corrosion is balanced by the amount of the precipitation all through the loop. It is the precipitation that sustains the corrosion in a non-isothermal liquid metal loop [35]. The precipitating corrosion product may be in the form of layers tightly adhering on the pipe wall or particles suspending in the liquid [35]. **Figure** Errore. Nel documento non esiste testo dello stile specificato.**-14** [36] illustrates a typical predicted profile of mass transfer in the hot leg, where deposition occurred over approximately the first quarter of the leg [36].

This deposition layer may provide a certain PRF in IHX tubes. However, literature data were not found, thus any PRFs coming from this deposition cannot be assumed. Moreover, some authors [35] states that it is more difficult to form solid stable oxide of Fe, Cr and Ni than sodium, but soluble ternary oxide can be formed in the form of FeO_nNa_2O.
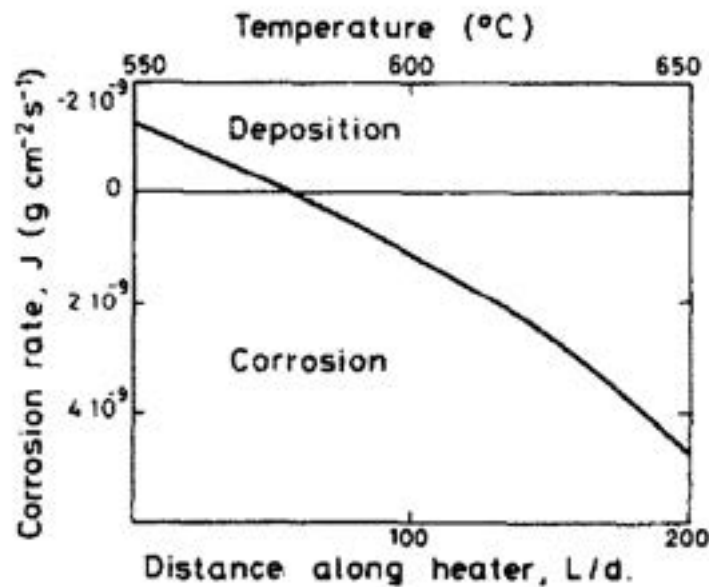
Figure Errore. Nel documento non esiste testo dello stile specificato.**-14 Typical predicted mass transfer profile along heater [36]**

Liquid metal corrosion depends on the liquid metal itself and impurities in it (i.e. oxygen concentration). Liquid sodium and sodium–potassium alloy are less corrosive than liquid lead and lead–bismuth alloy at the same operating conditions when impurities' effects are not considered [35]. If liquid lead or lead–bismuth is selected for the primary coolant of nuclear reactors, protective methods must be applied to mitigate the corrosion of structural materials. One of these methods is oxygen control technique which can control the oxygen concentration in the liquid in a certain range to form a protective oxide layer on structural material surfaces and to avoid the precipitation of the lead oxide from the liquid [35]. For liquid sodium and sodium– potassium alloy, the oxygen concentration has to be controlled as low as possible because the corrosion rate by liquid sodium and sodium– potassium increases significantly with oxygen concentration [35].

In conclusion, considering that sodium characterizes a reducing atmosphere, considering that oxygen must be kept as low as possible and considering that oxide deposition could occur only on the cold leg of a secondary sodium loop we can conservatively assume a PRF = 1 on surfaces wetted by liquid sodium.

Various hydrogen/tritium permeation barriers for SG tubes

Nickel-based alloys were selected as one of the promising class of materials based on experimental results of corrosion tests and mechanical tests before irradiation [37] for SG tubes in SFRs (see par. 0). These alloys show a high tendency to form a protective oxide film in water at high temperatures [37]. Based on its advantages, such as high strength and corrosion resistance at high temperatures, Incoloy 800 (a high nickel alloy), is one of the most candidate materials for SG tubes in SFRs [2], as shown in par. 0. The internal oxidation layer may be expected to appear because the oxygen affinity for Cr is larger than for Fe, therefore Cr oxidizes more readily by reacting with diffused oxygen [37]. Simultaneously the formation of this layer will decrease the oxygen potential at the oxide/metal interface making iron oxide less stable [37]. Different materials were tested by Serpekian [34]. All tested materials showed a basically similar behavior with time, which was characterized by a decrease in the rate of hydrogen permeation from a very high value initially to an equilibrium value two order of magnitudes lower [34]. A less recent analysis of status of permeation barrier development was carried out by Stöver et al [38]. Results of PRFs reviewed by Stöver are summarized in **Table** Errore. Nel documento non esiste testo dello stile specificato.**-12**, in which the PRF is called Hemmfaktor. Comparing PRFs values obtained for Incoloy 800 of **Table** Errore. Nel documento non esiste testo dello stile specificato.**-12** [38] to those of Serpekian [34] (ranging between 22 to 100), we note that both show two orders of magnitudes in the PRF values coming from natural oxidation of Incoloy 800. It must be to point out that results obtained by Serpekian come from experiment carried out in a secondary loop of an High Temperature Reactor, in which the SG operates with helium and water, and the oxidation is formed in the helium side by adding H_2 and H_2O at a fixed ratio [34], while the natural oxidation in SFR's SGs is expected (and also wished) on the water side. Therefore, these values are just illustrative of the tendency of these alloys to form natural oxides and the chemical and physical atmosphere operating on these materials is a relevant factor. For tritium transport analysis is relevant to consider that we cannot rely on PRFs coming from natural oxidation in SFR's SGs larger than a certain conservative value (i.e. the lowest value reported in **Table** Errore. Nel documento non esiste testo dello stile specificato.**-12**, which is 10).

As reported in par. 0, another class of steels for SG tubes is the ferritic one. Since no literature data were founded for PRFs coming from natural oxidation of ferritic steels, in this work will be considered that the maximum PRF values achievable are those coming from Incoloy 800 oxidation.

Table Errore. Nel documento non esiste testo dello stile specificato.**-12 Hemmfaktor's (or PRFs) obtained on austenitic steels from literature [32]**

Tritium/hydrogen cold traps

Control of tritium in the sodium coolant of SFRs is important for achieving as low as practicable release of radioactivity. Cold-trapping has been shown to be an effective method for controlling hydrogen in sodium and should be effective for controlling tritium as well [25]. Two mechanisms for removal of tritium from sodium are available:

- coprecipitation of hydrogen and tritium from solution in form of solid sodium hydride NaH and NaT respectively (see par. 0 and equilibrium reaction (2-2));
- isotopic exchange of tritium in sodium with hydrogen in solid NaH In a cold trap.

Some authors [25] have indicated that the coprecipitation mechanism is, as expected, much more effective in removing tritium from sodium than the isotopic exchange mechanism, thus hereafter will be considered only this mechanism in the cold trap modeling for our tritium transport analysis contest.

To keep the release as low as practicable, the cold traps will be required in order to remove at least the 90 % of tritium produced inside the core and released into the primary coolant [25].

Theory of tritium/hydrogen cold traps

Inside the cold traps basically occurs the process I of Barn-Haber cycle (see **Figure** Errore. Nel documento non esiste testo dello stile specificato.**-3)** and it is considered the physical mechanism of hydrogen and tritium removal from liquid sodium by means of hydrogen precipitation in form of solid impurity NaH (s) and NaT (s), while in sodium flowing inside the SFR heat transport facilities (core, IHX and SG), the process III is considered for tritium concentration evaluation (based on a solvation model), effectuated by means of the Sievert's law.

In the estimation of the amount of tritium removed by the cold traps cognizance has also to be taken of the hydrogen level in the sodium because the tritium concentration by itself does not reach its saturation level C_{sat}^H (about 0.057 wppm at 121 °C according to empirical relation reported in Eq. (2-4)), even at SFR cold trap temperatures T_{cold}^{CT} of 121°C [30]. The types of hydrogen source identified in the SFRs primary circuits are [22]:

- Protons formed by fission;
- Protons from neutron activation of the core materials;
- Cover gas moisture;
- Hydrogen and water adsorbed on fresh sub-assembly surfaces.

The hydrogen sources in the secondary sodium include:

- Corrosion of the SG steels by water;
- Atmospheric corrosion of the steel of the circuit;
- Atmospheric hydrogen diffusion through the steel of the circuit;
- Cover gas moisture.

Two other sources are taken into account at Phénix [22]:

- Diffusion of the molecular hydrogen dissolved in water;
- Hydrazine thermal decomposition.

Although hydrogen content is a crucial parameter to estimate tritium retention rate inside the cold traps, were not implemented any mass balance equation for hydrogen in the code, because was a simplified approach avoiding the hydrogen balances inside primary and secondary sodium as illustrated hereafter.

From the modeling point of view a cold trap is characterized by a removal efficiency ϵ_{CT} which is referred to the hydrogen removal rate from a certain total volume flow rate $\dot{Q}_{CT}$ of sodium flowing in it and defined as:

$$\epsilon_{CT} = \frac{\text{Recovered hydrogen molar flow rate}}{\text{maximun hydrogen molar flow rate recoverable}} = \frac{C^H_{in,CT} - C^H_{out,CT}}{C^H_{in,CT} - C^H_{sat}\left(T^{CT}_{cold}\right)} \qquad (4\text{-}3)$$

where C^H_{in} and C^H_{out} are the inlet and the outlet hydrogen concentrations in sodium flowing in the cold traps apparatus. From experimental results in AMPS test facility [25], this parameter is observed to range between $40 \div 100$ %. In **Figure** Errore. Nel documento non esiste testo dello stile specificato.**-15** is reported a cold trap arrangement in a SFR system.
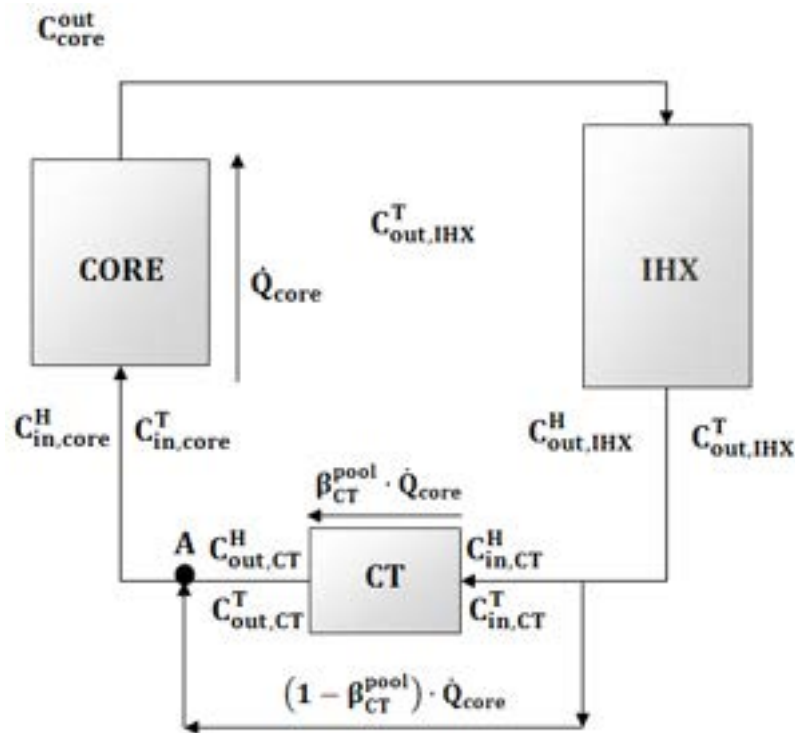
Figure Errore. Nel documento non esiste testo dello stile specificato.**-15 Cold trap arrangement in a SFR pool**

As reported in **Figure** Errore. Nel documento non esiste testo dello stile specificato.**-15**, cold traps in an SFR systems can be located both inside the pool (removing the tritium molar flow rate $\phi^{pool}_{CT}[mol/s]$ from the primary sodium coming from the IHX and entering into the core) and inside a secondary loop (removing the tritium molar flow rate $\phi^{sec}_{CT}[mol/s]$ from the secondary sodium coming from the SG and directed to the IHX). In case of sodium cold traps located inside the pool (see **Figure** Errore. Nel documento non esiste testo dello stile specificato.**-15**), a certain fraction β^{pool}_{CT} of core volume flow rate

$\dot{Q}_{core}$ flows inside a set of cold traps placed at the top of the pool, because the sodium in this region is less hot than that in the top region.

Assuming the reference configuration reported in **Figure** Errore. Nel documento non esiste testo dello stile specificato.**-15**, the hydrogen and tritium concentrations inside the sodium getting into the core and coming from the cold traps are calculated by means of steady state balances of hydrogen and tritium in the node A given by:

$$C_{in,core}^{H} = \beta_{CT}^{pool} \cdot C_{out,CT}^{H} + \left(1 - \beta_{CT}^{pool}\right) \cdot C_{out,IHX}^{H} \tag{4-4}$$

$$C_{in,core}^{T} = \beta_{CT}^{pool} \cdot C_{out,CT}^{T} + \left(1 - \beta_{CT}^{pool}\right) \cdot C_{out,IHX}^{T} \tag{4-5}$$

where $C_{out,IHX}^{H}$ and $C_{out,IHX}^{T}$ are the hydrogen and the tritium concentrations in sodium coming from IHX (coincident respectively to that of hydrogen and tritium inside sodium entering into the cold trap $C_{in,CT}^{H}$ and $C_{in,CT}^{T}$). Adopting the definition of the cold trap removal efficiency reported in Eq. (4-3), the hydrogen concentration inside the sodium directed to the core $C_{in,core}^{H}$ can be written as follows:

$$\begin{aligned} C_{in,core}^{H} &= \beta_{CT} \cdot \left[C_{out,IHX}^{H}(1 - \epsilon_{CT}) + \epsilon_{CT} \cdot C_{sat}^{H}\left(T_{cold}^{CT}\right) \right] + \left(1 - \beta_{CT}^{pool}\right) \cdot C_{out,IHX}^{H} = \\ &= C_{out,IHX}^{H}\left(1 - \beta_{CT}^{pool} \cdot \epsilon_{CT}\right) + \beta_{CT}^{pool} \cdot \epsilon_{CT} \cdot C_{sat}^{H}\left(T_{cold}^{CT}\right) \end{aligned} \tag{4-6}$$

Since the objective of this work is related to tritium and not to hydrogen content estimation in sodium, we need to find some expression to estimate tritium concentration inside sodium entering into the core $C_{in,core}^{T}$, in order to implement the correct boundary condition in the tritium mass balance equation for the core sodium. McPheeters and Raue [25] state that tritium should be precipitated with hydrogen in the cold trap in the same ratio as they exist in solution. This is the basic idea of the model for the coprecipitation mechanism. Hence it is assumed that the tritium/hydrogen ratio at the cold trap entrance is equal to that on the exit. Therefore we have:

$$\frac{C_{out,CT}^{T}(t)}{C_{out,CT}^{H}(t)} = \frac{C_{in,CT}^{T}(t)}{C_{in,CT}^{H}(t)} = \frac{C_{out,IHX}^{T}(t)}{C_{out,IHX}^{H}(t)} = \frac{C_{in,core}^{T}(t)}{C_{in,core}^{H}(t)} \tag{4-7}$$

Combining Eqs. (4-5), (4-6) and (4-7) the tritium concentration inside primary sodium entering into the core can be expressed as:

$$C_{in,core}^{T}(t) = C_{out,IHX}^{T}(t) \cdot \left[\left(1 - \beta_{CT}^{pool} \cdot \epsilon_{CT}\right) + \beta_{CT}^{pool} \cdot \epsilon_{CT} \cdot \frac{C_{sat}^{H}\left(T_{cold}^{CT}\right)}{C_{out,IHX}^{H}\left(t, T_{out,IHX}^{Na}\right)} \right] \tag{4-8}$$

In the following expression appears the term $C_{out,IHX}^H(t)$ which implies that hydrogen concentration has to be computed in the IHX primary sodium. In order to avoid this operation, it is assumed that, as a first approximation, the ratio $C_{sat}^H / C_{out,IHX}^H$ is equal to the ratio of the hydrogen Sievert's constants $K_S^{Na}(T_{cold}^{CT})$ and $K_S^{Na}(T_{out,IHX}^{Na})$ defined at the cold trap temperature T_{cold}^{CT} and at outlet temperature of primary sodium inside the IHX respectively. It is equivalent to assume that both for the saturation concentration C_{sat}^H and hydrogen concentration in primary sodium $C_{out,IHX}^H$ the Sievert's law is valid, and the hydrogen partial pressure p_{H_2} is assumed to be equal for both conditions. Hence, the inlet tritium concentration inside the core is given by:

$$C_{in,core}^T(t) = C_{out,IHX}^T(t) \cdot \left[1 - \beta_{CT}^{pool} \cdot \epsilon_{CT} \left(1 - \frac{K_S^{Na}(T_{cold}^{CT})}{K_S^{Na}(T_{out,IHX}^{Na})} \right) \right] \tag{4-9}$$

Adopting this modeling approach, the tritium retention molar rate removed from primary sodium by cold traps can be obtained combining Eqs. (4-3) and (4-7) and assuming the same hypothesis on the partial pressure constancy. Thus, the removal rate is defined as:

$$\Phi_{CT}^{pool} \left[\frac{mol}{s} \right] = \beta_{CT} \cdot \dot{Q}_{core} \cdot (C_{in,CT}^T - C_{out,CT}^T) = \beta_{CT} \cdot \dot{Q}_{core} \cdot C_{in,CT}^T \cdot \left(1 - \frac{C_{out,CT}^H}{C_{in,CT}^H} \right) =$$

$$= \beta_{CT} \cdot \epsilon_{CT} \cdot \dot{Q}_{core} \cdot C_{out,IHX}^T \cdot \left(1 - \frac{K_S^{Na}(T_{cold}^{CT})}{K_S^{Na}(T_{out,IHX}^{Na})} \right) \tag{4-10}$$

Assuming a cold trap temperature in a SFR $T_{cold}^{CT} = 121 \, ^{\circ}C$ [28] and the outlet temperature of primary sodium inside IHX $T_{out,IHX}^{Na} = 394 \, ^{\circ}C$ (value related to the Prototype Fast Breeder Reactor [39]) and considering the Sievert's constant measured by Vissers et al. [7] (see **Table** Errore. Nel documento non esiste testo dello stile specificato.**-3**), the ratio $K_S^{Na}(T_{cold}^{CT})/K_S^{Na}(T_{out,IHX}^{Na})$ is about 0.8 (0.729), which is quite similar to an effective concentration ratio $C_{sat}^H / C_{out,IHX}^H$ given by the ratio between the saturation hydrogen concentration at 121 °C (calculated as the solubility concentration at that temperature according to the expression reported in Eq. (2-4) and equal to 0.0572 wppm) and the hydrogen concentration inside primary sodium loop estimated by Kozlov [20] for a pool type 600 MW$_e$ reactor (BN-600) equal to 0.0708 wppm. In fact, with these values this ratio is equal to 0.813.

Here above was illustrated the modeling of primary sodium cold traps, but the approach remains the same for the cold traps located in the secondary loop, in which they remove a certain tritium removal rate Φ_{CT}^{sec} from secondary sodium coming from SG and entering into the IHX.

Therefore, adopting the same analytical approach, the inlet tritium concentration in the secondary sodium entering into the IHX $\left(C_{in,IHX}^{T}\right)$, can be expressed as a function of the outlet tritium concentration inside the secondary sodium coming from the SG $\left(C_{out,SG}^{T}\right)$, of the others parameters appearing in Eq. (4-9), of the outlet SG secondary sodium temperature secondary sodium $T_{out,SG}^{Na}$ and manly of the cold trapping rate operated inside the secondary loops cold traps β_{CT}^{sec}, defined by the ratio between the flow rate processed inside the secondary loop cold traps, and that flowing inside a secondary sodium loop flow rate. It can be written as follows:

$$C_{in,IHX}^{T}(t) = C_{out,SG}^{T}(t) \cdot \left[(1 - \beta_{CT}^{sec} \cdot \epsilon_{CT}) + \beta_{CT}^{sec} \cdot \epsilon_{CT} \cdot \frac{K_{S}^{Na}\left(T_{cold}^{CT}\right)}{K_{S}^{Na}\left(T_{out,SG}^{Na}\right)} \right] \tag{4-11}$$

The tritium removal rate extracted in a single secondary loop cold traps, is given by:

$$\phi_{CT}^{sec}\left[\frac{mol}{s}\right] = \beta_{CT} \cdot \epsilon_{CT} \cdot \dot{Q}_{sec}^{loop} \cdot C_{out,SG}^{T} \cdot \left(1 - \frac{K_{S}^{Na}\left(T_{cold}^{CT}\right)}{K_{S}^{Na}\left(T_{out,SG}^{Na}\right)}\right) \tag{4-12}$$

where $\dot{Q}_{sec}^{loop}[m^3/s]$ is the total volume flow rate of sodium circulating in a secondary loop.

In conclusion, the total tritium retention rate inside cold traps (both primary and secondary loop cold traps), is given by the sum of tritium removal rate extracted by both sets of cold traps and is defined as:

$$\phi_{CT}^{tot}\left[\frac{g}{y}\right] = \left(\phi_{CT}^{pool}\left[\frac{mol}{s}\right] + n_{sec}^{loop} \cdot \phi_{CT}^{sec}\left[\frac{mol}{s}\right]\right) \cdot PA_{T} \cdot N_{s}^{y} \tag{4-13}$$

where n_{sec}^{loop} is the total number of secondary loops, $PA_{T} \approx 3 \,[g/mol]$ is the tritium atomic weight and $N_{s}^{y} = 3.1536 \cdot 10^{7}\,[s/y]$ is the number of seconds per year.

Technical features of an experimental cold trap device: the AMPS cold traps

An experimental cold-trap section (AMPS) is shown schematically in **Figure** Errore. Nel documento non esiste testo dello stile specificato.**-16** and a detailed view of sodium flowing section is reported in **Figure** Errore. Nel documento non esiste testo dello stile specificato.**-17**.
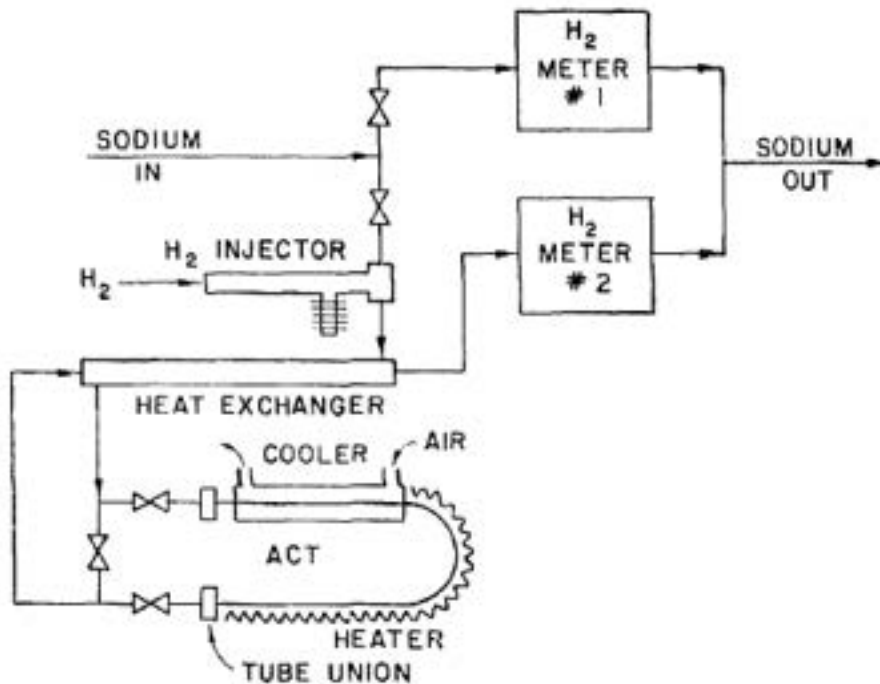
Figure Errore. Nel documento non esiste testo dello stile specificato.**-16 Flow diagram of experimental cold trap section [29]**
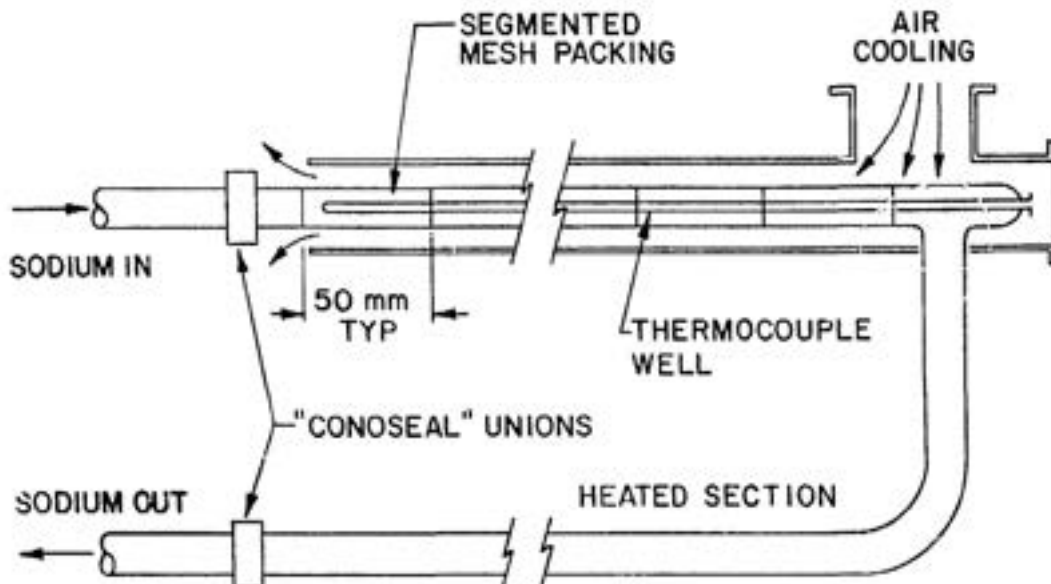
Figure Errore. Nel documento non esiste testo dello stile specificato.**-17 Detailed view of the sodium flowing section of a cold traps [29]**

The cold-trap used in this experimental device was of an integral economizer-crystallizer design with the economizer located in the upper half of a vertical pipe 16 mm O.D. x 7.1 nm wall thickness] and the crystallizer region In the lower half. Sodium flowed into the top of the cold trap,

downward through the economizer into the annulus of the crystallizer region. The crystallizer was packed with stainless-steel wire mesh and was air-cooled on the outer surface. The sodium continued up the center section of the crystallizer, through the economizer, and out the top of the cold trap. Temperature control was maintained by varying the input to heaters on the external surface of the cold trap while the air coolant flow was maintained constant. The volume of the crystallizer region was 9300 cm^3.

This test apparatus processes a small sodium flow rate of order of ∿ 10 g/sec [29] preleving from a main circulation circuit where a mass flow rate of 1.1 kg/sec circulates [29].

For our modeling contest the mass flow rate circulating inside the cold traps of operative SFR plants was not found in literature, but, as already mentioned, the cold traps should remove from the primary sodium at least the 90 % of total tritium release rate from fuel and boron. Thus, the sodium flow rate inside the cold traps should ensure this removal rate but it must pay attention to the sodium residence time inside the cold trap which influences the hydrogen removal efficiency as reported by McPheeters and Raue [25]. In **Figure** Errore. Nel documento non esiste testo dello stile specificato.**-18** is reported a plot showing the experimental results of the hydrogen removal efficiency as a function of the sodium residence time. This is quite obvious because the higher is the residence time and the larger is the possibility of tritium to be retained inside the cold trap. Therefore the sodium mass flow rate to be circulated inside cold traps has un upper limit given by the residence time and a lower limit fixed by the tritium removal rate. In order to guarantee a sufficiently high flow rates and residence times inside the cold trap a set of many in-parallel cold traps should adopted.

As already mentioned, cold trapping of sodium is an efficient method to remove hydrogen and tritium from sodium, but some problems may arise. In fact, in order to guarantee a suitable reliability during the lifetime, an hydrogen cold trap needs to be cooled, and this is a crucial point from engineering point of view, because it may be problematic to cool down a certain liquid sodium flow rate from about 400 °C to temperature values of order of 121 °C [28], necessary to have precipitation.
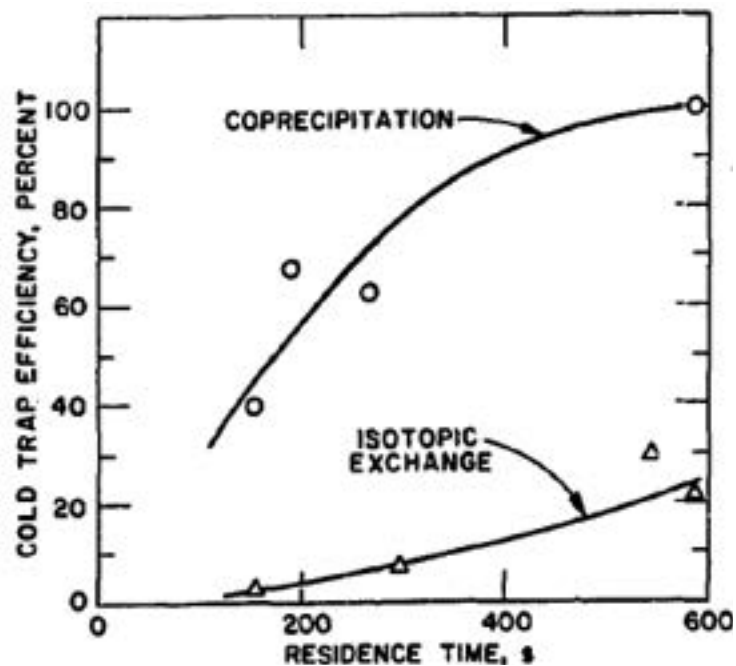
Figure Errore. Nel documento non esiste testo dello stile specificato.**-18 Cold-trapping efficiencies for coprecipitation and isotope exchange experiments [25]**

Moreover, a problem was discovered that could greatly reduce the attractiveness of the cold-trapping method for reactor sodium systems. This problem arises from water-side corrosion of the steam-generator tubes which releases hydrogen that diffuses through the tubes into the sodium system. Measurements of this corrosion rate and the resulting hydrogen source term with both experimental systems and full-scale reactor systems [29] have shown that the hydrogen source is so large that the capacity of the cold trap to retain the sodium hydride may be exceeded within one year of full-power reactor operation [29].

Results and discussions

Introduction

The tritium permeation barriers and the cold trap features were illustrated, from the theoretical and technical point of view in the two previous sections, and in the previous chapter a mathematical model, whose objective is to simulate the tritium transport in a SFR system, was developed and described. This model was implemented in a computational code called SFR-TPC, which will be used hereafter to perform a parametric study of the two tritium transport mitigation techniques

adopted in SFRs (permeation barriers and cold traps employment) necessary to reduce as low as reasonable achievable (ALARA) the tritium losses into the environment.

This parametric study is aimed to evaluate the behavior of total tritium losses and the total tritium inventory by varying the most influencing parameters, especially those related to tritium transport mitigation devices. After many simulations and according to the illustration of tritium permeation barriers and cold traps features, three essential parameters were individuated as the most influencing ones and they are:

- the permeation reduction factor on SG tubes $\left(PRF_{tube}^{SG}\right)$;
- cold trapping rate ratio β_{CT}^{pool} (ratio between the cold trapping rate inside primary sodium cold trap Q_{CT}^{pool} and the total core flow rate Q_{core});
- cold traps hydrogen removal efficiency (ϵ_{CT}).

The objective thus is to analyze the response in term of tritium losses and inventories coming from the variation of these parameters in a suitable range.

The current analysis was carried on an under construction prototype reactor, the Prototype Fast Breeder Reactor (PFBR) [37-43] since a large quantity of information are available for this reactor, and its typology (pool type design) is similar to that of other operating and dismissed reactors about which tritium measurements were carried out and therefore are known (e.g., Super-Phénix).

General description of the Prototype Fast Breeder Reactor (PFBR)

PFBR is a 500 MW_{elc} unit designed by Indira Gandhi Centre for Atomic Research, Kalpakkam. It is a sodium cooled, mixed oxide (MOX) fuelled, pool type fast reactor. The core thermal power is 1253 MW and the gross electrical output is 500 MW_{elc}. The reactor is located at Kalpakkam, 500 m south of Madras Atomic Power Station (MAPS). Kalpakkam is 60 km south of Chennai on the coast of Bay of Bengal. India started fast breeder reactor (FBR) program by constructing a $40\,MW_{th}/13.5\,MW_{elc}$ loop type fast breeder test reactor (FBTR) at Kalpakkam, which is in operation since 1985. This was followed by the design and development of PFBR.

The overall flow diagram is shown in **Figure** Errore. Nel documento non esiste testo dello stile specificato.**-19**. The nuclear heat generated in the core is removed by circulating sodium from cold pool at 670 K to the hot pool at 820 K [45]. The sodium from hot pool after transporting its heat to four intermediate heat exchangers (IHX) mixes with the cold pool. The circulation of sodium from

cold pool to hot pool is maintained by two primary sodium pumps and the flow of sodium through IHX is driven by a level difference (1.5m of sodium [45]) between the hot and cold pools. The heat from IHX is in turn transported to 8 steam generators [45] by sodium flowing in the secondary circuit. Steam produced in SG is supplied to turbo-generator [45].
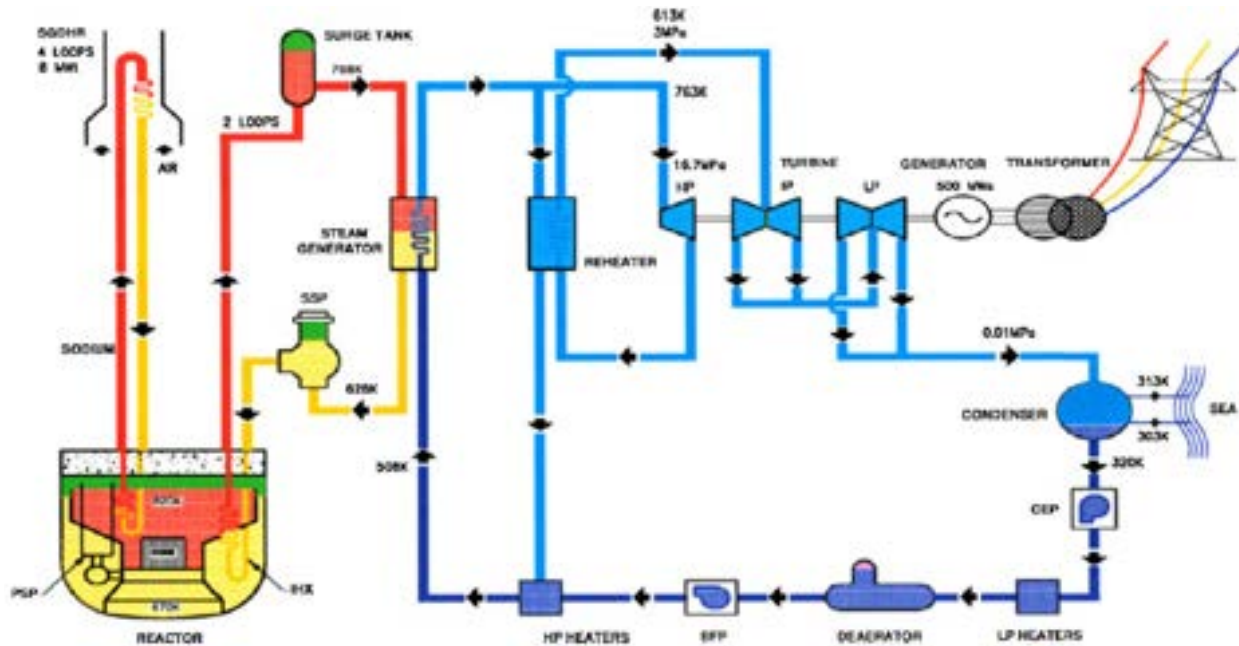
Figure Errore. Nel documento non esiste testo dello stile specificato.**-19PFBR Flow sheet [45]**

The main vessel (12.9 m diameter), is supported at the outer shell of the roof slab. The height of main vessel from the roof slab junction is 12.54 m. The vessel contains ~1150 tonnes of sodium.

SFR-TPC numerical input data for the simulation

In order to run the code a variety of input data must be inserted in it. In fact, the code needs geometrical and thermalhydraulics data of core, pool IHX and SG (e.g., heat transfer length, tube thickness and tubes number, pool and core assembly diameters, pool and core assembly heights and pool thickness), IHX and SG tubes materials, thermalhydraulics data (i.e., inlet and outlet temperatures, mass flow rates, etc) and other numerical settings (e.g., ODE MATLAB solver, number of finite volumes inside the IHX and the SG and relative and absolute tolerance of the adopted ODE solvers [26]). All numerical data adopted for the simulations [21] of the code are reported hereafter. The numerical input data for the PFBR core and for the pool are reported in **Table** Errore. Nel documento non esiste testo dello stile specificato.**-13** and in **Table** Errore. Nel documento non esiste testo dello stile specificato.**-14** respectively.

Parameter	Tag	Value
Thermal Power	$P_{th}[MW_{th}]$	1250
Inlet core Temperature	$T_{in}^{core}[°C]$	397
Outlet core Temperature	$T_{out}^{core}[°C]$	547
Sodium mass flow rate	$\dot{W}_{core}[kg/sec]$	6800
Fuel assembly diameter	$D_{FA}[m]$	6.35
Fuel assembly height	$H_{FA}[m]$	4.50
Volume Fraction of Sodium inside FA	χ_{Na}	0.368

Table Errore. Nel documento non esiste testo dello stile specificato.**-13 SFR-TPC Core Input Data for PFBR**

Parameter	Tag	Value
Pool material	–	SS_316L
Permeation Reduction Factor	PRF_{pool}	1
Main pool diameter	$D_{pool}[m]$	12.9
Main pool height	$H_{pool}[m]$	12.9
Main pool thickness	$t_{pool}[cm]$	2.5
Fraction of total core flow rate flowing inside primary loop cold traps	β_{CT}^{pool}	0
Cold trap efficiency	ϵ_{CT}	0

Table Errore. Nel documento non esiste testo dello stile specificato.**-14 SFR-TPC pool input data for PFBR**

SFR-TPC input data for PFBR IHX are listed in **Table** Errore. Nel documento non esiste testo dello stile specificato.**-15**.

Parameter	Tag	Value
IHX tube material	–	SS_316L
IHX shell material	–	SS_316L
Permeation reduction Factor of Tube	PRF_{tube}^{IHX}	1
Permeation reduction Factor of Shell	PRF_{shell}^{IHX}	1
Primary Sodium mass flow rate	$\dot{W}_{prim}^{IHX}[kg/sec]$	1649
Secondary Sodium mass flow rate	$\dot{W}_{sec}^{IHX}[kg/sec]$	1450
Inlet Primary Sodium Temperature	$T_{in,prim}^{IHX}[°C]$	544

Outlet Primary Sodium Temperature	$T^{IHX}_{out,prim}[°C]$	394
Inlet Secondary Sodium Temperature	$T^{IHX}_{in,sec}[°C]$	355
Outlet Secondary Sodium Temperature	$T^{IHX}_{out,sec}[°C]$	525
Outer tube diameter	$d^{IHX}_{out}[mm]$	19
Tube Thickness	$t^{IHX}_{tube}[mm]$	0.8
Shell Outer Diameter	$D_{IHX}[m]$	1.96
Outer Diameter of IHX Down-Comer	$D^{IHX}_{DC}[cm]$	40
Shell Thickness	$t^{IHX}_{shell}[mm]$	20
Heat Transfer Length	$L^{IHX}_{HT}[m]$	7.5
Number of tubes	n^{IHX}_{tube}	3600
Total number of IHX	n_{IHX}	4
Number of IHX per loop	n^{loop}_{IHX}	2

Table Errore. Nel documento non esiste testo dello stile specificato.-15 SFR-TPC IHX Input Data for PFBR

The steam generator (SG) is a shell and tube type of heat exchanger. In this exchanger, hot liquid sodium enters into the shell side through an inlet nozzle. It rises up in the annular space, enters into the window region of the tube bundle and flows downward. Water flows on tube side.

SG input data for SG PFBR configuration are listed in **Table** Errore. Nel documento non esiste testo dello stile specificato.**-16.**

Parameter	Tag	Value
SG Tube Material	–	INCOLOY 800
SG Shell Material	–	INCOLOY 800
Permeation Reduction factor of tube	PRF_{tube}^{SG}	1
Permeation Reduction factor of Shell	PRF_{shell}^{SG}	1
Water Mass Flow Rate in a single SG	$W_w^{SG}[kg/sec]$	70
Secondary Sodium mass flow rate	$W_{sec}^{SG}[kg/sec]$	725
Inlet Water Temperature	$T_{in}^w[°C]$	235
Outlet Water Temperature	$T_{out}^w[°C]$	493
Inlet Secondary Sodium Temperature	$T_{in,sec}^{SG}[°C]$	525
Outlet Secondary Sodium Temperature	$T_{out,sec}^{SG}[°C]$	355
Steam Pressure	$p_w[MPa]$	17.2
Inlet Hydrogen Concentration	$C_{H_2}^{in}[mol_{H_2}/m^3]$	10^{-4}
Outer tube diameter	$d_{out}^{SG}[mm]$	17.2
Tube Thickness	$t_{tube}^{SG}[mm]$	2.3
Shell Outer Diameter	$D_{SG}[m]$	0.8
Shell Thickness	$t_{shell}^{SG}[mm]$	15
Heat Transfer Length	$L_{HT}^{SG}[m]$	24.7
Economizer Heat Transfer Length	$L_{HT}^{eco,SG}[m]$	5
Evaporator Heat Transfer Length	$L_{HT}^{eva,SG}[m]$	15
Super-heater Heat Transfer Length	$L_{HT}^{sh,SG}[m]$	4.7
Number of tubes	n_{tube}^{SG}	547
Total number of SG	n_{SG}	8
Number of SG per loop	n_{SG}^{loop}	4
Fraction of total core flow rate flowing inside secondary loop cold traps	β_{CT}^{sec}	0

Table Errore. Nel documento non esiste testo dello stile specificato.**-16 SFR-TPC SG Input Data for PFBR**

Although the choice of the candidate materials for this application was directed to modified P91 ferritic martensitic steel [40], Incoloy 800 (already used for SuperPhénix [2]) ensures more accuracy in permeation parameters because hydrogen permeability of Incoloy 800 was has been investigated markedly, while hydrogen permeability in ferritic steels can be influenced by many factors (i.e., the trapping [46] or the composition [47] which can be variable depending on the adopted type of ferritic steels).

Numerical settings for our simulation are reported in **Table** Errore. Nel documento non esiste testo dello stile specificato.**-17**. All listed values are arbitrary and chose by the user of the code, thus, they do not require any reference, but they are only related to the user exigencies.

Parameter	Tag	Value
Number of Finite Volumes into IHX	n_{FV}^{IHX}	100
Number of Finite Volumes into SG	n_{FV}^{SG}	200
Solver	—	ode23tb
Absolute Tolerance	Tol_{abs}	10^{-7}
Relative Tolerance	Tol_{rel}	10^{-8}
Initial Time Step of Computation	$\Delta t_{init}[sec]$	10^{7}
Final Computation Time	$t_{fin}[sec]$	10^{8}

Table Errore. Nel documento non esiste testo dello stile specificato.**-17 SFR-TPC Numerical Input Settings for PFBR**

The above table shows different values related to numerical analysis issues, such as number of volume discretization, numerical solver, and tolerances. The *ode23tb* solver was observed to be the most accurate and fastest in tritium analysis, because it is a multistep method solver and it applies a suitable numerical method for stiff problems resolution [26].

Results and discussions without permeation barriers and cold traps

After this complete list of numerical values inserted inside SFR-TPC, the code is ready to be started. The typologies of available output plots are different (e.g., tritium concentration evolutions and distributions, tritium partial pressures evolutions and distributions, tritium losses, tritium inventories, and other auxiliary plots); for this reason we are going to report only the most relevant plots.

Before starting with the parametric study of the permeation barriers and of the cold traps, it might be useful to report some tritium losses and inventory results obtained without any mitigation measures (i.e., $PRF_{tube}^{SG} = 1$, $\beta_{CT}^{pool} = 0$, $\beta_{CT}^{sec} = 0$ and $\epsilon_{CT} = 0$) which corresponds to the worst scenario in terms of radiological risks related to tritium. The idea of this section is also to give an idea to the reader of all available outputs of the code.

As already mentioned, the code must elaborate different materials properties which are expressed as functions of temperature before staring the integration of the differential equations. Therefore a computation of the temperature distributions is necessary. The calculation approach is quite simplified and is based on inlet and outlet temperature of both fluids operating inside the IHX and the SG and, adopting some simplifying hypothesis [21], the steady state energy conservation law is solved, giving the temperature distribution of hot and cold fluids of both the IHX and the SG. The average tubes temperature distribution is calculated as the average value between hot and cold fluid temperatures. In **Figure** Errore. Nel documento non esiste testo dello stile specificato.**-20** are reported all temperature profiles along z_{IHX} and z_{SG}..
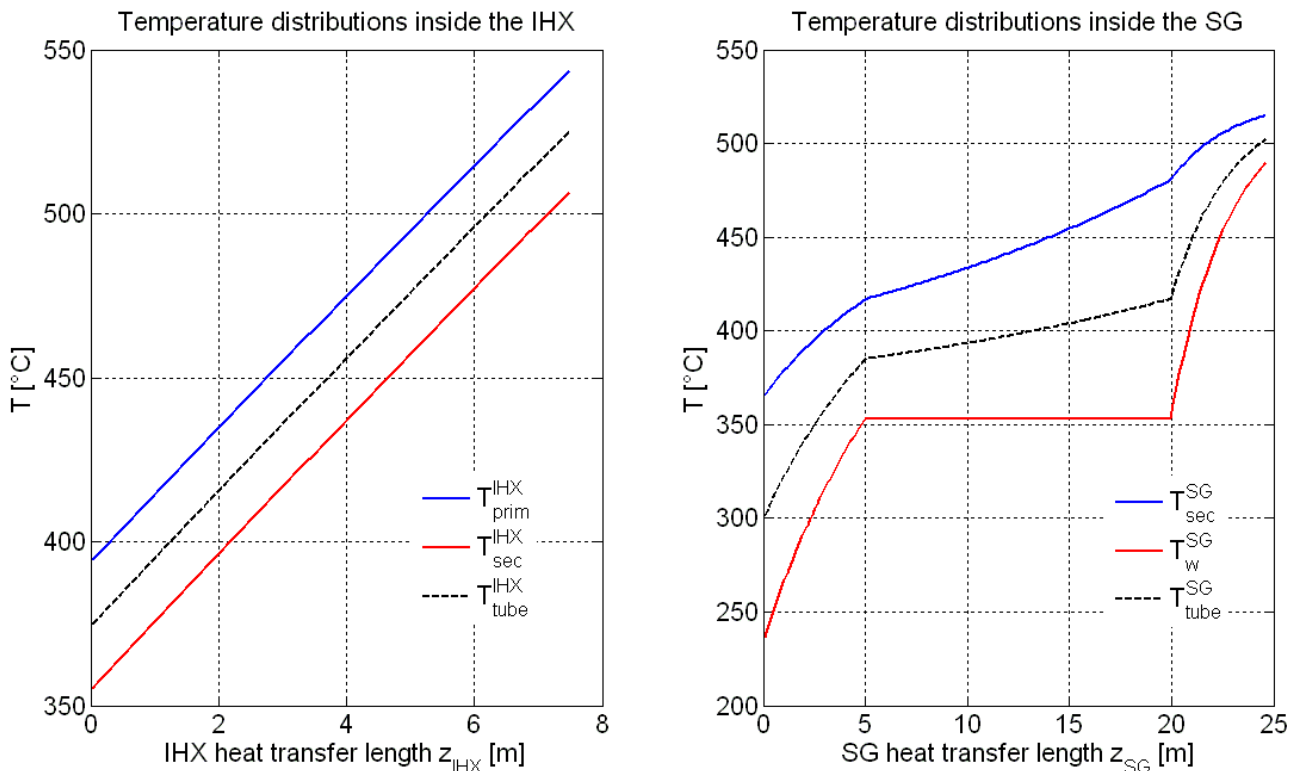
Figure Errore. Nel documento non esiste testo dello stile specificato.**-20 SFR-TPC Temperature profiles Vs space inside PFBR**

The assumption of a certain temperature profile is quite important, because the tritium permeabilities can vary of about one order of magnitudes in the operative temperature ranges (see **Figure** Errore. Nel documento non esiste testo dello stile specificato.**-12**).

In **Figure** Errore. Nel documento non esiste testo dello stile specificato.**-21** are reported the average tritium concentrations inside the primary sodium, secondary sodium and water. The term "average" means that an average value was calculated starting from a spatial tritium concentration distribution along the IHX and SG heat transfer coordinates (z_{IHX} and z_{SG} respectively), computed by the code, which computes the concentrations behavior in space and time giving the generic tritium concentration $C_{i,j,k}(z_k, t)$ (see par. 0).
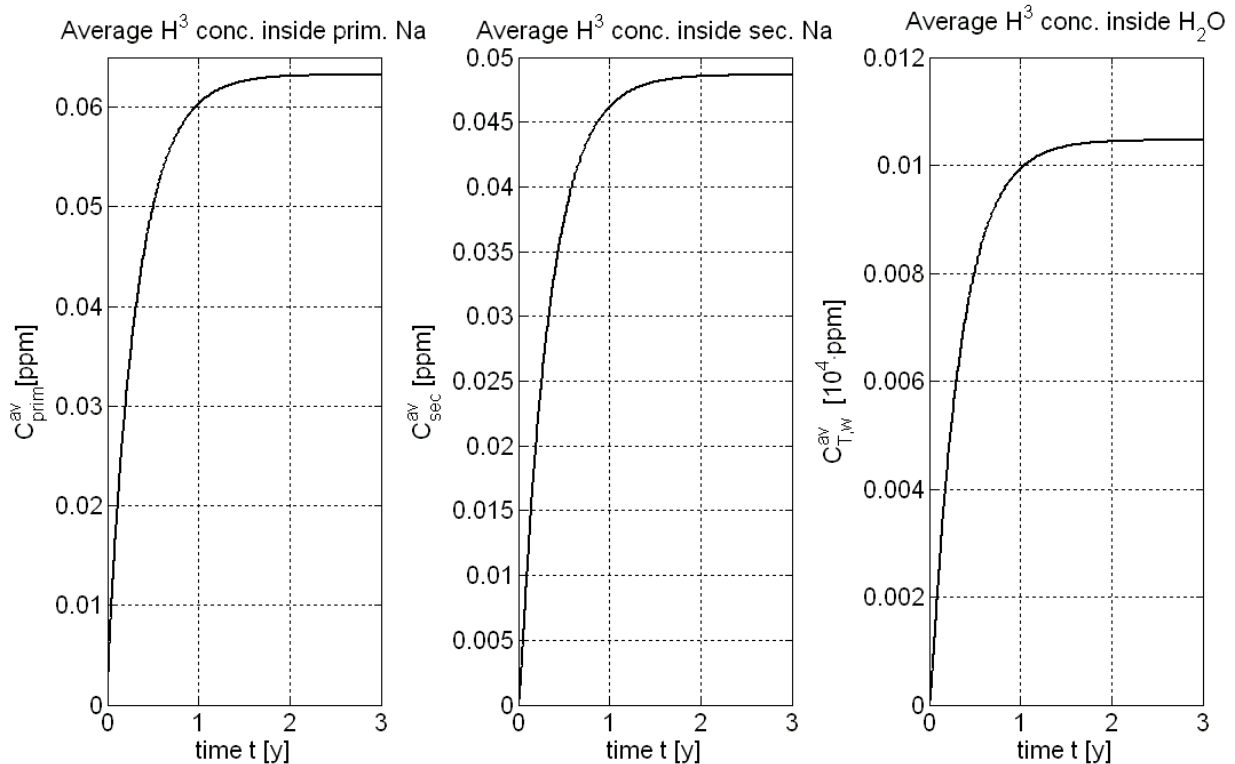
Figure Errore. Nel documento non esiste testo dello stile specificato.**-21 SFR-TPC Average tritium concentrations inside PFBR Vs time**
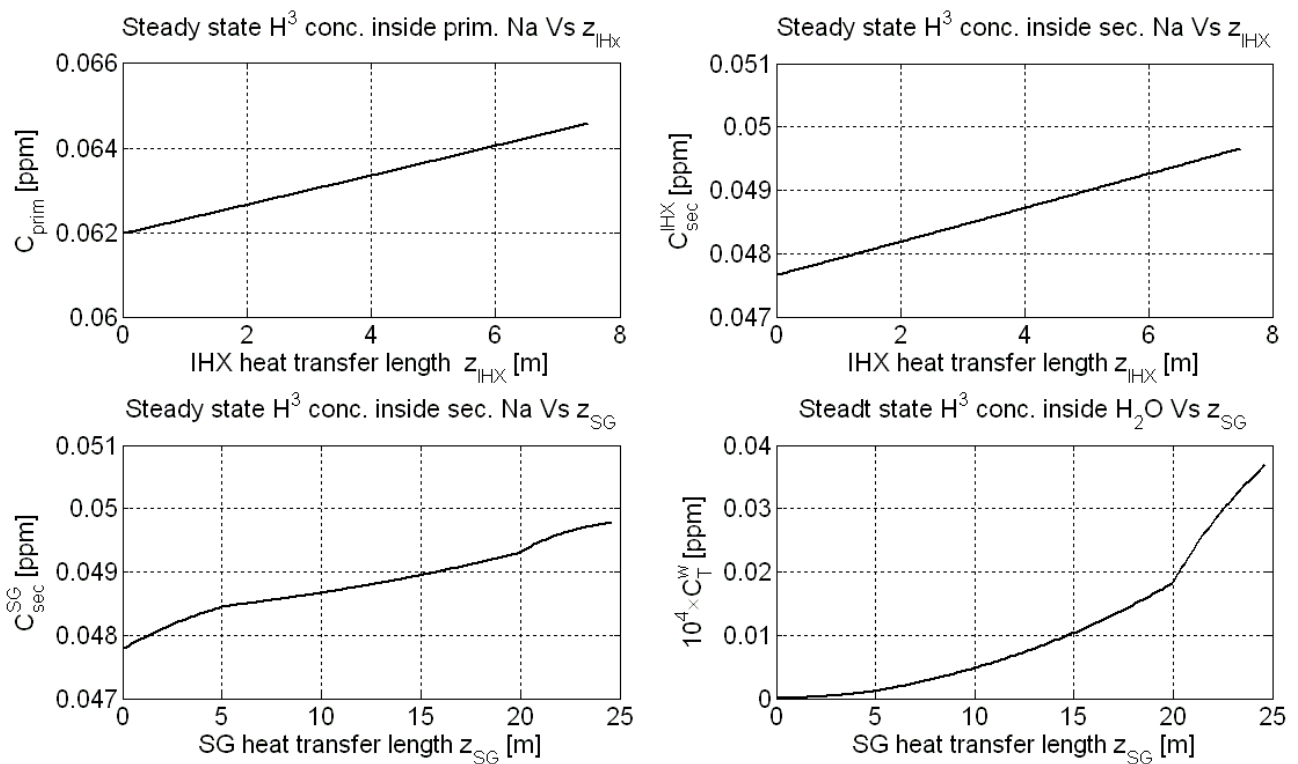$(\beta_{CT}^{pool} = 0, \beta_{CT}^{sec} = 0, \epsilon_{CT} = 0, PRF_{tube}^{SG} = 1)$

Observing the above graph, it can be seen that the tritium concentrations in sodium and water differ by four order of magnitudes. This means that hydrogen (or tritium) in water has an high dilution and the tritium removal by water could results a complicate and an uneconomic operation; therefore, as a first approximation, the tritium concentration in water can be neglected since it is very low compared to those in sodium, even at the worst scenario (no cold traps and permeation

barriers were present during this simulation). Moreover, the tritium concentration in water, in this plot, is meant as the total tritium concentration, which is given by the sum of the average HT and HTO concentrations computed by the code and averaged on the space coordinate z_{SG}.

From the tritium concentration values in sodium reported in the above plot, arises the confirm of the coprecipitation mechanisms principle (see par. 0) based on the idea that tritium concentration in primary sodium (the maximum one) will never reach the saturation value; therefore the tritium precipitation occurs only with hydrogen precipitation. In this simulation maximum tritium concentration ($\approx$ 0.06 ppm = 0.0026 wppm) does not approach neither the saturation concentration at cold temperature concentration (0.0576 wppm at 121°C).

In **Figure** Errore. Nel documento non esiste testo dello stile specificato.**-22** are reported the steady state tritium concentrations distribution along heat transfer tubes coordinates z_{IHX} and z_{SG}.

Figure Errore. Nel documento non esiste testo dello stile specificato.**-22 SFR-TPC Steady state tritium concentrations inside PFBR Vs heat transfer lengths**
($\beta_{CT}^{pool} = 0$, $\beta_{CT}^{sec} = 0$, $\epsilon_{CT} = 0$, $PRF_{tube}^{SG} = 1$)

Since numerical values are quite similar to those reported in **Figure** Errore. Nel documento non esiste testo dello stile specificato.**-21** at the steady state, what is interesting in this plot is the behavior of the curves. In fact, while in the IHX tritium concentrations are about linear along z_{IHX}, this is not true

for concentrations distributions inside the SG water, in which the inclination (or the gradient) of concentrations changes along z_{SG}. This fact is due to the change of constitutive law along z_{SG}, because water changes phase along it, and therefore the correlation between tritium concentration and partial pressure changes too (see par. 0) ranging from the Henry's law in the liquid water region (about in $z_{SG} = [0 \text{ m}, 5 \text{ m}]$) to the Dalton's law in the superheated steam region (about $z_{SG} = [20 \text{ m}, 25 \text{ m}]$).

Moreover, the increasing trend of all reported curves makes sense because inside the IHX sodium comes from the top $(z_{IHX} = L_{HT}^{IHX} = 7.5 \text{ m})$ and falling down through the IHX shell decreases its tritium concentrations, yielding a certain tritium flux to the secondary sodium that, on the contrary, flows from the bottom to the top of the IHX through the tubes side. The same mechanism is verified inside the SG, where the water comes from the bottom $(z_{SG} = L_{HT}^{SG} \approx 25 \text{ m})$ and goes up through the SG tubes and it is heated up by the secondary sodium that flows through the shell and falls down. If we observe the numerical values reported in the graph, we note that, at the steady state, the variation of tritium concentrations in sodium are quite low with respect to those in water, because it is supposed to enter into the SG free of tritium atoms and thus the tritium concentration in water along z_{SG} ranges between zero and that at the exit.

In order to complete the illustration of tritium concentration profiles along heat transfer coordinates, in **Figure** Errore. Nel documento non esiste testo dello stile specificato.**-23** are reported the HT and HTO concentrations distributions along z_{SG}.

Figure Errore. Nel documento non esiste testo dello stile specificato.**-23 SFR-TPC Steady state HT and HTO concentrations Vs SG heat transfer length**
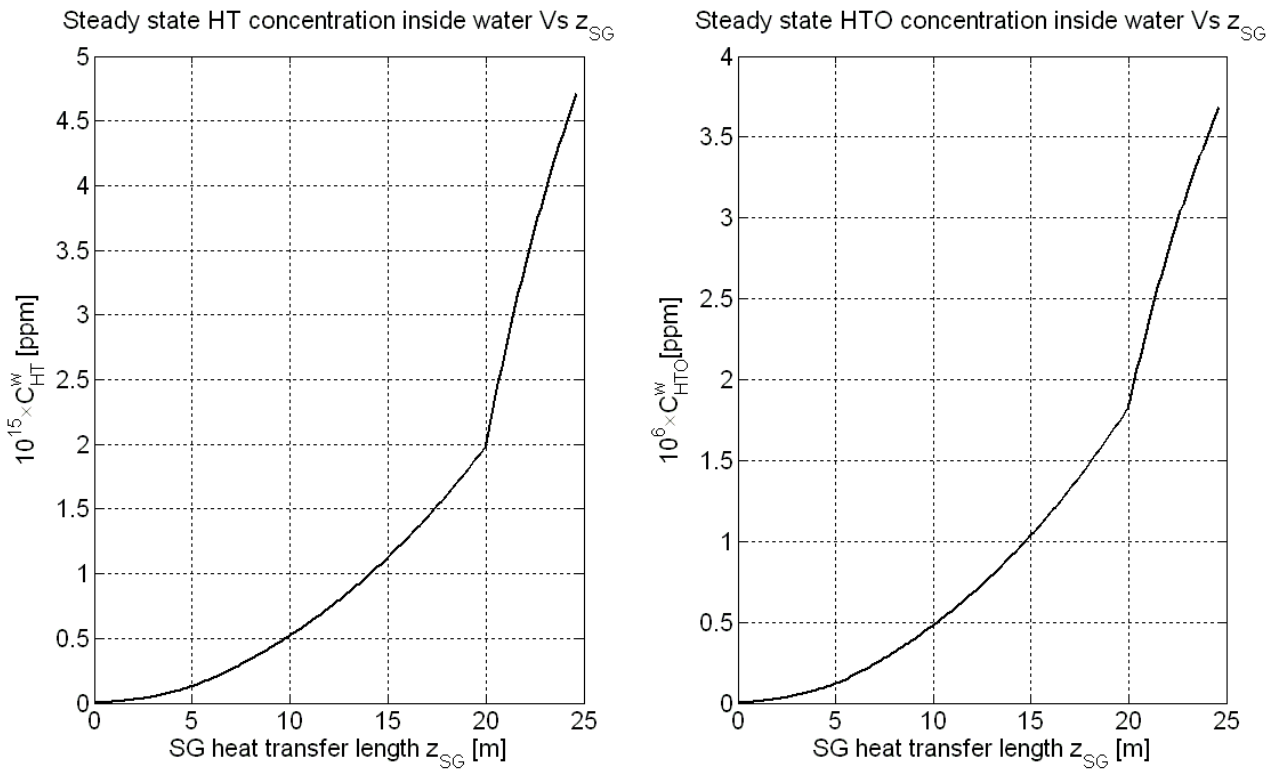$(\beta_{CT}^{pool} = 0, \beta_{CT}^{sec} = 0, \epsilon_{CT} = 0, PRF_{tube}^{SG} = 1)$

The concentrations inside water, as shown in the above figure, is almost totally attributed to HTO contributions, since values of HTO concentrations are comparable with those of HT larger of nine orders of magnitudes. The HTO concentration in water is much larger than that of HTO because of the net offset of chemical equilibrium written in (2-1), which is mostly shifted to the product direction. The partial pressure here will be not reported.

Since the objective of this work remains to evaluate tritium losses and inventories, in **Figure** Errore. Nel documento non esiste testo dello stile specificato.**-24** are reported the total tritium losses $\phi_{tot}[g/y]$ (see Eq. (3-10) and par. 0) and consequently **Figure** Errore. Nel documento non esiste testo dello stile specificato.**-25** the total tritium inventory $I_{tot}[g]$ (see Eq. (3-22) and par. 0) obtained by running the code avoiding the utilization of the cold traps and considering the IHX and SG tubes to be coated with any permeation barrier.
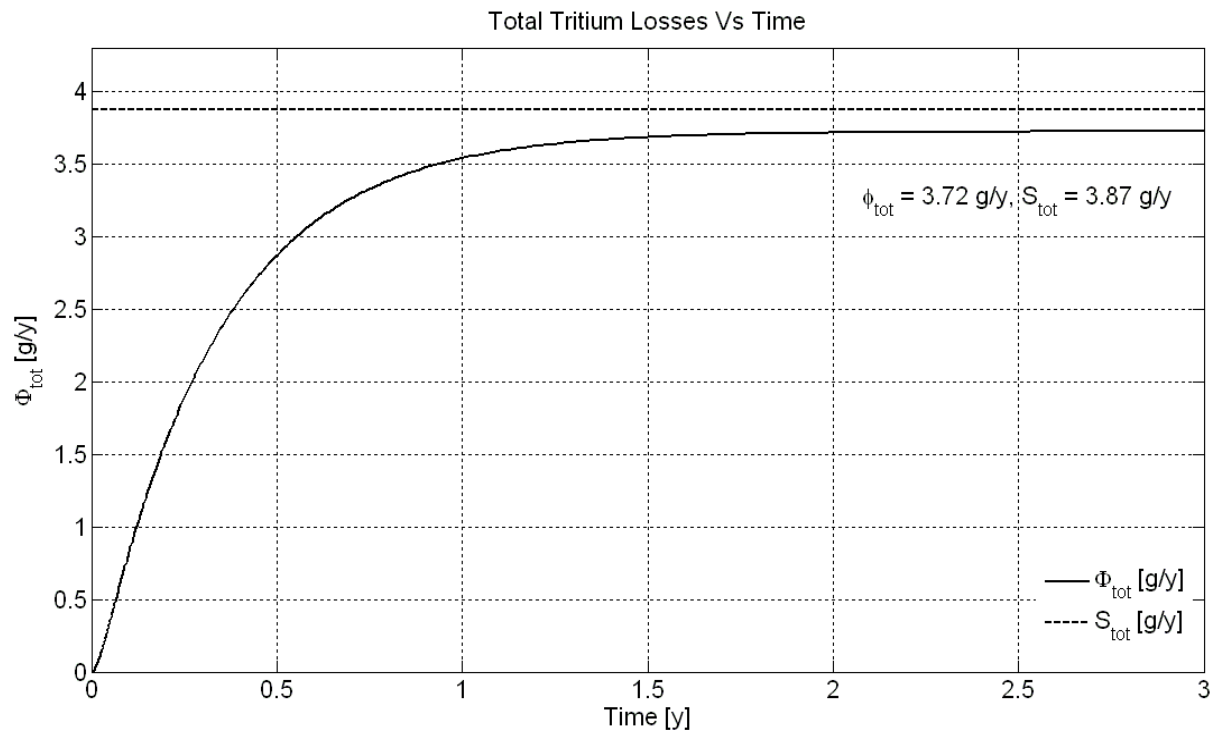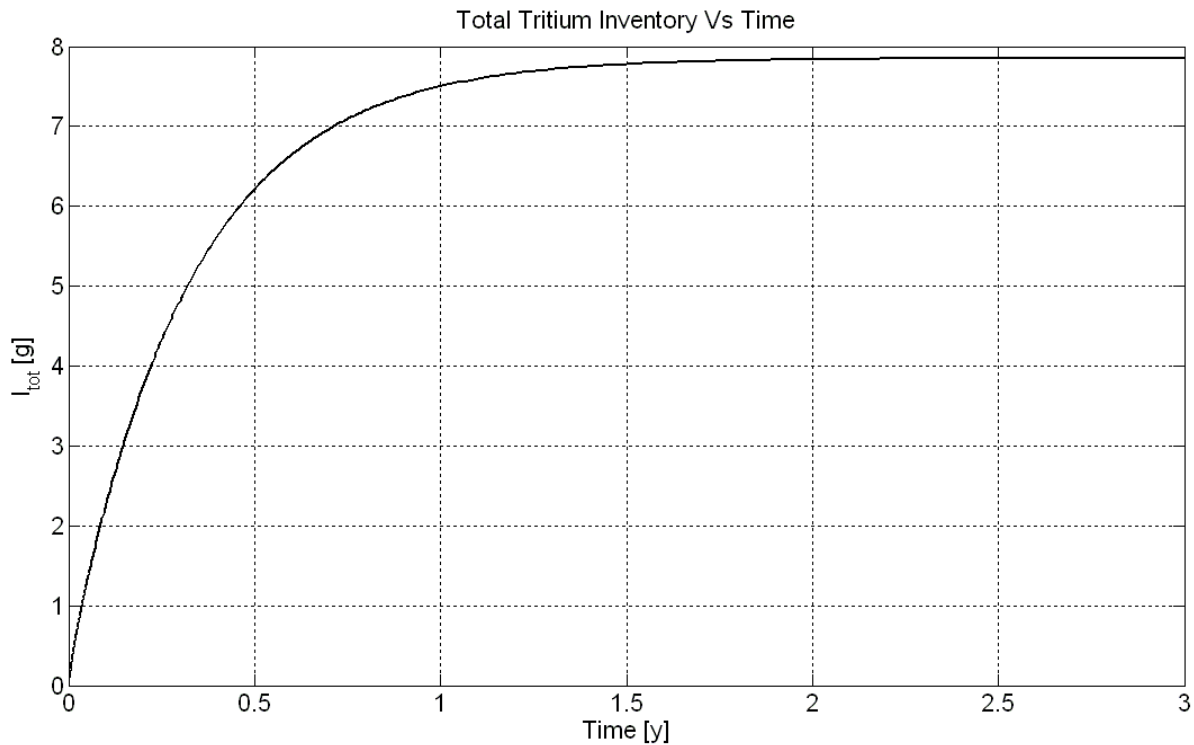
Figure Errore. Nel documento non esiste testo dello stile specificato.**-24 SFR-TPC Total Tritium Losses from PFBR Vs time ($\beta_{CT}^{pool} = 0$, $\beta_{CT}^{sec} = 0$, $\epsilon_{CT} = 0$, $PRF_{tube}^{SG} = 1$)**

Figure Errore. Nel documento non esiste testo dello stile specificato.**-25 SFR-TPC Total Tritium Inventory inside PFBR Vs time ($\beta_{CT}^{pool} = 0$, $\beta_{CT}^{sec} = 0$, $\epsilon_{CT} = 0$, $PRF_{tube}^{SG} = 1$)**

From **Figure** Errore. Nel documento non esiste testo dello stile specificato.**-24** arises the fundamental aspect of the current work, because, as shown in the graph, the total tritium losses at steady state are equal to 3.73 g/y which correspond to the 96 % of total tritium release rate into the primary sodium (S_{tot} = 3.87 g/y). This is a clear indicator that mitigation techniques are absolutely necessary in order to retain inside the plant a significant and suitable tritium portion, with respect to the total amount reaching the primary sodium from the core. Moreover the above results are in accordance with those founded by Taylor [28] (whose model was develop to estimate the tritium quantity escaping into the water/steam system as a function of the purification rate of primary and secondary coolant). In fact these results show that the percentages of tritium calculated to be released into the steam system was about the 98% of total generated tritium, which is quite similar to the SFR-TPC results.

From the tritium inventory plot it is possible to note that at steady state this quantity amounts to about 8 g of tritium. This quantity is not so worrying from the radiological point of view because it is referred to the total tritium amount inside the entire SFR plant. Moreover it comes from some conservative assumptions (i.e., tritium concentration inside the sodium contained into the pool it is supposed to be equal to that inside core sodium). However, tritium inventories inside sodium and

steels may increase if some permeation barriers (i.e., $PRF_{tube}^{SG} > 1$) are foreseen, as expected. As already mentioned in par. 0, tritium inventories inside cold traps were calculated into the code because cold traps after a certain operation period, must be restored or plugged; therefore, adopting the cold traps inside primary and secondary loops, tritium inventories inside sodium would decrease. However, tritium flux retained inside cold trap is a key parameter in order to quantity the effects of cold traps on tritium losses reductions. In general tritium inventory inside a fission plant does not constitute a big concern, unlike fusion reactors where tritium amount cycling inside fusion power plant is quite larger than a fission one. For this reason the parametric study in this work is mainly devoted to evaluate tritium losses instead of tritium losses.

**Results and discussion with permeation barriers and cold traps**

As already discussed, it is interesting to assess the evolution of tritium losses and inventory versus the variation of the parameters and to determine what sets of parameters could allow satisfying the target, which is to get a significant reduction of tritium losses from the maximum value (3.72 g/y = 96 % of total tritium source) to more suitable and less worrying values (i.e., retaining more than 90 % of fission-generated tritium, or reducing tritium losses under a certain fixed value or imposing a maximum value on tritium concentration inside water). This reduction would come from the two main tritium transport mitigation techniques already discussed in pars.0 and 0.

The two basic tritium transport mitigation techniques are given by the permeation barriers providing a certain permeation reduction factor (PRF), and the employment of a set of sodium cold traps inside the pool sodium and the secondary sodium, able to process the operative volume flow rates of sodium $\dot{Q}_{CT}^{pool}$ and $\dot{Q}_{CT}^{sec}$ respectively (expressed by means of the fraction of the core volume flow rate β_{CT}^{pool} and the fraction of the secondary loop volume flow rate β_{CT}^{sec}) with an efficiency ϵ_{CT} (see Eq. (4-3)).

As reported in the introduction of this section, three essential parameters were individuated as the most influencing ones:

- the permeation reduction factor on SG tubes $\left(PRF_{tube}^{SG}\right)$;
- cold trapping rate ratio β_{CT}^{pool} (ratio between the cold trapping rate inside primary sodium cold trap Q_{CT}^{pool} and the total core flow rate Q_{core});
- cold traps hydrogen removal efficiency $\left(\epsilon_{CT}\right)$.

In **Figure** Errore. Nel documento non esiste testo dello stile specificato.**-26** is reported the total tritium losses evolution varying the PRF inside the SG tubes $\left(\text{PRF}_{tube}^{SG}\right)$ considering the typical PRFs listed in **Table** Errore. Nel documento non esiste testo dello stile specificato.**-12** varying between 10 to 400 for Incoloy 800.
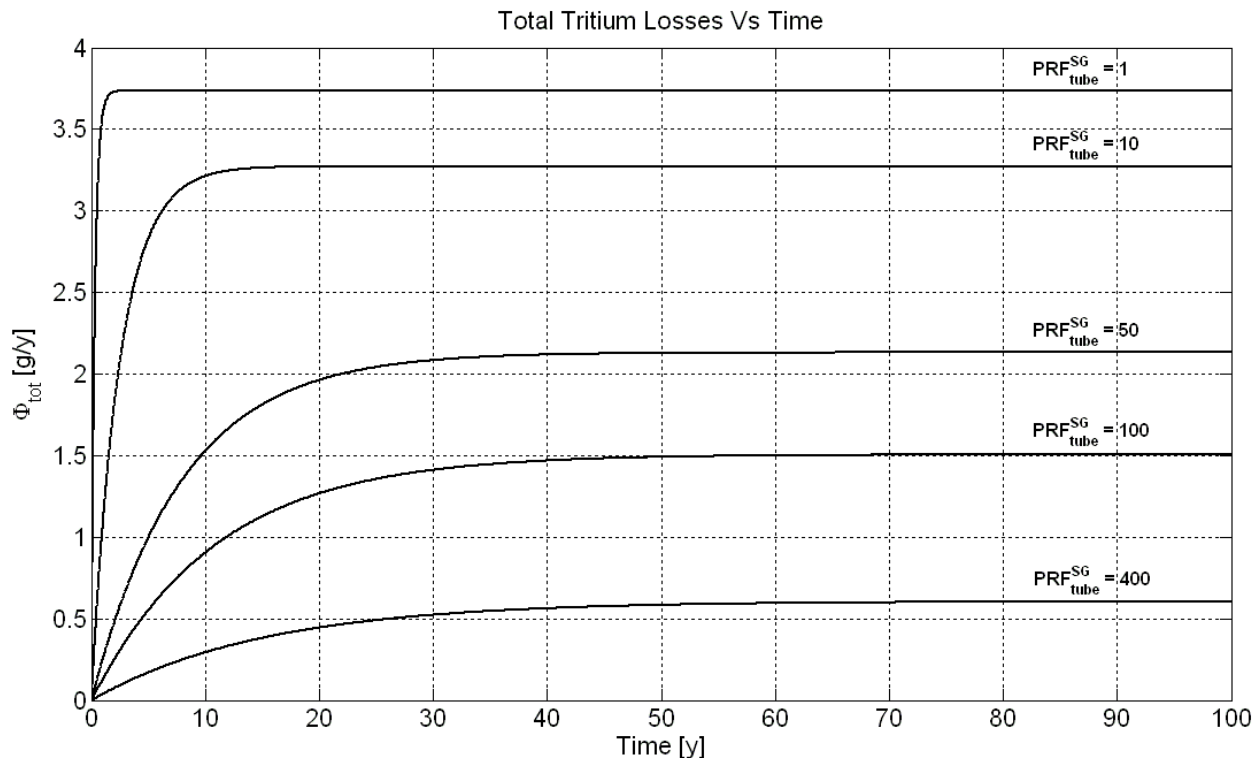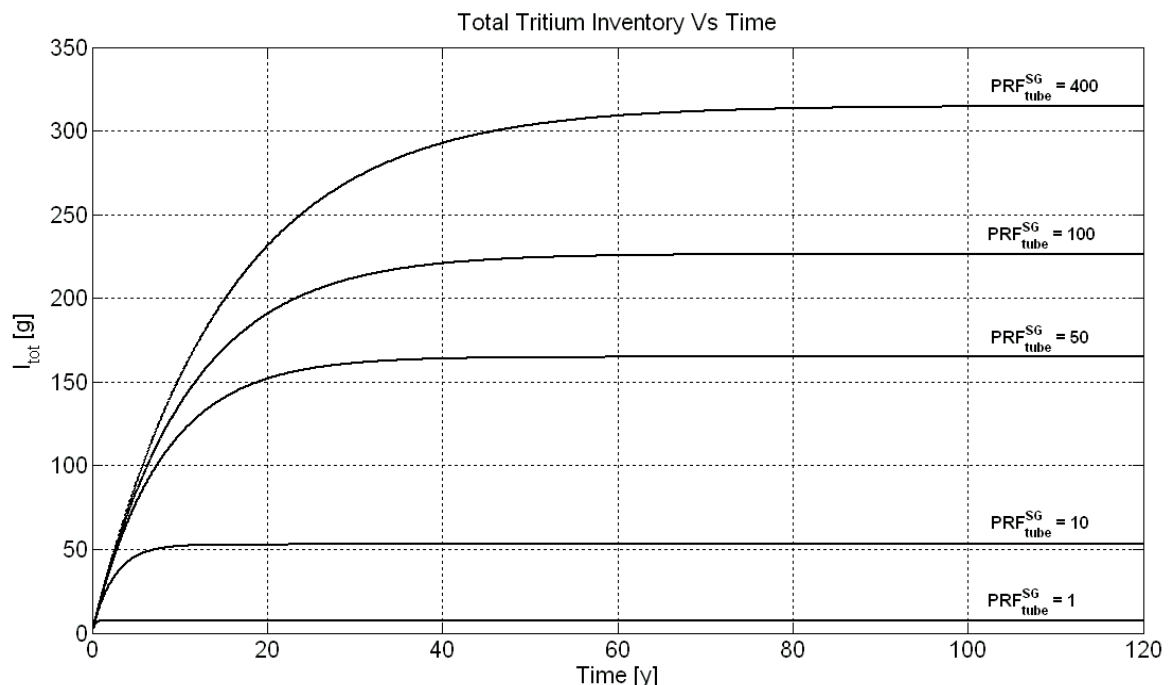

Figure Errore. Nel documento non esiste testo dello stile specificato.**-26 SFR-TPC Total Tritium Losses from PFBR Vs time Vs PRF_{tube}^{SG} ($\beta_{CT}^{pool} = 0$, $\beta_{CT}^{sec} = 0$, $\epsilon_{CT} = 0$)**

Although was observed a PRF even equal to 400 inside SG tubes coming from the natural oxidation in the water side, this last value could appear too optimistic and quite difficult to be reached; therefore here is reported just to see how much tritium losses can be reduced with this PRF value.

This parametric study does not care about any PRF inside IHX tubes for two reasons: (i) it is not a much influencing parameter because permeation fluxes through the permeation walls are proportional to the difference of the square root of the high and the low tritium partial pressures (see Eq. (2-10)) and this difference is much larger in the SGs than that in the IHXs; (ii) the PRF inside the IHX can be obtained only by means of coated tube, but this choice can be quite uneconomic and complicated (see par. 0). As shown in the above graph,. $\text{PRF}_{tube}^{SG} = 1$ provides the same tritium losses results obtained in **Figure** Errore. Nel documento non esiste testo dello stile specificato.**-24** where no

PRFs were considered. The permeation reduction factor acts also on evolution time scale, as expected. In fact, the larger is PRF_{tube}^{SG} and the higher is the difficulty for the system to reach the equilibrium conditions. However in term of tritium losses reduction, a PRF = 100 on SG pipes provide a 50 % reduction, lowering the losses until about 1.5 g/y, while, assuming that a PRF = 400, tritium losses can be reduced even until 0.6 g/y, but as already mentioned, it is not possible to rely on such an optimistic value. This results gives once again the confirm that cold trapping is needed to reach suitable tritium losses values. In **Figure** Errore. Nel documento non esiste testo dello stile specificato.**-27** is reported the same parametric study performed for total tritium inventory, varying PRF_{tube}^{SG}.
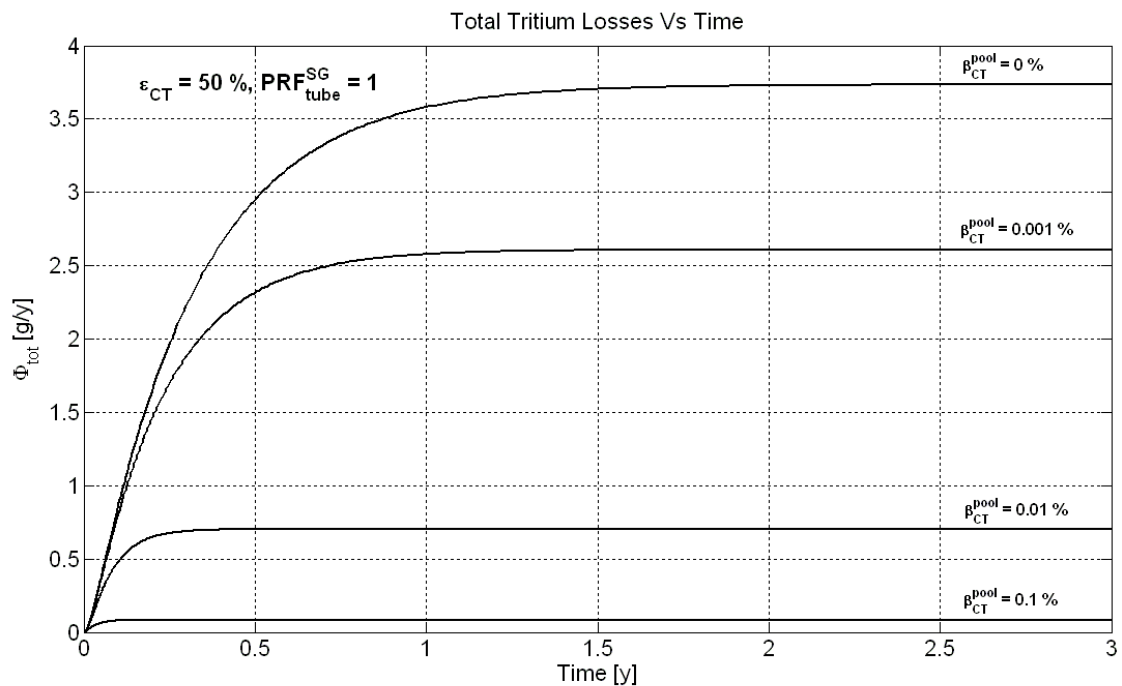

Figure Errore. Nel documento non esiste testo dello stile specificato.**-27 SFR-TPC Total Tritium Inventory inside PFBR Vs time Vs PRF_{tube}^{SG} ($\beta_{CT}^{pool} = 0$, $\epsilon_{CT} = 0$)**

In **Figure** Errore. Nel documento non esiste testo dello stile specificato.**-27** is verified the opposite tendency with respect to that reported in **Figure** Errore. Nel documento non esiste testo dello stile specificato.**-26,** because here the tritium inventory was observe to increase with the PRF_{tube}^{SG} increasing. This is quite obvious since the permeation barrier reduces the tritium capability to escape outside SFR facilities into the environment.

Since from **Figure** Errore. Nel documento non esiste testo dello stile specificato.**-26** it can be seen that cold traps are needed, the objective becomes to evaluate the tritium losses reduction obtained by the

employment of the cold traps. According to the theoretical discussion performed in par. 0 and to the reference configuration reported in **Figure** Errore. Nel documento non esiste testo dello stile specificato.**-15,** locating a set of cold traps at the core entrance, a portion of tritium dissolved inside the primary sodium coming out from IHX would be retained in it. The cold traps parameters are the cold trapping flow rate β_{CT}^{pool} (referred to total volume flow rate of sodium into the core $\dot{Q}_{core}$) and the removal efficiency. In **Figure** Errore. Nel documento non esiste testo dello stile specificato.**-28** is reported the parametric study of tritium losses varying β_{CT}^{pool}, between the 0% and the 0.1% of the total primary sodium flow rate with a cold trap removal efficiency fixed at $\varepsilon_{CT} = 50\ \%$ and considering that any PRFs and any cold traps into the secondary sodium loops are present.

Figure Errore. Nel documento non esiste testo dello stile specificato.**-28 SFR-TPC Total Tritium Losses from PFBR Vs time Vs β_{CT}^{pool} (PRF$_{tube}^{SG}$= 1, β_{CT}^{sec} = 0 % ε_{CT} = 50 %)**

The plot of **Figure** Errore. Nel documento non esiste testo dello stile specificato.**-28** visualizes the great influences on tritium losses results coming from the variations of the cold trapping rate; in fact Φ_{tot} decreases by almost two order of magnitudes (0.08 g/y) by adopting a cold trap flow rate equal to the $0.1\ \%$ of the total core sodium flow rate (≈ 8 lt/sec) flowing inside the core with an efficiency $\varepsilon_{CT} = 50\ \%$. This maximum cold trapping rate ratio inside primary sodium cold trap used for the

simulation is quite difficult to be overcame. In fact, as already mentioned in par. 0, the sodium mass flow rate to be circulated inside the cold traps has un upper limit given by the residence time and a lower limit fixed by the tritium removal rate. In the real technical situation, this order of magnitude for the cold trapping rate is verified and utilized in order models. In fact, in the results obtained by Taylor [28] the cold trapping rate was assumed equal to 380 lt/min ($\approx$ 6.33 lt/sec) which is the 0.07 % of total primary sodium flow rate and thus almost equal to the maximum value used for this parametric study. However, with this values (obtained adopting only primary sodium cold traps), as mentioned above, total tritium losses are equal to 0.08 g/y, which corresponds to the 2.1 % of total tritium release rate from core into primary sodium (S_{tot} = 3.87 g/y). With this operative cold trapping rate, Taylor found that the tritium release rate into the SG water (and therefore considered losses into the environment) was about the 0.7 % of the total generated one and release into primary sodium. This divergence is due mainly to the fact that in Taylor results the cold trapping of 380 lt/min was operated both in primary and secondary sodium cold traps, thus increasing the tritium removal rate. In **Figure** Errore. Nel documento non esiste testo dello stile specificato.**-29** is reported the same parametric study but now considering to operate the tritium purification with both primary and secondary sodium cold trap with the same cold trapping rate ratios adopted for the plot in **Figure** Errore. Nel documento non esiste testo dello stile specificato.**-28** and considering again a removal efficiency of the 50%. It can be seen that the effects are stronger, and the reduction in term of tritium losses results are deeper and assuming a cold trapping rate ratio of the 0.1 % inside both primary and secondary sodium cold traps, the tritium losses amount to about 10 mg/y, which correspond to the 0.28 % of the total tritium generation rate inside the primary sodium. This result, as a first approximation is in accordance with that obtained by Taylor, in which, as mentioned here above, tritium release rate into SG water was the 0.7 % of the tritium introduced into primary sodium.

Significant variations on tritium losses can be obtained also by forcing some variations on the efficiency on the cold traps (see **Figure** Errore. Nel documento non esiste testo dello stile specificato.**-30**). This actions simulates the normal situation during the operation phase, in which the usury and obsolescence of cold traps determine some decreases in the retention capabilities of the latter. However, as shown in **Figure** Errore. Nel documento non esiste testo dello stile specificato.**-18**, hydrogen removal efficiency can range from about 30 % to 100 %. Therefore in this part of the parametric study, the parameter ϵ_{CT} was made to range between 0 – 100 % assuming that both primary and

secondary sodium cold traps are operating with a reasonable value of the cold trapping rate ratios β_{CT}^{pool} and β_{CT}^{sec} of 0.05 % and that any PRFs are present.

From this last plot, it can be seen that hydrogen removal efficiency is an highly influencing parameter too. In fact, if ϵ_{CT}=100 %, tritium losses can reach the low value of about 10 mg/y, which is further reduced and corresponds to the 0.26 % of total the tritium entering into the primary sodium (S_{tot}).
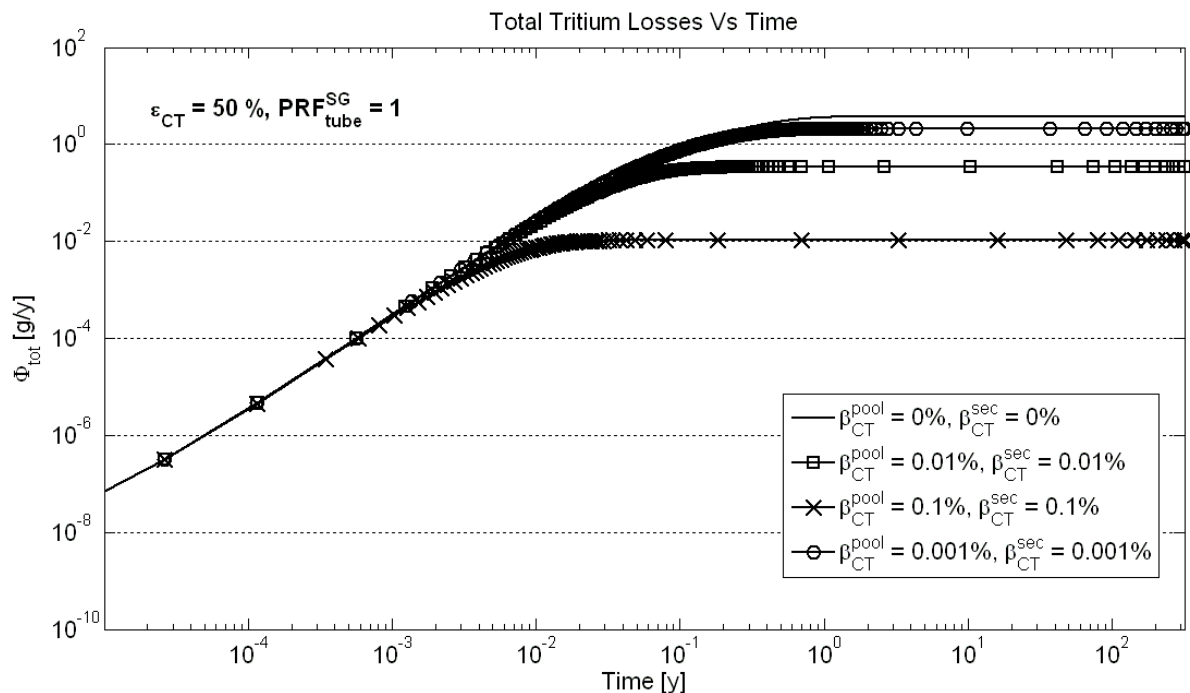

Figure Errore. Nel documento non esiste testo dello stile specificato.**-29 SFR-TPC Total Tritium Losses from PFBR Vs time Vs β_{CT}^{pool} and β_{CT}^{sec} (PRF$_{tube}^{SG}$= 1, ϵ_{CT} = 50 %)**
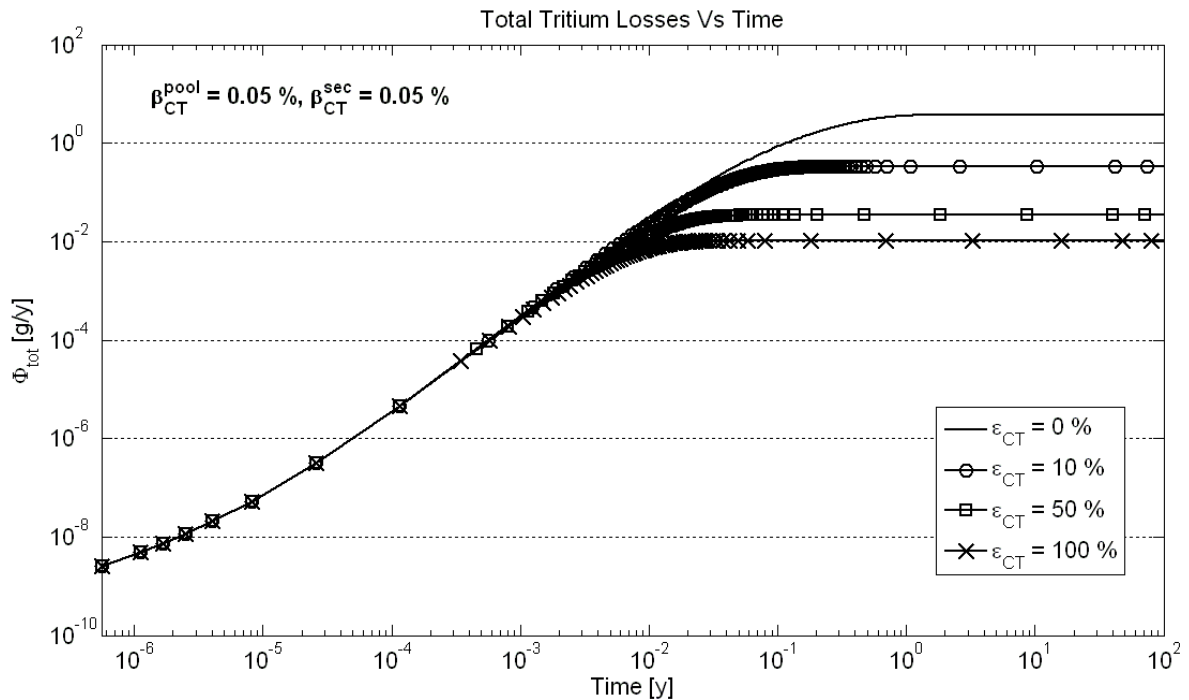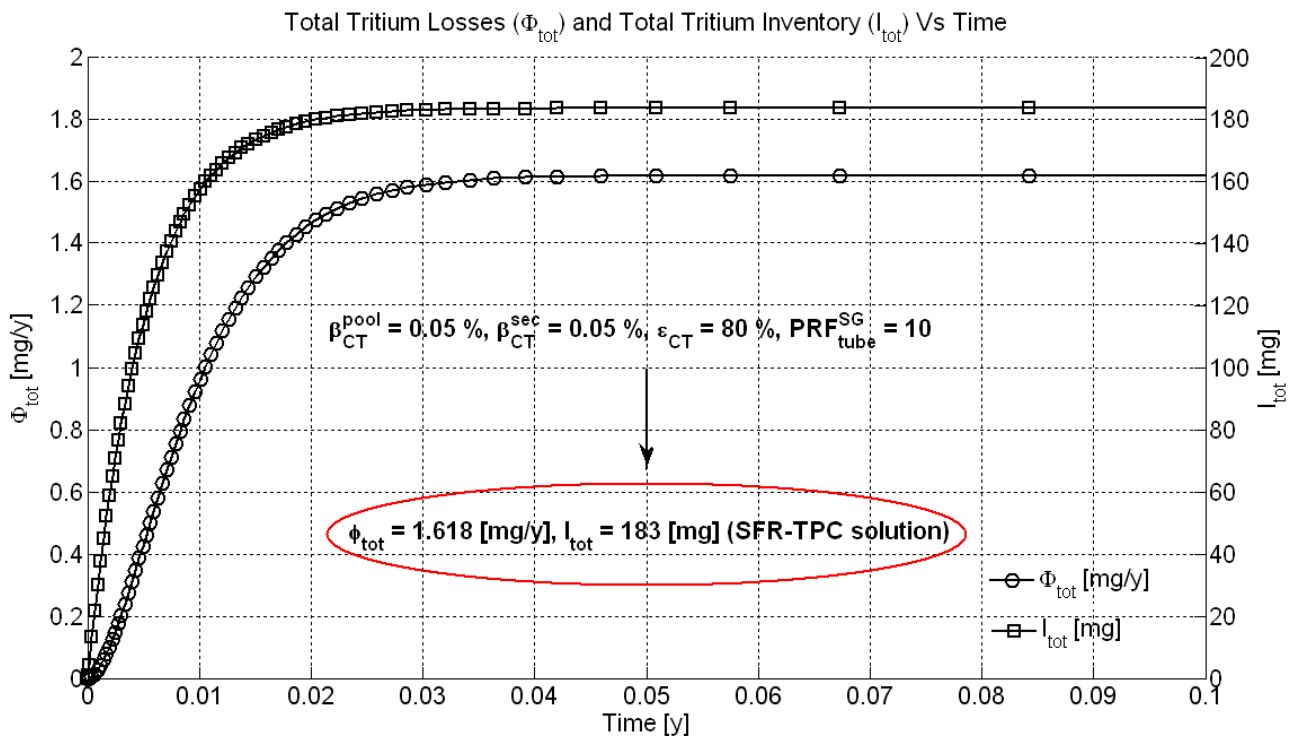
Figure Errore. Nel documento non esiste testo dello stile specificato.**-30 SFR-TPC Total Tritium Losses from PFBR Vs time Vs ϵ_{CT}**
($PRF_{tube}^{SG} = 1$, $\beta_{CT}^{pool} = 0.05$ %, $\beta_{CT}^{sec} = 0.05$ %)

Observing the results reported in the three above figures, the first consideration to be remarked regards the different influences of the two different mitigations techniques adopted (cold traps and permeation barrier utilization) on the tritium losses results. In fact, the effects produced by the cold traps usage are very powerful; a small portion of 0.01 % of the core volume flow rate processed inside cold traps produces a decrease in tritium losses of almost two order of magnitudes. However, relevant effects of permeation barriers are observed also for PRF inside SG tubes of order of 100 (a nominal PRF = 100 is considered as a reference value difficult to be overcame). Therefore, utilization of cold traps in SFR plants is required in order to keep low tritium losses through the overall plant heat installations.

After this parametric analysis, a final simulation of SFR-TPC will be repeated inserting inside the input settings a suitable combination of all parameters studied here above; this combination is given by a PRF inside SG tubes $PRF_{tube}^{SG} = 10$ (obtained by natural oxidation processes), a cold trapping rate ratio equal to 0.05 % inside both primary and secondary sodium cold traps and an hydrogen removal efficiency equal to the 50 %. This set of parameters are representative of the operative situation from the plant exercise point of view because these values

are in general quite common in nuclear power plant, especially in SFR plants, where sodium cold traps are adopted also for sodium purifications from hydrogen impurities. Tritium losses obtained by adopting this numerical inputs are reported in **Figure** Errore. Nel documento non esiste testo dello stile specificato.**-31**. The obtained results are crucial because it is possible to point out that they represent the final results of the tritium transport analysis in SFRs system. In fact, the input parameters of PRF_{tube}^{SG}, β_{CT}^{pool}, β_{CT}^{sec} and ϵ_{CT} listed above are quite representative of the actual operative conditions of an SFR but are quite conservative too. From the numerical point of view, it can be seen that at steady state the total tritium losses are equal about to 1.618 mg/y (the 0.04 % of total fission-generated introduce inside the primary sodium) while the total tritium inventory inside the plant is about 183 mg (as already mentioned this value does not take into account of the tritium inventory inside the cold traps, because they are subjected to maintenance operations and therefore to restoration or plugging). Comparing this steady state tritium inventory value (obtained considering the presence of both cold traps and permeation barriers) with that reported in the plot of **Figure** Errore. Nel documento non esiste testo dello stile specificato.**-25** ($\approx$ 8 g), it is shown that a great reduction occurred also in the tritium inventory value. This is quite in contrast with the tendency visualized in **Figure** Errore. Nel documento non esiste testo dello stile specificato.**-27**, where the tritium inventory increased with the increasing of the barrier entity (PRF_{tube}^{SG}). This behavior is justified by the fact that total tritium inventory are mainly characterized by tritium inventory inside primary sodium I_{pool}^{Na} and secondary sodium I_{sec}^{loop} (see par. 0). Since, as already mentioned, the tritium inventory inside the cold traps does not participate in the total tritium inventory estimation, when cold traps are adopted, a big tritium quantity will be retained inside them and therefore does not enter into the primary and secondary sodium giving a string reduction of $I_{tot}[g]$. The indicative parameter of the cold traps performances is the tritium removal rate inside them. Using this set of values, the total tritium removal rate inside the cold trap is 3.854 g/y which is equal to the 99.5 % of the total tritium quantity released inside the primary sodium. From this results it is point out that the cold traps are more powerful than the permeation barrier to retain tritium inside the plant; moreover we can state that tritium does not constitute a big radiological concern, unless adequate systems of tritium transport mitigations are foreseen.

Figure Errore. Nel documento non esiste testo dello stile specificato.**-31 SFR-TPC Total Tritium Losses and Inventory from and inside PFBR Vs time**
(β_{CT}^{pool} = 0.05 %, β_{CT}^{sec} 0.05 %, PRF_{tube}^{SG} = 10 and ϵ_{CT} = 80 %)

In conclusion, SFR-TPC simulation, obtained by analyzing SFR components from core until SG, gave us results quite satisfactory because they reflected all assumptions and simplifying hypothesis carried out from the beginning of this work.

Comparison of the results with various radiological limits

A perplexing challenge at the current stage of the NGNP(Next Generation Nuclear Plant) is to set a provisional limit on the allowable tritium contamination both in sodium (primary and secondary) and inside the process steam.

Regarding limits inside primary and secondary, there no safety limits related to tritium specific activity inside sodium to be kept under control during the plant operation, but some requirements for the re-use of sodium into the industry and for the transportation are fixed by Radiation Safety Standards (RSS) [48] and defined as:

- 1000 MBq/kg for the reuse of spent sodium in the nuclear industry;
- 10 MBq/kg for the transportation.

It has to be remarked that these limits are referred to spent sodium, thus the comparison between these values and those obtained from a SFR-TPC simulation could be performed but it has to be considered not as a strong constrain in the SFR tritium transport analysis, but just a reference values of tritium specific activity in sodium to be labeled as a low one.

Regarding the limits in the steam/water process (nominal conditions) the international regulatory standards for allowable tritium contamination in air and drinking water vary remarkably (see **Table** Errore. Nel documento non esiste testo dello stile specificato.**-18** [23]). Tritium specific activity into steam/water are fixed by the US EPA (Environmental Protection Agency) [23]:

- 20 pCi/g ($7.4 \cdot 10^{-4}$ MBq/kg) during all operation phase.

This recommended NGNP limit should not be considered a formal requirement for the NGNPs but an early and ambitious figure of merit.

However, we want to verify if our SFR plant, adopting the cold trap settings discussed in the previous paragraph and the value of PRF_{tube}^{SG} = 10 respects this programmatic limit. In **Figure** Errore. Nel documento non esiste testo dello stile specificato.**-32** are reported the average tritium specific activities for the primary sodium $\left(A_{prim}^{av}\,[MBq/kg]\right)$, for the secondary sodium $\left(A_{sec}^{av}\,[MBq/kg]\right)$ and the tritium specific activity inside the outgoing water coming from the SG outlet $\left(A_{w}^{out}[MBq/kg]\right)$. These values are based on the tritium concentrations expressed in ppm units and converted into Bq/kg.

Organization	H-3 Limit	Value
Regulatory Limits		
US NRC	Air	84 pCi/g (100 pCi/l)
US EPA	Drinking Water	20 pCi/g (20,000 pCi/l)
France, Germany, UK	Drinking Water	2.7 pCi/g (100 Bq/l)
Canada (Ontario)	Drinking Water	189 pCi/g (7000 Bq/l)
Australia	Drinking Water	2057 pCi/g (76,103 Bq/l)
IAEA	Exemption Limits	27×10^6 pCi/g (10^6 Bq/g)
Programmatic Limits		
PNP (FRG)	H-3 in syn gas	10 pCi/g
KINS (Korean "ACRS")	H-3 in hydrogen (IAEA limit)	27×10^6 pCi/g
KAERI (Korea)	Air	6284 pCi/g (232.5 Bq/g)
KAERI (Korea)	Water	1081 pCi/g (40 Bq/g)
JAERI (Japan)	H-3 in hydrogen	1510 pCi/g
NGNP	H-3 in hydrogen/steam	[20/20] pCi/g (EPA H_2O)

Table Errore. Nel documento non esiste testo dello stile specificato.**-18 International Limits on Tritium Contamination in Various Media [23]**
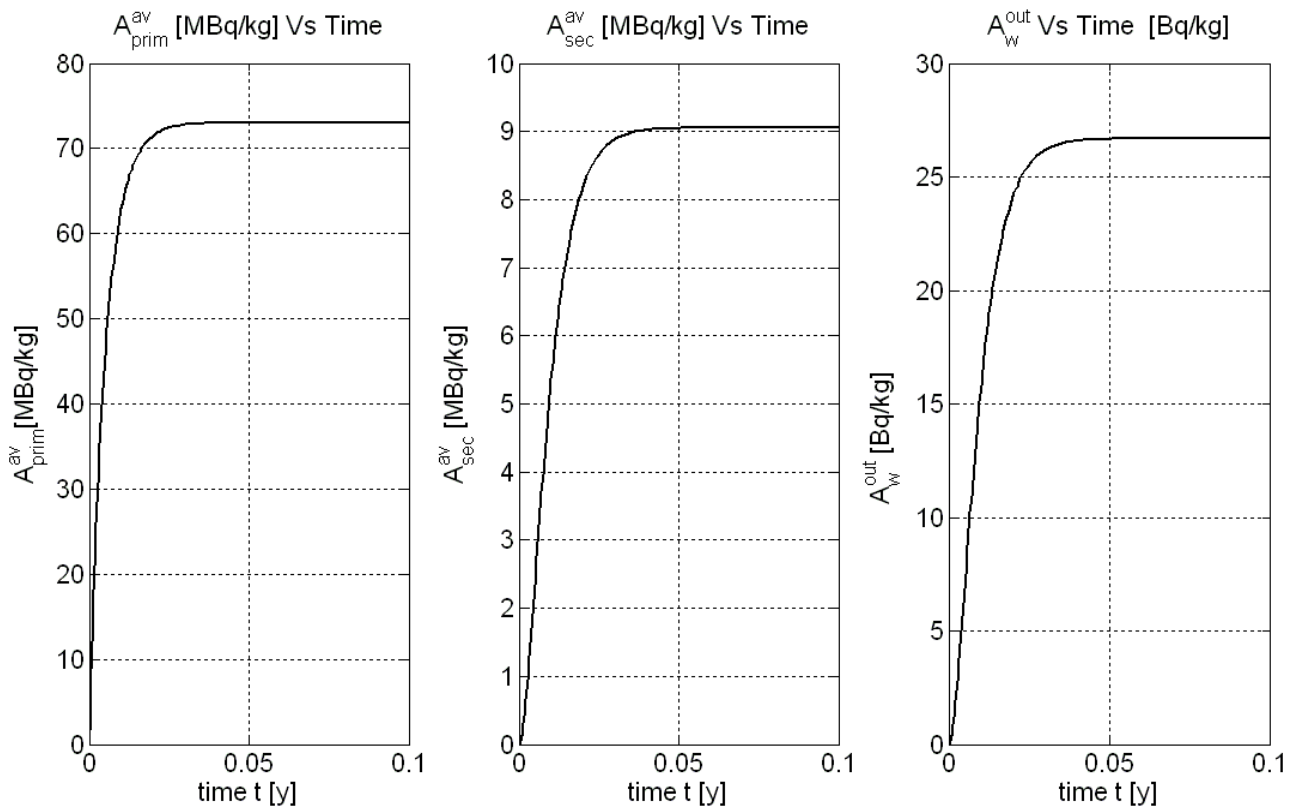
Figure Errore. Nel documento non esiste testo dello stile specificato.**-32 SFR-TPC Specific Activities inside PFBR Vs Time**
(β_{CT}^{pool} = 0.05 %, β_{CT}^{sec} 0.05 %, PRF_{tube}^{SG} = 10 and ϵ_{CT} = 80 %)

From the plot of **Figure** Errore. Nel documento non esiste testo dello stile specificato.**-32** it can be seen that neither primary or secondary sodium must be purified from tritium in order to be reused inside the nuclear industry, while for transportation the primary sodium exceeds the fixed limit (10 MBq/kg). The specific activity inside the outgoing water into the SG is very far from exceeding the programmatic limit fixed by the US EPA (740 Bq/kg). Moreover, from the above results it appears that, using the cold traps devices, radiological limits on primary sodium, secondary sodium and water can be guaranteed. In fact, observing concentration values reported in **Figure** Errore. Nel documento non esiste testo dello stile specificato.**-21** we can be seen that nor of the above listed limits are respect. In fact tritium concentration in primary sodium was found to be equal to 0.06 ppm (3036 MBq/kg), in secondary sodium equal to 0.048 ppm (2242 MBq/kg) and inside water equal to 0.012 $\times 10^{-4}$ ppm (71.6 kBq/kg). All three tritium specific activities were exceeding deeply the fixed limits of 1000 MBq/kg for sodium and 740 Bq/kg for water. Therefore from this results it can be pointed out again that cold traps are needed during the SFR operation.

Validation of the code

In order to have an idea of the quality of the obtained results, a brief comparison with some other's models results and measurements effectuated on some operating reactors (or in decomissioning phase) should be performed. These measurements regard essentially the tritium specific activities inside the primary sodium, the secondary sodium and inside the water, as those reported in **Figure** Errore. Nel documento non esiste testo dello stile specificato.**-32**. The analyzed reactors belong both to the loop primary circuit configuration and to the pool primary circuit one (see par. 0). Although this strong design difference, it will be shown that the tritium specific activities measured for the analyzed reactors are quite similar between them, and therefore, even if the analysis was not carried out on one of the analyzed reactors, it is not so meaningless to compare tritium concentrations values obtained from the SFR-TPC simulations for the Prototype Fast Breeder Reactor (PFBR) with those measured on SuperPhénix or on BN-600, which are quite similar to the studied one (each reactors adopt the pool-type primary circuit configuration, as PFBR does).

During the development of the parametric study performed in par. 0, a comparison between SFR-TPC results and other model's results (not measurements) was done. In fact was found that total tritium losses (in term of fraction of tritium generation rate) was quite similar to that evaluated by Kozlov [20] (<1 %), by Court (3 %), by Taylor (0.7 %) and by Kumar (0.07 %). These values are quite different because were obtained by testing the respective models on different test reactors. However, as a first approximation, our results are quite closer to the above results. In fact the total tritium losses were equal to about 1.6 mg/y adopting a not too much optimistic cold trapping rate (the 0.05 % of primary and sodium flow rate) and efficiency (80 %). This tritium losses value correspond to the 0.04 % of the total generation rate (3.87 g/y). Therefore, comparing the SFR-TPC results with other models results it can be pointed out that it produces tritium losses values, tritium inventory values and tritium specific activity values already founded by other models.

Since the comparison with in-reactor measurements are the most powerful meaning to validate a code, a brief comparison with some tritium specific activities measured on some operating and shutdown reactors should be effectuated. In **Table** Errore. Nel documento non esiste testo dello stile specificato.**-19** are reported in the same units the measured specific activity for different experimental, prototype and commercial reactors ([22], [39], [49]).

Reactor	Primary circuit configuration	Primary sodium [Bq/kg]	Secondary sodium [Bq/kg]	Water [Bq/kg]
EBR-II	pool	$1.8 \cdot 10^{6}$	$5.5 \cdot 10^{4}$	$1.8 \cdot 10^{2}$
Phénix	pool	$1.0 \cdot 10^{6}$	$5.5 - 11 \cdot 10^{4}$	$2.2 \cdot 10^{3}$
FFTF	loop	$1.2 \cdot 10^{7}$	$(2.2 - 3.9) \cdot 10^{6}$	–
BN-350	loop	$1.0 \cdot 10^{7}$	$0.5 \cdot 10^{6}$	–
PFR	pool	$3.7 \cdot 10^{7}$	–	–
Super-Phénix	pool	$(5 - 20) \cdot 10^{6}$	–	–

Table Errore. Nel documento non esiste testo dello stile specificato.**-19 Tritium specific activities measured in different SFRs ([22], [39], [49])**

As mentioned above, in **Table** Errore. Nel documento non esiste testo dello stile specificato.**-19** are reported the tritium specific activities for both loop and pool type design reactors. Since sodium volumes are quite larger for pool-type reactors than that of the loop-type ones, the tritium concentrations inside primary sodium are expected to be lower than those inside reactors built with loop design. In fact, between the reactors listed in **Table** Errore. Nel documento non esiste testo dello stile specificato.**-19**, only FFTF and BN-350 adopt a loop-type primary circuit configuration, and in fact, primary sodium and secondary sodium activities are almost one order of magnitudes larger than those of others pool-type design reactors (except for the pool-type reactor PFR where the larger concentrations obtained at PFR, compared with those of others systems with the same primary circuit configuration, are probably due to the fact that the primary cold-trap on PFR only operates periodically and only one cold-trap operates sequentially on the three secondary loops, thus reducing the amount of tritium removed per cycle of plant operation). This suggests that the values quoted in the above table are not absolute values as they will vary with time of operation and cold trapping rate. In fact, considering the results of tritium specific activities reported in **Figure** Errore. Nel documento non esiste testo dello stile specificato.**-32**, tritium specific activities inside primary and secondary sodium (74 MBq/kg and 9 MBq/kg respectively) are one order of magnitude larger than those reported in **Table** Errore. Nel documento non esiste testo dello stile specificato.**-19**, whereas the same quantity in water (27 Bq/kg) was observed to be much lower than that reported in the same table. This could suggest to think that some mistakes or too much large uncertainties are present, but these last results was obtained from arbitrary choices of some very highly influencing parameters (i.e., the cold trapping rate inside primary and secondary sodium (β_{CT}^{prim} and β_{CT}^{sec} respectively), the hydrogen

removal efficiency β_{CT}^{pool} and the PRF inside the SG tubes PRF_{tube}^{SG}), because specific information about the operative cold traps parameters of all these reactors were not found and therefore the comparison must be effectuated very carefully. However, the primary sodium specific activity is quite closer to that recorder in SuperPhénix (SPX), and since PFBR and SPX are quite similar from the primary circuit specifications (temperature, pool geometries, etc.), this analogy of the results is quite satisfactory Moreover, tritium specific activities calculated by Kozlov [20] for the reactor BN-600 (pool type design) are equal to 33.3 MBq/kg for the primary sodium circuit, 4.88 MBq/kg for the secondary sodium circuit and 7÷35.2 Bq/kg for the water circuit, which are very closer to values obtained from the SFR-TPC simulation. From this last consideration, one may be suggested to try to increase the cold trap performances parameters; increasing the cold trapping rate inside both primary and secondary sodium cold traps from 0.05 % to the 0.5 % of the total core flow rate and secondary sodium loop flow rate respectively specific activities become as reported in **Figure** Errore. Nel documento non esiste testo dello stile specificato.**-33.**

The reported values show that tritium concentrations, as expected, are further reduced until they reach specific activity values quite in accordance with the in-reactors measurements reported in **Table** Errore. Nel documento non esiste testo dello stile specificato.**-19.** It has to be remarked that the cold trapping rate equal to the 0.5 % of total primary and secondary sodium loops could appear a too much high value to guarantee a removal efficiency of the 80 %. Thus, it must pay attention to these parameters and it must be sure that there will be the physical possibility to operate such a cold trapping rate, because they are the most relevant ones in tritium transport analysis.

Observing the plot reported in **Figure** Errore. Nel documento non esiste testo dello stile specificato.**-33** primary and secondary sodium tritium specific activities pass from 74 MBq/kg and 9 MBq/kg respectively to about 8 MBq/kg and 0.11 MBq/kg (similar to the BN-350 and the SPX measurements), while tritium activities in water passes from 26.7 Bq/kg to 0.32 Bq/kg. However, this last results is deeply influenced also by the PRF inside SG tubes. Therefore, the divergences between the SFR-TPC results (in terms of tritium concentration inside water) and the measurements could be justified by the fact that, for the simulation, PRF_{tube}^{SG} was choose arbitrarily and therefore, since the SG tubes surfaces are unknown at the time of the measurements (or better during the operation lifetime), it may be not so representative of the real conditions of these surfaces.
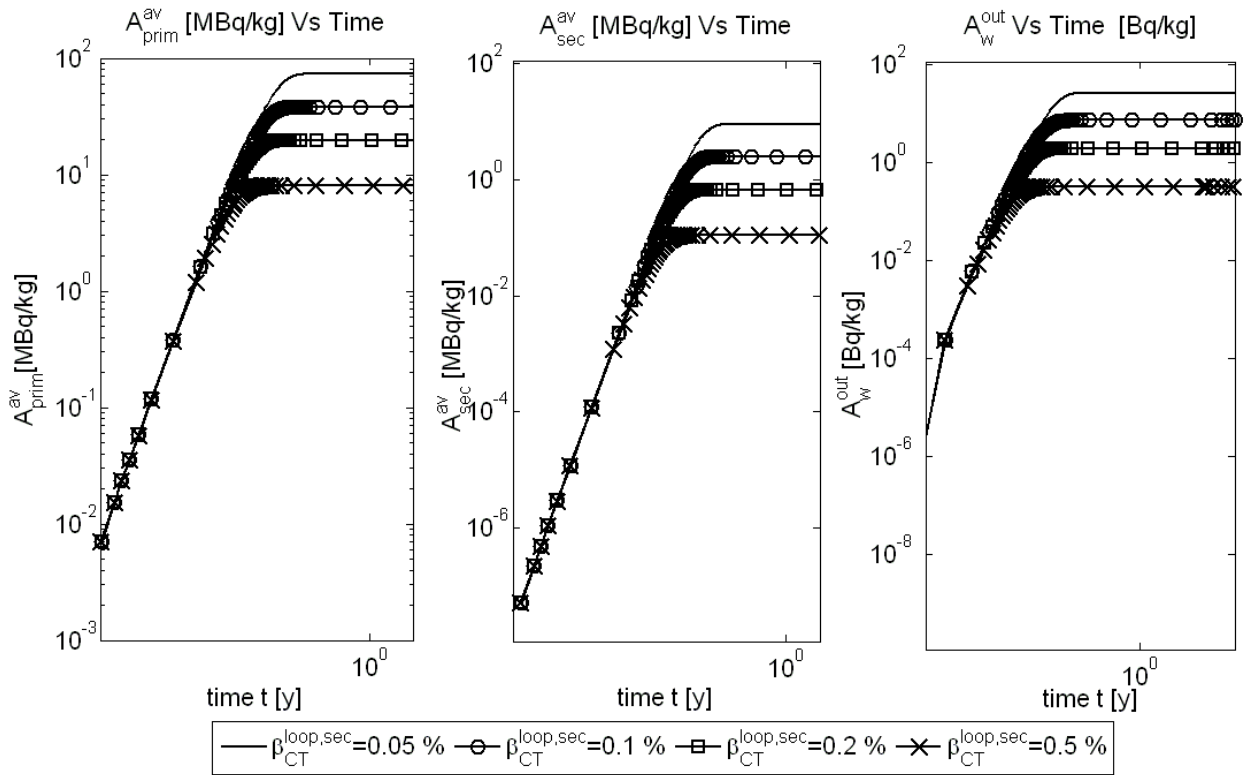
Figure Errore. Nel documento non esiste testo dello stile specificato.**-33 SFR-TPC Specific Activities inside PFBR Vs Time Vs β_{CT}^{pool} Vs β_{CT}^{sec} (PRF_{tube}^{SG} = 10 and ϵ_{CT} = 80 %)**

Conclusions and discussions

In this work the problem of tritium transport in Sodium-Cooled Fast Reactors (SFRs) from the primary coolant through heat exchangers and other plant facilities to the environment has been studied and analyzed by means of a computational code called Sodium-Cooled Fast Reactor Tritium Permeation Code (SFR-TPC).

The Sodium-Cooled Fast Reactor (SFR) system features a fast-spectrum reactor and closed fuel recycle system. The majority of natural uranium is the isotope U^{238} making up about 99.3 %. The remaining 0.7 % is U^{235} the isotope required for thermal fission in modern light water reactors.

The primary coolant system can either be arranged in a pool layout schematized in **Figure** Errore. Nel documento non esiste testo dello stile specificato.**-1** (a common approach, where all primary system components are housed in a single vessel), or in a compact loop layout, favored in Japan. The total thermal power generated in the reactor core is exchanged by a set of IHXs in the reactor vessel. IHX is in general a straight tube heat exchanger of counter current shell and tube type. Liquid sodium is circulated through the core using one/two primary sodium pumps. The sodium enters the core and leaves at an higher temperature. The hot primary sodium is radioactive and is not used directly to produce steam, in fact it transfers the heat to secondary sodium through set of IHXs. The non-radioactive secondary sodium is circulated through a certain number of independent secondary loops, each having a sodium pump, a given number of intermediate heat exchangers and of steam generators (SG).

In order to perform a tritium transport analysis in SFR systems, some data on materials attitudes to allow tritium transport (i.e. tritium permeabilities and solubilities). For this reason attention will be focused on pool containment, IHX and SG materials. In SFRs austenitic stainless steels are employed in the entire liquid sodium system even if the temperatures of some components are low enough to use less expensive ferritic steels [2]. **Table** Errore. Nel documento non esiste testo dello stile specificato.**-1** lists the structural materials selected for major components such as reactor vessel, intermediate heat exchanger (IHX), and piping in currently operating or designed Fast Breeder Reactors (FBRs) all over the world. Materials selected for SFR steam generator application should meet requirements of high temperature service such as high temperature mechanical properties

including creep and low cycle fatigue, resistance to loss of carbon to liquid sodium which leads to reduction in strength, resistance to wastage in case of small leaks leading to sodium-water reaction and resistance to stress corrosion cracking in sodium and water media [2]. For SFR steam generators, a range of materials starting from ferritic steels (2.25Cr- 1Mo, Nb stabilized 2.25Cr-1Mo, 9Cr-1Mo (grade 9), Modified 9Cr-1Mo (grade 91)), austenitic stainless steels (AISI 304/316/321) and Nickel alloys (Incoloy 800) were examined [2].

Hydrogen dissolves in and permeates through most materials, thus it is important to understand the permeation, diffusion and dissolution of atomic hydrogen in materials in which hydrogen and its isotopes are present. Tritium permeation inside solid materials is characterized by bulk process and surface processes. An important parameter that measures the attitude of materials to dissolve a gas is called Sievert's constant K_S. Sievert's constant derive from the chemical equilibrium between the diatomic hydrogen molecule(gas phase) and hydrogen atoms in a metal (solid phase) (or phase of host material), expressed by means of Sievert's law; this law correlates partial pressure of hydrogen in gas phase (p_{H_2}) and the concentration inside host materials (C_{H^-}), by means of Sievert's constant $(C_{H^-} = K_S(T) \cdot \sqrt{p_{H_2}})$. Others important parameters describing the attitude of hydrogen to permeate inside a solid materials are the permeability P, and the diffusivity D, to put inside the Richardson's law $(P = K_S \cdot D)$. Permeation model, thus, rely on a mathematical model in which the hydrogen permeation flux is directly proportional to the permeability coefficient and to the square root of the partial pressure. This mathematical form is involved inside diffusion equation and solved. Sievert's constant (as the permeability and the diffusivity) is in general expressed as a function of the temperature by means of the Arrhenius law $K_S(T) = K_{S,0} \cdot \exp(-Q_S/RT)$. The same relation is needed also for the permeability $P(T)$.

Since we are dealing with SFR systems, we treated, in a theoretical way, all chemical issues regarding presence of hydrogen (and its isotopes), in liquid sodium, especially regarding solubility of hydrogen in sodium and Sievert's constant data.

Na – Na-H binary system exhibits a monotectic reaction, which is a case of a non complete solubility between Na and Na-H system (as shown in **Figure** Errore. Nel documento non esiste testo dello stile specificato.**-2**). Dissolution of hydrogen in sodium can be represented by a Barn-Heber cycle [7]. Below the monotectic temperature (see **Figure** Errore. Nel documento non esiste testo dello stile specificato.**-2**), hydrogen dissolves in sodium up to a concentration beyond which solid sodium hydride saturated with sodium metal precipitates. The hydrogen dissolved in sodium can origin

solid sodium hydride NaH(s) (see process I of Born – Heber cycle reported in **Figure** Errore. Nel documento non esiste testo dello stile specificato.**-3**). This mechanism is verified inside the sodium cold traps (see par. 0), that are needed in order to remove significant tritium quantities from primary and secondary sodium, in order to reduce tritium losses and inventories

After a detailed description of the chemistry of the Na-NaH system, some literature data of hydrogen Sievert's constant in sodium were analyzed. The reported data show that variation of Sievert's constant is negligibly small in the temperature range of 603-843 K and in order to visualize more clearly all listed data, in this case they are reported in a linear scale plot instead of a log scale plot. Sievert's constant experiments clearly indicate also an increase in its measured values with the increasing of dissolved oxygen concentration [7]. Presence of oxygen impurity would lead to an interaction with dissolved hydrogen.

After this quantitative analysis, we compared the hydrogen Sievert's constant in sodium to that in the most important liquid breeders utilized in fusion reactors, such as liquid lithium (which is very high and therefore leads designers to deal with tritium inventory problems) and liquid lead-lithium alloy (which is very low and thus may cause problem of tritium permeation). In fact, according to the Sievert's law, the higher is the Sievert's constant and the lower is the tritium partial pressure. Hence, the purpose to verify the entity of sodium Sievert's constant referred to these two extreme cases and, putting function $K_S(T)$ on the same Arrhenius plot, we observed an intermediate position of hydrogen Sievert's constants in sodium, included between that in liquid lithium (largest values) and that in liquid lead-lithium.

The steam/water system inside the nuclear reactors may contain H_2. A chemical equilibrium between hydrogen species HT, H_2, HTO and H_2O occurs, and the isotopic exchange rate of this equilibrium was studied, since it participates into the tritium mass balance equations. Observing all the theoretical analysis of the hydrogen isotopes in matter, we concluded that chemical equilibrium tritium concentration is characterized by different expressions depending on the case in which tritium is dissolved in sodium (Sievert's law), in liquid water (Henry's law) or in superheated steam (Dalton's law).

One potential problem of using SFR is the tritium permeation from the primary coolant through heat exchangers into the environment. In SFRs tritium mostly comes from ternary fission of the fuel and neutron capture reactions inside boron-containing materials [22], such as control rods and neutron flux shielding blocks. A 1000 MW$_e$ SFR reactor gives a total generation rate of 7.75 g/y,

which characterizes another confirm that tritium is a concern in SFRs. To keep the release as low as practicable, the cold traps will be required to remove at least 90 % of this tritium burden.

In order to study all the tritium sources and sink mechanisms, the computational code SFR-TPC were developed. The SFR-TPC code solves the 1D time dependent tritium mass balance equation for the i species (with i = T⁻, HT and HTO) into the fluid j (with j = primary sodium, secondary sodium and water) inside the k component (with k = core, IHX and SG) and computes the tritium concentrations. Once the concentrations listed above are calculated, the code proceeds with a post elaboration, evaluating tritium losses and inventories, which are the objective of the code.

In order to avoid a large amount of tritium dissolved in primary sodium and potentially permeated into secondary sodium and steam, a set of tritium containment tools are foreseen in an SFR system. The main mitigation measures are referred to:

- application of tritium permeation barriers on the heat exchanger tubes surfaces (i.e., coating the tubes surfaces with a certain material before the installation or forming an oxidation layer during the operation);
- Cold trapping of primary and secondary sodium.

The experimental proof of the barrier efficiency is a relative reduction of the steady-state permeation flux measured at the identical conditions (p, T). Its definition is the ratio of the steady-state permeation rate through the uncoated membrane versus one through the coated membrane, termed "the permeation reduction factor" (PRF).

Some studies [34] show that oxide layers can decrease the hydrogen permeation rates even by more than two orders of magnitude and that the oxidation potential and temperature may be essential for the formation and the structure of oxide layer, and consequently for the permeation rate [34]. Since IHX deals with liquid sodium at high temperature on both sides (primary and secondary sodium), the corrosion of structural steels by liquid metals could be of interest in the oxide formation and deposition and therefore, in the tritium permeation reduction. The precipitating corrosion products may be in the form of layers tightly adhering on the pipe wall or particles suspending in the liquid [35]. This deposition layer may provide a certain PRF in IHX tubes. However, literature data on this topic were not found, thus any PRFs coming from this deposition cannot be assumed. Moreover, some authors [35] states that it is more difficult to form solid stable oxide of Fe, Cr and Ni than sodium, but soluble ternary oxide can be formed in the form of

FeO_nNa_2O. In conclusion, we can conservatively assume a PRF = 1 on surfaces wetted by liquid sodium. Regarding the possibility to get a PRF>1 from the natural oxidation of the SG tubes, nickel-based alloys (e.g., Incoloy 800) were selected as one of the promising class of materials based on experimental results of corrosion tests and mechanical tests before irradiation [37] (see par. 0). A less recent analysis of status of permeation barrier development was carried out by Stöver et al [38] and by Serpekian [34]. The results show two orders of magnitudes in the PRF values coming from natural oxidation of Incoloy 800, ranging from 10 to 400. However, for our tritium transport analysis purposes it is relevant to consider that we cannot rely on PRFs coming from natural oxidation in SFR SGs larger than a certain conservative value fixed to 10.

Control of tritium in the sodium coolant of SFRs is important for achieving as low as practicable release of radioactivity. Cold-trapping has been shown to be an effective method for controlling hydrogen in sodium and should be effective for controlling tritium as well [25]. Two mechanisms for removal of tritium from sodium are available:

- coprecipitation of hydrogen and tritium from solution in form of solid sodium hydride NaH and NaT respectively (see par. 0 and equilibrium reaction (2-2));
- isotopic exchange of tritium in sodium with hydrogen in solid NaH In a cold trap.

To keep the release as low as practicable, the cold traps will be required in order to remove at least the 90 % of tritium produced inside the core and released into the primary coolant [25]. In the estimation of the amount of tritium removed by the cold traps, cognizance has also to be taken of the hydrogen level in the sodium because the tritium concentration by itself does not reach its saturation level C_{sat}^H (about 0.057 wppm at 121 °C according to empirical relation reported in Eq. (2-4)), even at SFR cold trap temperatures T_{cold}^{CT} of 121°C [30]. The sodium mass flow rate to be circulated inside cold traps has un upper limit given by the residence time and a lower limit fixed by the tritium removal rate exigences.

The current analysis was carried on an under construction SFR plant, the Prototype Fast Breeder Reactor (PFBR) [37-43]. PFBR is a 500 MW_{elc} unit designed by Indira Gandhi Centre for Atomic Research, Kalpakkam. It is a sodium cooled, mixed oxide (MOX) fuelled, pool type fast reactor. The core thermal power is 1253 MW and the gross electrical output is 500 MW_{elc}.

Before starting with the parametric study of the permeation barriers and of the cold traps, it was reported some tritium losses and inventory results obtained without any mitigation measures (i.e., $PRF_{tube}^{SG} = 1$, $\beta_{CT}^{pool} = 0$, $\beta_{CT}^{sec} = 0$ and $\epsilon_{CT} = 0$) which corresponds to the worst scenario in terms

of radiological risks related to tritium. Adopting this configuration the total tritium losses at steady state are equal to 3.73 g/y, which correspond to the 96 % of the total tritium release rate into the primary sodium ($S_{tot} = 3.87$ g/y), while the total tritium inventory is equal to about 8 g. This is a clear indicator that mitigation techniques are absolutely necessary in order to retain inside the plant a significant and suitable tritium portion, with respect to the total amount reaching the primary sodium from the core.

The objective of this work is to perform a parametric study of the tritium transport in SFRs, looking mainly to those parameters that are able to provide a significant reduction of tritium losses from the maximum value (3.72 g/y = 96 % of total tritium source) to more suitable and less worrying values (e.g., retaining more than 90 % of fission-generated tritium or reducing tritium losses under a certain fixed value or imposing a maximum value on tritium concentration inside water).

The three essential parameters able to accomplish these missions are:

- the permeation reduction factor on SG tubes (PRF_{tube}^{SG});
- cold trapping rate ratio β_{CT}^{pool} (ratio between the cold trapping rate inside primary sodium cold trap Q_{CT}^{pool} and the total core flow rate Q_{core});
- cold traps hydrogen removal efficiency (ϵ_{CT}).

In term of tritium losses reduction, a PRF = 100 on SG pipes provide a 50 % reduction, lowering the losses until about 1.5 g/y, while, assuming that a PRF = 400, tritium losses can be reduced even until 0.6 g/y, but as already mentioned, it is not possible to rely on such an optimistic value.

Assuming a cold trapping rate ratio of the 0.1 % inside both primary and secondary sodium cold traps with a 50 % of the removal efficiency, the tritium losses decreases from 3.72 g/y to about 10 mg/y, which correspond to the 0.28 % of the total tritium generation rate inside the primary sodium. This result, as a first approximation is in accordance with that obtained by Taylor, in which, as mentioned here above, tritium release rate into SG water was the 0.7 % of the tritium introduced into primary sodium.

Significant variations on tritium losses can be obtained also by forcing some variations on the efficiency on the cold traps (see **Figure** Errore. Nel documento non esiste testo dello stile specificato.**-30**). This action simulates the normal situation during the operation phase, in which the usury and

obsolescence of cold traps determine some decreases in the retention capabilities of the latter. Therefore in this part of the parametric study, the parameter ϵ_{CT} was made to range between 0 – 100 % assuming that both primary and secondary sodium cold traps are operating with a reasonable value of the cold trapping rate ratios β_{CT}^{pool} and β_{CT}^{sec} of 0.05 % and that any PRFs are present. With this operative settings and with ϵ_{CT}=100 %, tritium losses can reach the low value of about 10 mg/y, which corresponds to the 0.26 % of total the tritium entering into the primary sodium (S_{tot}).

Inserting inside the SFR-TPC input settings a suitable combination of all parameters studied in this work ($PRF_{tube}^{SG} = 10$, $\beta_{CT}^{pool} = 0.05\,\%$, $\beta_{CT}^{sec} = 0.05\,\%$, $\epsilon_{CT} = 80\,\%$) which is representative of the operative situation from the plant exercise point of view, the total tritium losses are equal about to 1.618 mg/y (the 0.04 % of total fission-generated introduce inside the primary sodium) while the total tritium inventory inside the plant is about 183 mg. Comparing these steady state results with those obtained with any permeation barriers and cold traps, the reduction in terms of tritium losses and inventories are clear. In fact tritium losses an inventory in that case was equal to 3.72 g/y and 8 g respectively. Moreover, the total tritium removal rate inside the cold trap is 3.854 g/y which is equal to the 99.5 % of the total tritium quantity released inside the primary sodium (3.87 g/y). From this results it is point out that the cold traps are more powerful than the permeation barrier to retain tritium inside the plant and we can state that tritium does not constitute a big radiological concern, unless adequate systems of tritium transport mitigations are foreseen. In fact, observing the tritium specific activities inside primary sodium, secondary sodium and water (74 MBq/kg, 9 MBq/kg and 26.7 Bq/kg respectively), it can be seen that neither primary or secondary sodium must be purified from tritium in order to be reused inside the nuclear industry (1000 MBq/kg) and the specific activity inside the outgoing water into the SG is very far from exceeding the programmatic limit fixed by the US EPA (740 Bq/kg).

In order to have an idea of the quality of the obtained results, a brief comparison with some other's models results and measurements effectuated on some operating reactors (or in decomissioning phase) should be performed. Comparing these last results with in-reactors measurements, it can be seen that tritium specific activities calculated with SFR-TPC are quite larger than those measured because, for example, we might assumed some parameters too conservatively, especially the cold trapping rates and the efficiency. In fact assuming the primary and the secondary sodium cold trapping rates equal to the 0.5 % of total core volume flow rate and secondary sodium loop flow rate respectively, an hydrogen removal efficiency equal to the 50 %

and a PRF inside the SG tubes equal to 1, primary and secondary sodium tritium specific activities pass from 74 MBq/kg and 9 MBq/kg respectively to about 8 MBq/kg and 0.11 MBq/kg, while tritium activities in water passes from 26.7 Bq/kg to 0.32 Bq/kg. These last results are similar to the BN-350 and the SPX measurements, where primary sodium tritium specific activities are found equal to 10 and between 5and 20 MBq/kg respectively (see **Table** Errore. Nel documento non esiste testo dello stile specificato.**-19**) and the measured secondary sodium tritium specific activities is equal to 0.1 MBq for BN-350 and 0.11 for Phénix). However, this last results is deeply influenced also by the PRF inside SG tubes.

References

[1] U.S. DOE Nuclear Energy Research Advisory Committee and the Generation IV International Forum. *A Technology Roadmap for Generation IV Nuclear Energy Systems.* December 2002. GIF-002-00.

[2] Indira Gandhi Centre for Atomic Research Department of Atomic Energy Kalpakkam-603 102, INDIA. Prototype Fast Breeder Reactor. SELECTION OF MATERIALS FOR PROTOTYPE FAST BREEDER. *BHAVIN web site.* [Online] February 2004. http://www.igcar.ernet.in/igc2004/PFBR.pdf.

[3] C. Boyer, L.Vichot , M.Fromm, Y.Losset, F.Tatin-Frouxa, P.Guétat, P.M.Badot. Tritium in plants: A review of current knowledge. *Environmental and Experimental Botany.* 67 (2009) 34–51.

[4] Chang H. Oh, Eung S. Kim. Development and Verification of Tritium Analyses Code for a Very High Temperature Reactor. [Prepared for the U.S. Department of Energy Office of Nuclear Energy Under DOE Idaho Operations Office Contract DE-AC07-05ID14517] September 2009. INL/EXT-09-16743.

[5] A.Pisarev. Hydrogen solubility in liquid Li-Pb alloys. *Report SIEC-245.* 2000.

[6] C. San Marchi, B.P.Somerday, S.L.Robinson. Permeability, solubility and diffusivity of hydrogen isotopes in stainless steels at high gas pressures. *International Journal of Hydrogen Energy.* 32 (2007) 100–116.

[7] T.Gnanasekaran. Thermochemistry of binary Na-NaH and ternary Na-O-H systems and the kinetics of reaction of hydrogen/water with liquid sodium - a review. *Journal of Nuclear Materials.* 274 (1999) 252-272.

[8] J. Trouvé, G. Laplanche. Diffusion et permeation de l'hydrogene dans le sodium. *Journal of Nuclear Materials.* 115 (1983) 56-62.

[9] A.Aiello, A.Ciampichetti, G.Benamati. Determination of hydrogen solubility in lead lithium using sole device. *Fusion Engeneering and Design.* 81 (2006) 639–644.

[10] Y.C. Chan, E. Veleckis, A thermodynamic investigation of dilute solutions of hydrogen in Li–Pb alloys, *Journal of Nuclear Materials*. 123 (1984) 935–940.

[11] H. Moriyama, S.Tanaka, D.K. Sze, J. Reimann, A.Terlain. Tritium recovery from liquid metals. *Fusion Engineering and Design.* 28 (1995) 226-239.

[12] Tetsuaki Takeda, Alice Ying, Mohamed A. Abdou. Analysis of tritium extraction from liquid lithium by permeation window and solid gettering processes. *Fusion Engineering and Design.* 28 (1995) 278-285.

[13] Andrea Ciampichetti. Tritium Technology for HCLL Blanket. *PHD Thesys, Politecnico di Torino, Febrary 2005.*

[14] L.A.Sedano, Tritium Cycle Design for He-cooled blankets for DEMO, Report for TASK of the EFDA Technology Programme TW4-TTB-COMPU. January 2006.

[15] S.Tosti, V.Violante, A.Natalizio. Analysis of tritium permeation in the steam generators of the SEAFP/SEAL fusion power reactor. *Fusion Engineering and Design.* 43 (1998) 29–35.

[16] R.Sander.*Compilation of Henry's Law Constants for Inorganic and Organic Species of Potential Importance in Environmental Chemistry.* [Air Chemistry Department-Max-Planck Institute of Chemistry].

[17] http://www.en.wikipedia.org/wiki/Henry's_law.

[18] Innovative SFR: alternative options related to mitigation of Na-water interaction & Some other tracks for R&D. Christian Latgé. CEA-ENEA Bologna Meeting 2010 April 7th.

[19] R. Kumar. *Tritium Transport in an LMFBR*. AEC Report ANL-8089, August 1974.

[20] F.A.Kozlov, V.M.Poplavskii, V.V.Alekseev, A.G.Tsikunov, T.A.Vorob'eva**.** Simulation of tritium mass transfer in a three loops Sodium-Cooled Nuclear Power System. *Atomic Energy.* 98 (2005) 163-169.

[21] F. Franza. *Tritium Transport Analysis in Advanced Sodium-Cooled Fast Reactors*. Thesis for a Master Degree in Nuclear Engineering, Politecnico di Torino, Italy (2011).

[22] International Atomic Energy Agency (IAEA). *Fission and corrosion products behavior in liquid metal fast breeder reactors (LMFBRs).* Vienna, 1993. IAEA-TECDOC-687, ISSN 1011-4289.

[23] General atomics.*Engineering Services For The Next Generation Nuclear Plant (NGNP) With Hydrogen Production.* [NGNP Contamination Control Study] 2008. GA Project 30283.

[24] Sunil Sunny Chirayath, Gordon Hollenbeck, Jean Ragusa, Paul Nelson. Neutronic and nonproliferation characteristics of (PuO2–UO2) and (PuO2–ThO2) as fast reactor fuels. *Nuclear Engineering and Design.* 239 (2009) 1916–1924.

[25] *Control of tritium in LMFBR sodium by cold trapping.* C.C.McPheeters, D.Raue. 1976. International Conference on Liquid Metal Technology in Energy Production

[26] Fausto Saleri, Alfio Quarteroni. *Scientific Computing with MATLAB and Octave.* s.l.: Springer. 88-470-0480-2.

[27] T.Yokoo, H.Ohta. ULOF and UTOP Analysis of a Large Metal Fuel FBR Core Using a Detailed Calculation System. *Journal of Nuclear Science and Technology.* 2001, Vol. 38, 6,(444-452).

[28] L.E.Trevorrow, B.J.Kullen, R.L.Jarry, M.J.Steindler. *Tritium and noble gas fission products in the nuclear fuel cycle. I. reactors.* October 1974. ANL-8102 Waste Management (UC-70).

[29] C.C.McPheeters, D.J.Raue.*Sodium Hybride Precipitaion in sodium cold trap.* December 1974, ANL-79-101.

[30] Internation Atomic Energy Agency. *Liquid Metal Cooled Reactors: Experience in Design and Operation.* December 2007. ISBN 978–92–0–107907–7.

[31] G.W.Hollenberg, E.P.Simonen, G.Kalinin, A.Terlain. Tritium/hydrogen barrier development. *Fusion Engineering and Design* . 28 (1995) 190-208.

[32] D.Stuver, H.P.Buchkremer, R.Hecker, H.J.Leyers. Status of tritium permeation barrier development on austenitic structural alloys . *Journal of Nuclear Materials*. 122-123 (1984) 1541-1546.

[33] B.Zajec. Hydrogen permeation barrier - Recognition of defective barrier film from transient permeation rate. *Internation Journal of Hydrogen Energy*. 36 (2011) 7353-7361.

[34] H.D.Rohrig, R.Hecker, J.Blumensaat. J.Schaefer. Studies on the permeation of hydrogen and tritium in nuclear process heat installations. *Nuclear Engineering and Design*, 34 (1975) 157-167.

[35] J.Zhang, P.Hosemann, S.Maloy. Models of liquid metal corrosion. *Journal of Nuclear Materials*, 404 (2010) 82–96.

[36] M.V.Polley, G.Skyrme. An analysis of the corrosion of pure iron in sodium loop system. *Journal of Nuclear Materials,* 66 (1977) 221-235.

[37] M.Fulger, D.Ohai, M.Mihalache, M.Pantiru, V.Malinovschi. Oxidation behavior of Incoloy 800 under simulated supercritical water conditions. *Journal of Nuclear Materials*, 385 (2009) 288–293.

[38] D.Stöver, H.P.Buchkremer, R.Hecker, H.J.Leyers. Status of tritium permeation barrier development on austenitic structural alloys . *Journal of Nuclear Materials,* 122-123 (1984) 1541-1546.

[39] International Atomic Energy Agency (IAEA). *Fast Reactor Database 2006 Update.* December 2006. IAEA-TECDOC-1531.

[40] Indira Gandhi Centre for Atomic Research Department of Atomic Energy Kalpakkam-603 102, INDIA. Prototype Fast Breeder Reactor. Preliminary Safety Analysis Report. Chapter 1: General Description of Plant. *BHAVIN web site.* http://www.bhavini.nic.in/GenDesc.pdf.

[41] K.Devan, A.Riyas, M.Alagan, P.Mohanakrishnan. A new physics design of control safety rods for prototype fast breeder reactor. *Annals of Nuclear Energy* . 35 (2008) 1484–1491.

[42] R.Gajapathy, K.Velusamy, P.Selvaraj, P.Chellapandi, K.Velusamy, P.Selvaraj, P.Chellapandi. Thermal hydraulic investigations of intermediate heat exchanger in a pool-type fast breeder reactor. *Nuclear Engineering and Design,* 238 (2008) 1577–1591.

[43] S.C.Chetal, et al. Conference Article: Conceptual design of heat transport systems and components of PFBR-NSSS. *Internation Atomic Energy Agency (IAEA) Web Site.* [Online] http://www.iaea.org/inisnkm/nkm/aws/fnss/fulltext/28014320.pdf.

[44] S.C. Chetal et al. The design of the Prototype Fast Breeder Reactor. *Nuclear Engineering and Design* . 236 (2006) 852–860.

[45] P. Chellapandi, P.Puthiyavinayagam, V.Balasubramaniyan, S.Ragupathy, V. Rajanbabu, S.C.Chetal, B.Raj. Design concepts for reactor assembly components of 500MWe future SFRs. *Nuclear Engineering and Design.* 240 (2010) 2948–2956.

[46] C. Hurtado Norena, P.Bruzzonib. Effect of microstructure on hydrogen diffusion and trapping in a modified 9%Cr–1%Mo steel. *Materials Science and Engineering A.* 527 (2010) 410–416.

[47] P.Jung. Compositional variation of hydrogen permeability in ferritic alloys ans steels. *Journal of Nuclear Materials.* 238 (1996) 189-197.

[48] Radiation Safety Standards (NRB-96), Goskomsanepidnadzor of Russian Federation, Moscow, Russian Federation (1996).

[49] Technical Meeting on *"Operation and decomissioning experiences with Fast Reactors"*. Internation Atomic Eneregy Agency (IAEA). Cadarache, France., 11-15 March 2002. IAEA-TM-25332, TWG-FR/109.